Status Report for Experiment AD-4/ACE
Biological Effectiveness of Antiproton Annihilation

Michael Holzscheiter[1], Jan Alsner[2], Angelo Angelopoulos[3], Niels Bassler[2,4], Gerd Beyer[5], Fred Currell[6], John DeMarco[7], Michael Doser[8], Dragan Hajdukovic[9], Oliver Hartley[5], Joy Kavanagh[6], Kei Iwamoto[7], Oliver Jäkel[4], Ioannis Kantemiris[3], Helge Knudsen[10], Sandra Kovacevic[9], Bill McBride[7], Søren Pape Møller[10], Jens Overgaard[2], Jørgen Petersen[2], Osman Ratib[5], Giuseppe Schettino[6], David Timson[6], Brita Singers-Sørensen[2], Timothy Solberg[11], Sanja Vranjes[12], and Brad Wouters[13]

[1] University of New Mexico, [2]Aarhus University Hospital, [3] University of Athens, [4] Deutsches Krebsforschungszentrum, [5] Geneva University Hospital, [6] Queens University of Belfast , [7] University of California at Los Angeles , [8] CERN, [9] University of Montenegro, [10] Aarhus University, [11] University of Texas, [12] Vinca Institute of Nuclear Sciences, [13]University of Maastricht.

CERN-SPSC-2009-002 / SPSC-SR-039
17/01/2009

Summary

The AD-4/ACE collaboration has been studying the biological effects of antiproton beams on living cells since its inception in 2003. Initial experiments using a beam at 46.7 MeV kinetic energy readily available at CERN did show a significant enhancement of the biological effective dose ratio (BEDR) for antiprotons compared to protons. The experimental methods and analysis as well as the definition of terms used here are described by Holzscheiter et al. [1]. Based on this initial success the collaboration requested delivery of a higher energy beam (502 MeV/c), providing deeper penetration into the target and allowing the use of a clinically relevant spread-out Bragg peak (SOBP). We have used this beam setting for three run periods and have collected data on dosimetry of the mixed radiation field produced by the annihilation of antiprotons as well as on cell survival of V79 Chinese Hamster cells and Human FaDu cells (a human epithelial cell line derived from a squamous cell carcinoma of the hypopharynx).

Using dosimetric measurements with ionization chambers and alanine pellets we have successfully benchmarked the FLUKA Monte Carlo code [2], which now allows precise dose planning of the irradiation experiments. Using the calculated dose values along the beam path together with reference measurements using the same materials and methods and a standard ^{60}Co radiation source we can now extract the Relative Biological Efficiency (RBE) instead of using the Biological Effective Dose Ratio (BEDR) utilized in the initial experiments. RBE, while still a complex quantity and dependent on a variety of physical and biological parameters, can be compared more easily across different radiation modalities and used to analyze the differences in therapeutic potentials for different radiation qualities.

Early 2007 we also performed a set of irradiations using the same methods and materials at GSI with carbon ions giving the same calculated penetration depth and the same calculated width of the Spread Out Bragg Peak (SOBP) as the antiprotons at CERN.

A number of published papers describe the materials, methods, and results of the dosimetric measurements and the related Monte Carlo calculations (some more recent publications are attached as appendices to this report). A publication of the biological results is in preparation and expected to be submitted once the data analysis of the 2008 run cycle is completed. While a continuation of cell survival measurements is necessary to base any assessment of the therapeutic potential of antiprotons and any

necessary to base any assessment of the therapeutic potential of antiprotons and any comparison to other particle beam modalities on a well-founded scientific basis, the collaboration has initiated additional work on studying potential detrimental effects on cells placed outside the primary beam area (peripheral effects). Measurements of cell survival beyond the Bragg peak can be used for an initial assessment of the relevance or severity of these effects, but as the relevant biological endpoint in this area is not tumour control but normal tissue complication, other methods that are sensitive to DNA damage on the cellular level seem more appropriate. In 2008 we performed first experiments studying the development of foci using the γ-H2AX assay (see section V for details), and based on preliminary results we plan to perform a systematic study of cell damage outside the direct beam due to cell signaling through the medium and long range secondary products from the annihilation events during the next run cycle. In parallel, these studies will also yield information on the chemically mediated bystander effect where cells not subject to irradiation show effects due to the irradiation of cells with which they share medium; they are bystanders to the irradiation. By performing comparative experiments with otherwise identical geometry but where cells can or cannot share medium it is possible to distinguish between effects of long range secondary particles and chemically mediated bystander effects. Since the chemically mediated effects are expected with any radiation modality, this provides a benchmark against which the effects of long range secondary particles can be compared.

In addition we have dedicated a percentage of the available beam time to the study of new dosimetric methods that promise direct measurements of linear energy transfer (LET) in the beam.

Initial Monte Carlo calculations for realistic treatment situations have been performed, based on physical dose alone [3]. Publications of these results are in preparation and will be forthcoming soon. But while these can give a first glimpse at the complexity of a face-to-face comparison of different treatment modalities, to make these comparisons on a fair and realistic fashion, a thorough understanding of biological effects are needed, as is a the detailed understanding of oxygen enhancement ratios (OER). This will require a continuation of experimental cell work to link our data to the large body of biological data available from proton, carbon ion, pion, and neutron therapy studies.

I. **Introduction:**

The overall goal of the AD-4 Experiment is to study the biological effect of antiprotons in order to validate earlier theoretical predictions that antiprotons could produce a better therapeutic ratio for the treatment of well defined tumors. This prediction is based on two observations:

1. The physical dose should be augmented near the end of range due to the additional energy deposited locally when antiprotons annihilate.
2. Some of the additional energy deposited results from low energy heavy ion recoils produced in the annihilation event, which are expected to exhibit a higher biological efficiency.

For this purpose several studies are needed. One is a detailed measurement of the dose deposition of an antiproton beam of a specific energy entering a biological target, which then can be compared to Monte Carlo calculations and can be used to

benchmark different available codes. The second piece of information needed is the relative biological effect with respect to a standard radiation type (typically a ^{60}Co source) along the path of the antiproton beam, preferably for a number of different cell lines extensively used in cancer therapy. Once these two questions are answered one can then use these results as input data for treatment planning tools and develop comparative treatment plans for a specific tumor for antiprotons, carbon ions, and protons. Based on these plans we would then be able to determine specific incidences of cancer where antiprotons could provide a significant benefit to patients.

Since antiproton annihilation also yields a significant component of medium and high-energy secondary particles, which will leave the annihilation vertex, a third, very critical, issue to be studied is the biological effect of this background on cells outside the direct target area.

II. **Biological Measurements:**

Overview:

In 2006, 2007, and 2008 we were assigned 1 week of antiproton beam time each, using a special extraction method providing a beam of 502 MeV/c antiprotons. As this extraction method is very different from normal AD operation it was decided to lump all beam time into a single run of 7 days of 24 hours. Typically, the first two days of the week were needed for beam set-up and dosimetry studies. Only when the desired beam quality was achieved, the biological measurements could be initiated. As cell viability in the gelatin medium used is limited to 48 – 72 hours, this had to be orchestrated precisely and we typically allowed some extra time before the start of biological measurements which was (in case that set-up of the beam was completed faster) used beneficially for physics studies of dosimetry systems, beam monitors, and to collect dose data for Monte Carlo benchmarking.

The 502 MeV/c antiproton beam from the AD provides a penetration into our target of approximately 10 cm. We used a set of passive degraders to generate a spread-out Bragg peak of 10 mm depth, irradiating a volume of approximately 300 mm^3. This is much more closely resembling possible therapeutic situations encountered in realistic treatment scenarios than what was possible with the 300 MeV/c beam available before 2006. It also allows a much clearer separation between the entrance channel, where we expect low LET (and thereby low RBE) to dominate from the high LET/RBE region around the end of range. A typical dose-depth profile for antiprotons is shown in figure 1.

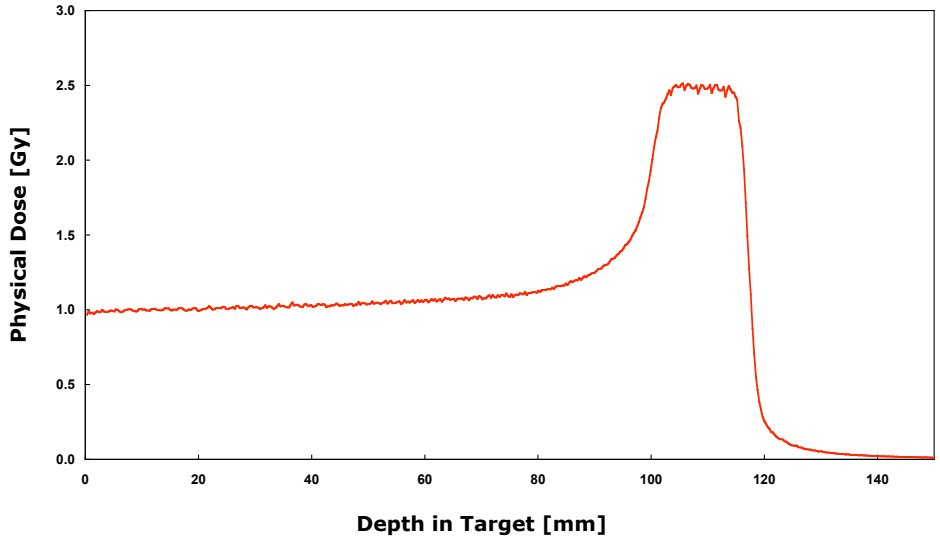

Fig. 1: Typical depth dose profile for antiprotons obtained from FLUKA (normalized to 1 Gy plateau dose).

In addition to the antiproton experiments at CERN we performed a comparison measurement using carbon ions at the heavy ion therapy unit at GSI in Darmstadt, Germany and a number of low LET calibration measurements needed for RBE analysis. For the carbon ion measurements a spread-out Bragg Peak (nearly) identical to the one shown above for antiprotons was programmed into the beam delivery software of the GSI treatment system.

Carbon Ion Measurements

In order to compare our studies with antiprotons to the gold standard of high LET particle therapy an experiment using carbon ions was conducted in early 2007 at GSI. Here a beam of clinical quality and absolute dosimetry was available and irradiations of 8 samples with plateau dose values between 0.3 and 4.0 Gy were performed. Survival data vs. depth are shown in figure 2.

The cell kill in the plateau region is noticeably higher for carbon ions than for antiprotons at similar plateau dose. This is due to the elevated RBE of carbon ions already in the entrance channel. Also there is an earlier and more gradual increase of cell kill for carbon ions compared to antiprotons.

Figure 3 shows the results of our analysis for the carbon ion experiment. Defining the plateau as data points 1 and 2 and the peak as points 9 – 14 of the depth survival curve (figure 2) we can plot survival vs. absolute dose for peak and plateau. In addition we plot survival vs. dose for a reference X-ray source with low LET and a RBE of 1. Using a biological endpoint of a survival rate of 10% we extract the $RBE_{0.1}$ for carbon ions as 1.38 in the plateau and 2.17 in the peak.

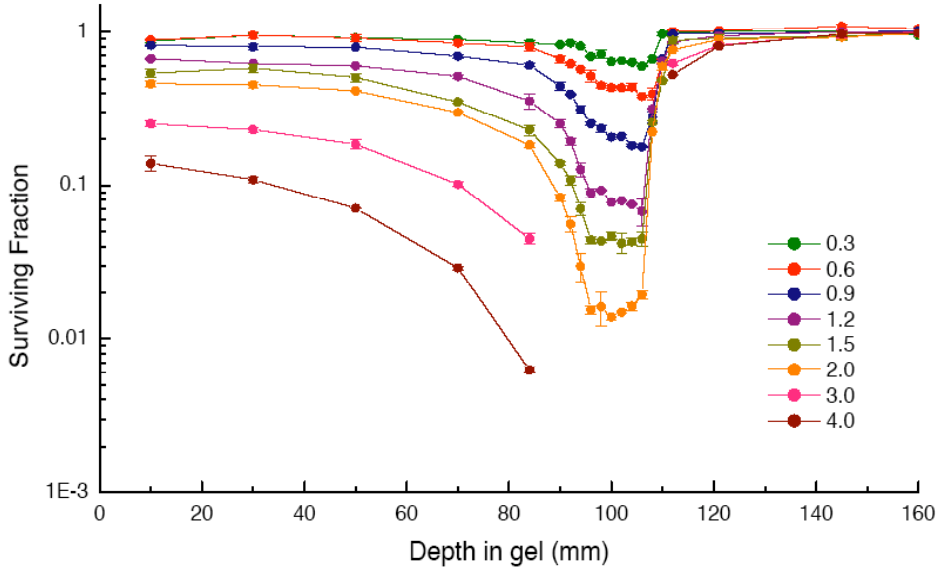

Figure 2: Survival fraction vs. depth in the target for V79 Chinese Hamster cells irradiated with carbon ions

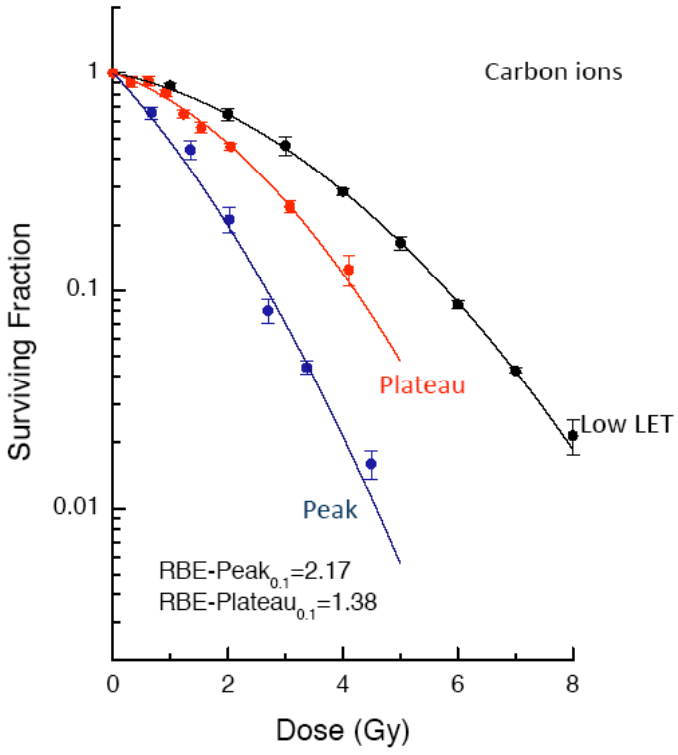

Figure 3: Survival fraction vs. absolute dose for V79 Chinese Hamster cells irradiated with carbon ions. By comparing the dose needed to achieve a survival of 10% using low LET X-rays to the dose needed when using carbon ions we extract a relative biological efficiency of 1.38 in the plateau and 2.17 in the peak

Antiproton Measurements – V79 Chinese Hamster Cells

In 2006 we performed 4 different irradiations with nominal dose values of 0.25, 0.5, 1, and 5 Gy. Due to high uncertainties in estimating the absolute dose only the lowest three dose values yielded useful data, which were presented in the last report (SPSC-2007-020/M-756). For the 2007 run period we had improved our dosimetry capabilities and were able to control the absolute dose delivered to the target to within 10%, allowing us to augment above data sets. We performed irradiations on V79 cells for 6 different dose values. These dose values were selected using FLUKA based on dosimetric information obtained before the irradiation together with a best guess for the dose response curve based on previous measurements to achieve specific desired survival values in the peak and/or plateau region. Dosimetric control measurements between different badges were performed to assure the stability of the beam delivery system. The raw data obtained in 2007 are shown in figure 4 below.

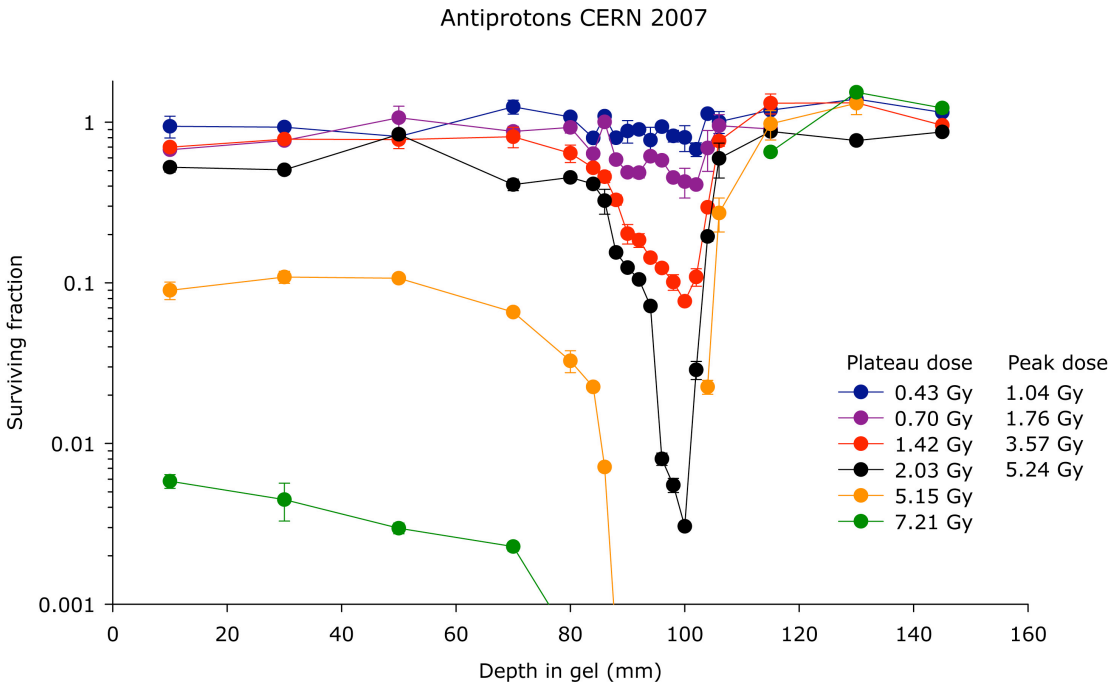

Fig. 4: Survival fraction vs. depth in the target for V79 Chinese Hamster cells irradiated with antiprotons. The dose values for the individual runs were estimated from FLUKA calculations using the number of antiprotons delivered and the radial beam profile obtained from radiochromic film irradiated simultaneously with the cell samples and analyzed after the run.

In figure 5 below we display the preliminary data analysis for antiproton irradiations performed at CERN in 2007. 4 survival values in the peak region and 6 values in the plateau region could be obtained. A reference measurement using the same cells, gelatine material, and preparation and analysis methods was obtained using low LET radiation sources at the DKFZ (Deutsches Krebsforschungszentrum) in Heidelberg and Aarhus. For 10% cell survival we find dose values of 5.17 for plateau antiprotons, 5.09 Gy for low LET radiation, and 3.31 Gy for peak antiprotons. This initial analysis indicates an RBE of unity in the plateau region, and an RBE of 1.56 in the peak of an antiproton beam.

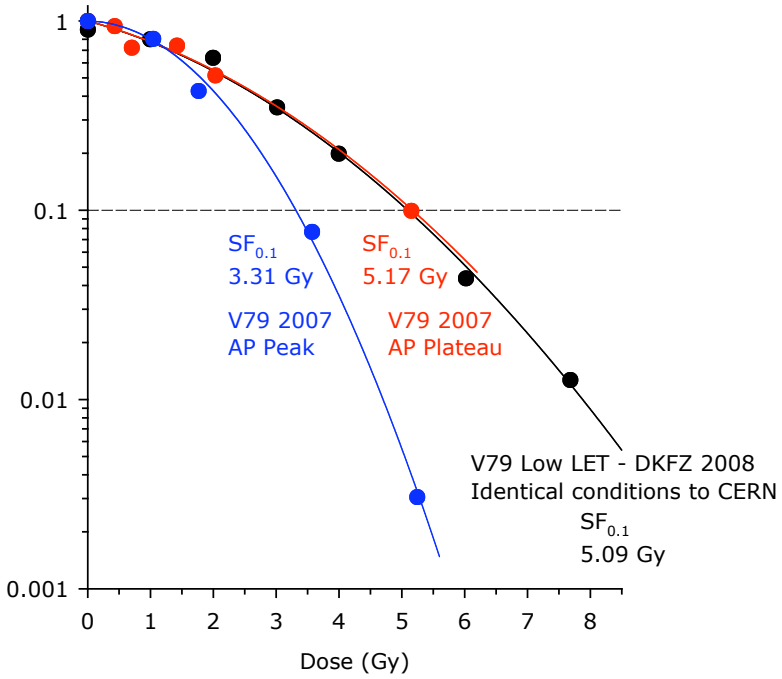

Fig. 5: Survival of V-79 cells irradiated with antiprotons in the plateau (red) and peak (blue) region. A reference measurement with low LET radiation was performed at DKFZ and is shown in black.

The statistical quality of the data was sufficient to analyse the RBE for each slice taken from the 6 sample tubes (see figure 6 for a lay-out of the analysis) resulting in the representation of RBE vs. depth shown in Figure 7.

We see that the antiproton RBE remains equal to 1 up to the proximal edge of the Bragg peak, where it rises sharply. As a matter of fact, the slope of the RBE increase is dominated by the admixture of low LET/RBE components in the antiproton beam that are aimed at a deeper penetration depth in order to generate a spread-out Bragg peak. This is distinctly different from the RBE vs. depth relationship for carbon ions, and such differences need to be taken into account when discussing specific tumour incidents where one or the other modality could be superior.

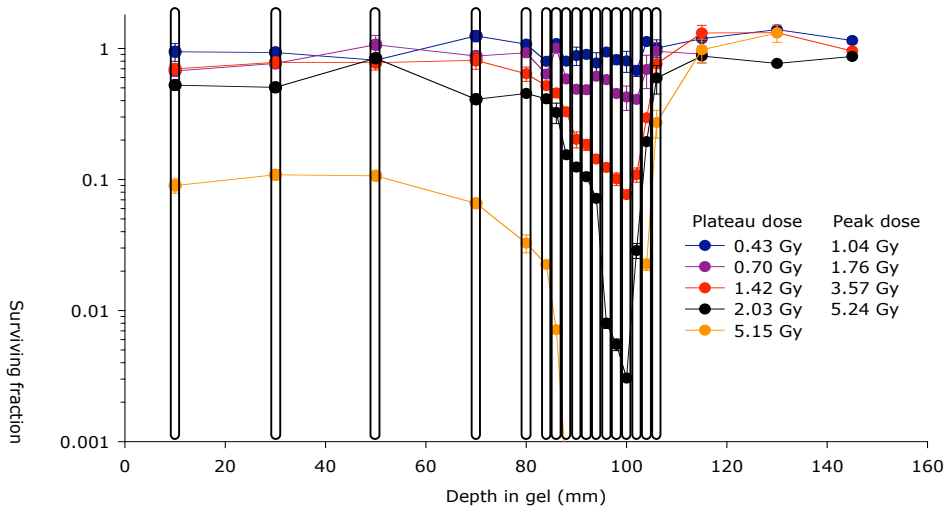

Figure 6: Slice position used for RBE analysis of antiproton irradiation of V79 Chinese Hamster cells.

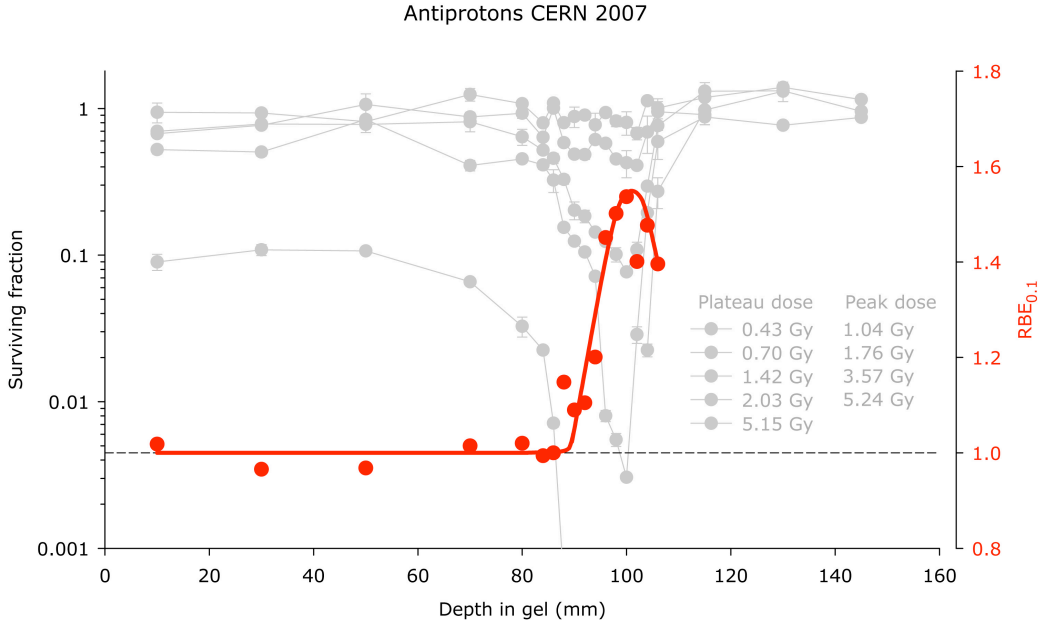

Figure 7: RBE vs. depth in target for antiprotons (overlaid on cell survival data). One can clearly see the rapid increase of RBE at the beginning of the SOBP

These are preliminary results and may change somewhat when the analysis of the 2008 run is completed and all data (2006 – 2008) are combined in a single analysis. One topic which needs careful attention (and probably more experimental work) is the fact that the biological effect in the plateau appears to be identical to the low LET reference radiation, in contrast to the expectation that inflight annihilation should

produce a fraction of high LET radiation already in the plateau, which was confirmed recently by Monte Carlo calculations [4].

Figure 8 shows a graph of the raw data from the October 2008 data run. We have further improved our dose calculation and achieved a Spread-Out Bragg Peak with a reasonably flat peak region. Also, the sensitivity of the clonogenic assay could be further improved and we were able this year to measure survival fractions as low as 1 x 10^{-4}.

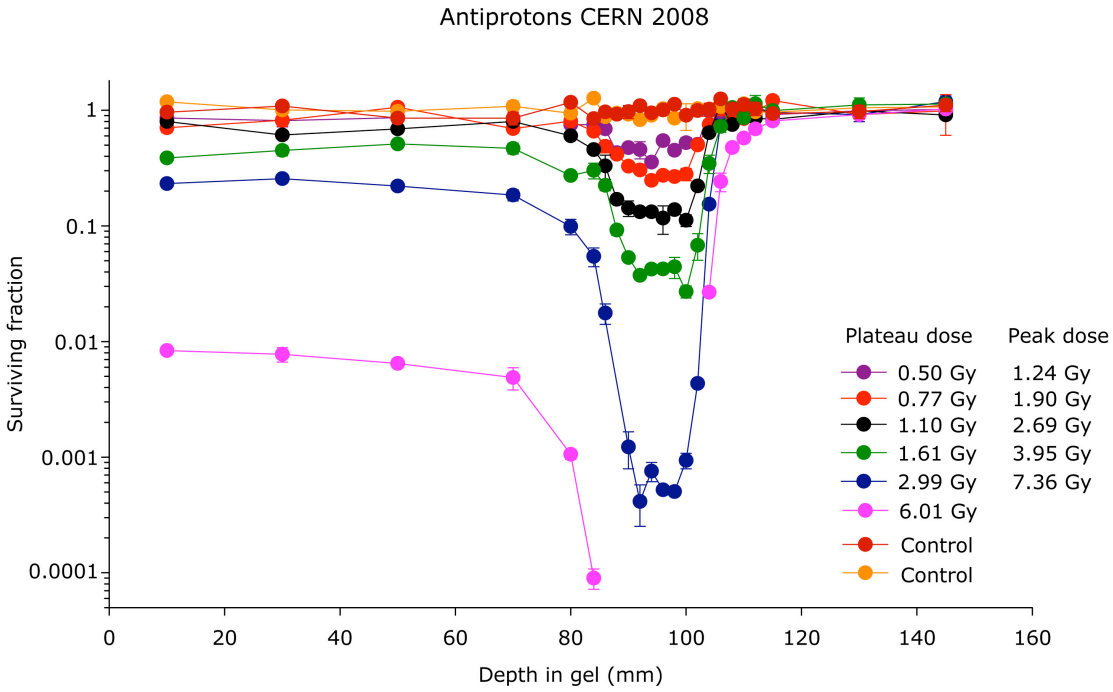

Fig. 8: Survival fraction vs. depth in the target for V79 Chinese Hamster cells irradiated with antiprotons during the 2008 run period.

Analysis of these data is ongoing.We need to determine the exact dose delivered to each depth point on each individual survival curve from the recorded shot-by-shot readings from the ionisation chamber and from the beam profiles measured with GAF chromic film between the different irradiations. We also need to complete a second control measurement with low LET radiation, to be done at the University Hospital in Aarhus. At that point we will be able to combine these data points with earlier measurements for a complete RBE analysis, but already now a coarse visual inspection indicates good agreement with the 2007 data set.

Antiproton Irradiation – FaDuDD

In addition to the studies on V-79 Chinese Hamster cells we irradiated a batch of tubes seeded with $FaDu_{DD}$ cells (a cell line derived from human head and neck tumor cells). These measurements were aimed primarily at the detection of cancer specific gene expressions. Using micro array analysis methods we identified commonalities to cells irradiated with X-rays in the expression of cancer specific genes and are encouraged to continue these studies in the future. Having these sample tubes available allowed us in addition to perform clonogenic survival analysis, preliminary

results of which are shown below. Additional measurements are needed to confirm the low LET response and confirm the RBE values extracted.

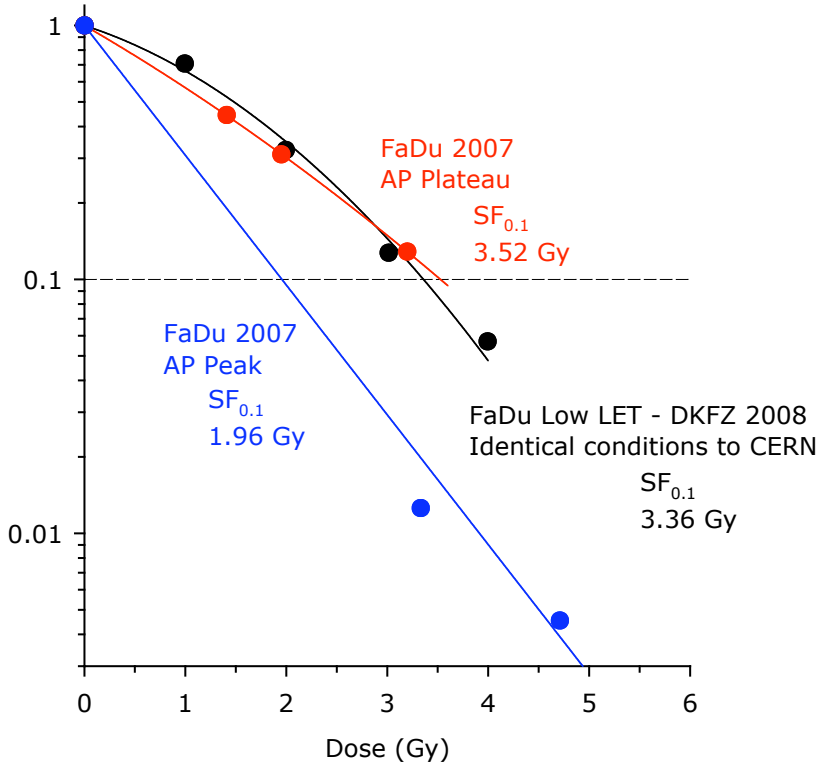

Figure 9: Surviving fraction for FaDuDD cells irradiated with antiprotons plotted vs. dose for peak and plateau. A biological endpoint of 10% cell survival is reached for 1.96 Gy in the peak and for 3.52 Gy in the plateau. This results in a Peak RBE of 1.8 with a plateau RBE of 1.0.

III. Liquid ionization chambers for LET determination

Introduction

The aim of the present measurements with a liquid ionization chamber (LIC) in the anti-proton beam is to determine the Linear Energy Transfer (LET) and the ionization density along the path of an anti-proton and to compare these parameters with proton and heavy ion tracks. The ionization density and the LET are related to the radiation's Relative Biological Effectiveness, RBE.

Air filled ionization chambers are the most commonly used ionization chambers in clinical settings for precision dosimetry. The methods are well established and the necessary conversion and correction factors needed to convert the reading into absorbed dose are known with high accuracy.

Ionization chambers filled with a liquid have some advantages over air filled chambers, e.g. the much higher sensitivity. The high sensitivity of the liquid ionization chambers is attractive as they can be made with small volumes without substantial loss of measured charge. Small volumes are desirable, e.g. in high dose gradients that exists at points beyond the Bragg peak or at the edge of the beam.

Due to the higher density of a liquid compared to that of air, the mobility of the ions in a liquid is much smaller than in air resulting in an increased ionic

recombination rate. In contrast to air filled ionization chambers, liquid ionization chambers never reach saturation, but there is always some fraction of ions that recombine.

Recombination can be classified either as general or initial. In general recombination, charged particles created by different incident ionizing particles recombine. General recombination is therefore dependent on the density of incident particle tracks, i.e. on the particle fluence. This means that general recombination depends on the dose rate.

Initial recombination occurs amongst ions created by the same incident ionizing particle and can further be divided into three groups:

a) Geminate recombination - the liberated electron recombines with its parent ion
b) Cluster recombination - the ions created in a group that is "localized" in space, recombine
c) Columnar recombination - ions created by one incident ionizing particle recombine.

The grouping above is not "water tight" as there is some overlapping, but is convenient as they are treated by different theories. Geminate recombination has been treated by Onsager [5], cluster recombination by Kara-Michailova and Lea [6] and columnar recombination by Jaffé [7].

Of interest in the present case is the columnar recombination. As the ionization density along the incident particle track increases, so does also the columnar recombination. Thus, an increase in this type of recombination indicates an increase in the LET and ionization density.

Materials & Methods

The liquid ionization chamber that was used in the present measurements in the antiproton beam is a plane parallel chamber with an electrode radius of 2.5mm and electrode spacing of only 0.3mm. The chamber was filled with the non-polar liquid ISOOCTANE (C8H18).

In all measurements, the antiproton beam was monitored with an air filled plane parallel chamber as described by Bassler et al. [8]. All readings with the liquid ionization chamber were corrected for beam fluctuations obtained from the readings of the monitor chamber.

Measurements were carried out in water at 21mm depth and at several depths on both sides of the Bragg-peak. At few depths, measurements were carried out with voltages from 100V up to 800V in 100V steps. Due to beam time constraints, at most of the depths the voltages ranged from 200V to 800V in steps of 200V.

The liquid ionization chamber is sensitive to voltage changes and each voltage was therefore measured 7 times, in order to allow sufficient time for the chamber to stabilize.

Results and discussion

Figure 10 shows a typical measurement result with the liquid ionization chamber. The LIC's charge is normalised with the monitor chamber reading. It is obvious from the curve in Figure 10 that saturation is not obtained in the voltage range shown.

In general, it is assumed that the linear part of the curve is due to initial recombination only and is therefore a measure of the beam's LET. The steeper the slope the higher is also initial recombination corresponding to a higher LET.

Specifically, if a linear fit to the measured values is made,

$$Q = aE + b \qquad (1)$$

then the ratio b/a is a measure of the LET. Initial recombination is independent of dose rate, and therefore the ratio must be independent of the dose rate. This is indeed the case as shown by several authors [9, 10, 11]. The procedure that is usually employed is to extrapolate the linear part of the curve to Q=0, and determine the so called extrapolated voltage, E_{ex}=-b/a. It has been noticed that the extrapolated voltage increases with the LET of the beam.

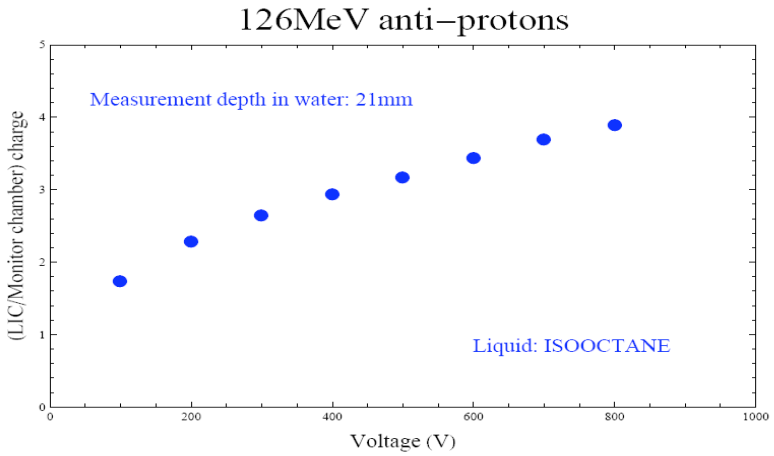

Figure 10. Charge versus voltage curve measured with the liquid ionization chamber.

Figure 11 illustrates the procedure in which linear fits have been made to the measurement at 21mm depth and at the Bragg peak in the 126 MeV antiproton beam. In Figures 10 and 11 the linear fits are made to measured values ranging from 400V up to 800V.

The extrapolated voltage in Figure 11 at the Bragg-peak is -578V whereas it is -819V at the 21mm depth. This then shows that the LET at the Bragg-peak is higher than at 21mm depth.

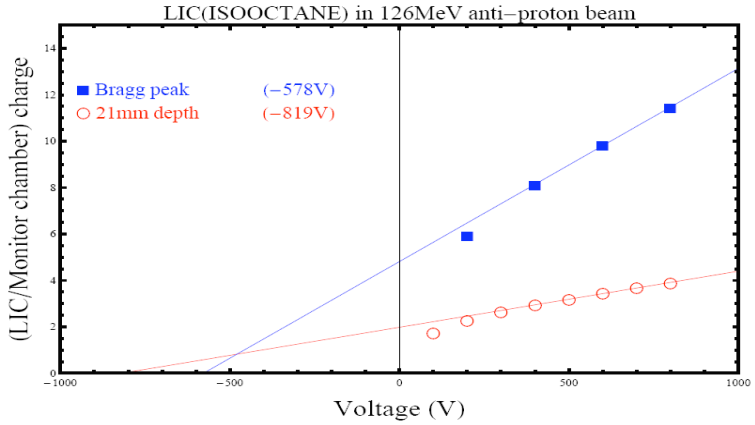

Figure 11. Linear fit to measurements in water at 21mm depth and at the Bragg peak.

In a similar manner, in figure 12 extrapolated voltages at Bragg peak minus 13mm, Bragg peak minus 2mm and at the Bragg peak are compared. The extrapolated voltages shows that as the Bragg peak is approached, the LET increases.

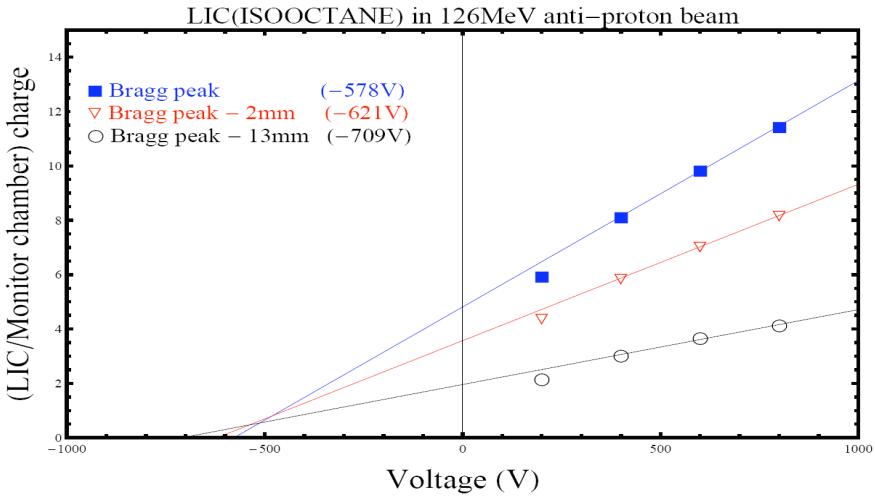

Figure 12. Linear fit to measurements in water at the Bragg peak and at 2mm and 13mm before the Bragg peak. The extrapolated voltages are indicated in the insert.

However, the values indicated have a high degree of uncertainty. A significant contribution to the uncertainty is the uncertainty in the correction for general recombination. The correction for general recombination in air filled ionization chambers, Boag's [112] theory is frequently employed. It has been shown by Johansson et al [13] that the same theory can also be applied to liquid ionization chambers, provided that the collection efficiency is at least 80% (for air filled chambers, the corresponding limit is 70%). This means that the method can be used in such cases where the measured charge is close to the saturation charge.

The theory by Boag is developed mainly for pulsed clinical beams in which the dose per pulse is modest, of the order of 1mGy/pulse. The dose per pulse in the anti-proton beam is much higher, between 10mGy/pulse and 20mGy/pulse. Consequently, higher general recombination can be expected in the antiproton beam than in conventional clinical pulsed beams.

Another point that may contribute to the uncertainty is the fact that the Jaffé theory on columnar recombination assumes cylindrical symmetry. For ionization chamber measurements, these assumptions mean that the incident particles passes through the chamber, leaving a cylindrical column of ions in the chamber. At the Bragg-peak and at points beyond, a large fraction of the incident particles will stop inside the ionization chamber and produce an ion distribution that should have a spherical distribution. This is clearly a violation to the Jaffé theory, but its effect is probably not as severe as it may look at a first glance; this will be investigated by us in more detail at the next run period.

Conclusions and future work with liquid ionization chambers

Due to their small size, liquid ionization chambers are extremely useful in measurements of radiation fields with high gradients, such as at points beyond the Bragg-peak or in the radial penumbra of a spot-scanned beam. In addition, the substantial initial recombination provides information about the LET and its variation in the beam.

Our goal for the present LIC measurements is to compare the linear energy transfer of antiprotons to that of protons.

A most interesting problem would be to determine the restricted LET in antiproton-, proton- and ion beams. Restricted LET takes into account energy transfer up to some predetermined limit and gives a measure of the ionization density in the close vicinity of the incident particle track. This type of information is possible already hidden in the measured values shown in the figures above but unfortunately, Jaffé's theory does not include the possibility to extract restricted LET.

In order to check the consistency of our results it would be desirable to use several chambers filled with different liquids, i.e. Isooctane and Tetramethylsilane.

IV. Studies of cell damage in the peripheral region using γ-H2AX

Brief description of the experiment

In order to accurately investigate the implications of antiproton irradiation of living cells, it is important to analyze genetic complications that may arise in cells in regions peripheral to the targeted volume and cause tumorigenesis and thus cancer development in previously healthy tissue; so called late normal tissue complication. Therefore an experiment which allows sensitive and accurate measurement of critical DNA lesions is required.

Double strand DNA breaks (DSBs) are highly cytotoxic lesions which if unrepaired or repaired incorrectly can cause cell death or mutations in DNA of daughter cells [14]. DNA damage can be caused by a number of extrinsic factors such as ionizing radiation, intrinsic factors such as reactive oxygen species and endogenous damage. As few as one DSB can cause cell death or genetic mutations leading to disregulation of cell growth and tumorigenesis.

Cells have a complex DNA damage response with which to deal with such assaults on their genetic material. Once a lesion is detected in healthy cells a number of proteins are released which trigger cell signaling pathways to initiate DNA damage checkpoints (the cell cycle is temporarily halted) and DNA repair [15]. A key event in repair of a DSB is the phosphorylation of the histone H2AX necessary to unwind the DNA and allow repair proteins to access the DSB site.

The γ-H2AX is a very sensitive and specific immunocytochemical assay based on antibodies which recognize, and bind to, the phosphorylated H2AX histone as an accurate indicator of a DNA DSB. A secondary fluorescing antibody is then introduced to the cells which will bind to the primary antibody so the aggregate (or focus) around the DSBs can be analyzed by fluorescence microscopy It has been shown [16] that there is an excellent 1:1 relationship between the number of γ-H2AX foci and the DSB induced. This assay is used frequently to investigate DNA damage induction by heat shock, chemotherapeutic agents, ionizing radiation, bystander signaling and other DNA damage agents.

In order to assess the applicability of the γ-H2AX assay to studies of DNA damage in cells present in the target during irradiation with antiprotons but located outside of the direct beam path a number of preliminary studies were performed.

After preparation in the laboratory at Queen's University Belfast human fibroblast cells (cell line AGO 1522), seeded on glass coverslips situated in 24-well plates were transported at room temperature in culture media (20% bovine serum + 25 mM Hepes buffer to maintain suitable pH conditions) from Belfast to CERN. At CERN the 24-well plates (6 wide, 4 high) were mounted inside the water phantom perpendicular to the beam direction at the location of the Bragg peak in such a way that the centre of the beam was aiming at the second well from the left in the lowest row. This set-up gave optimum access to the remaining well plates for the bystander experiments. The plates received estimated antiproton doses of 0 (control), 0.2, 0.5, 0.75, 1.0, 1.5 and 2.0 Gy. The temperature of the water phantom was kept at 34 degree Celsius during irradiation. In addition to examining cells directly irradiated in the water phantom, culture media was transferred from directly irradiated wells for each dose point into well plates with cells that had not been placed into the phantom. This was done to quantify the effect of the chemical signaling of cells damaged by antiproton irradiation to other cells (bystander experiment). This is a critical step to investigate and determine the effect of secondary particles in cells which are not directly irradiated. Cells were fixed 1 hour after irradiation and transported back to Belfast.

Plates were washed in PBS and cells stained with anti-γ-H2AX antibody, a routinely used marker of DNA damage induced by ionizing radiation, and a secondary fluorescing antibody (Alexa Fluor 488) before the nuclei were stained with DAPI (a fluorescent stain that binds strongly to DNA). Cells were mounted on slides and viewed with a fluorescence microscope.

Images of the cells show the nuclei stained blue and DNA damage (foci) shows up as bright green spots within the nuclei.

Results.

Directly irradiated cells show a significant increase in number of foci per cell compared to the controls. Foci measured in the irradiated samples are also larger than those measured in the controls (caused by endogenous reaction and/or environmental stress) clearly indicating radiation-induced DNA damage.

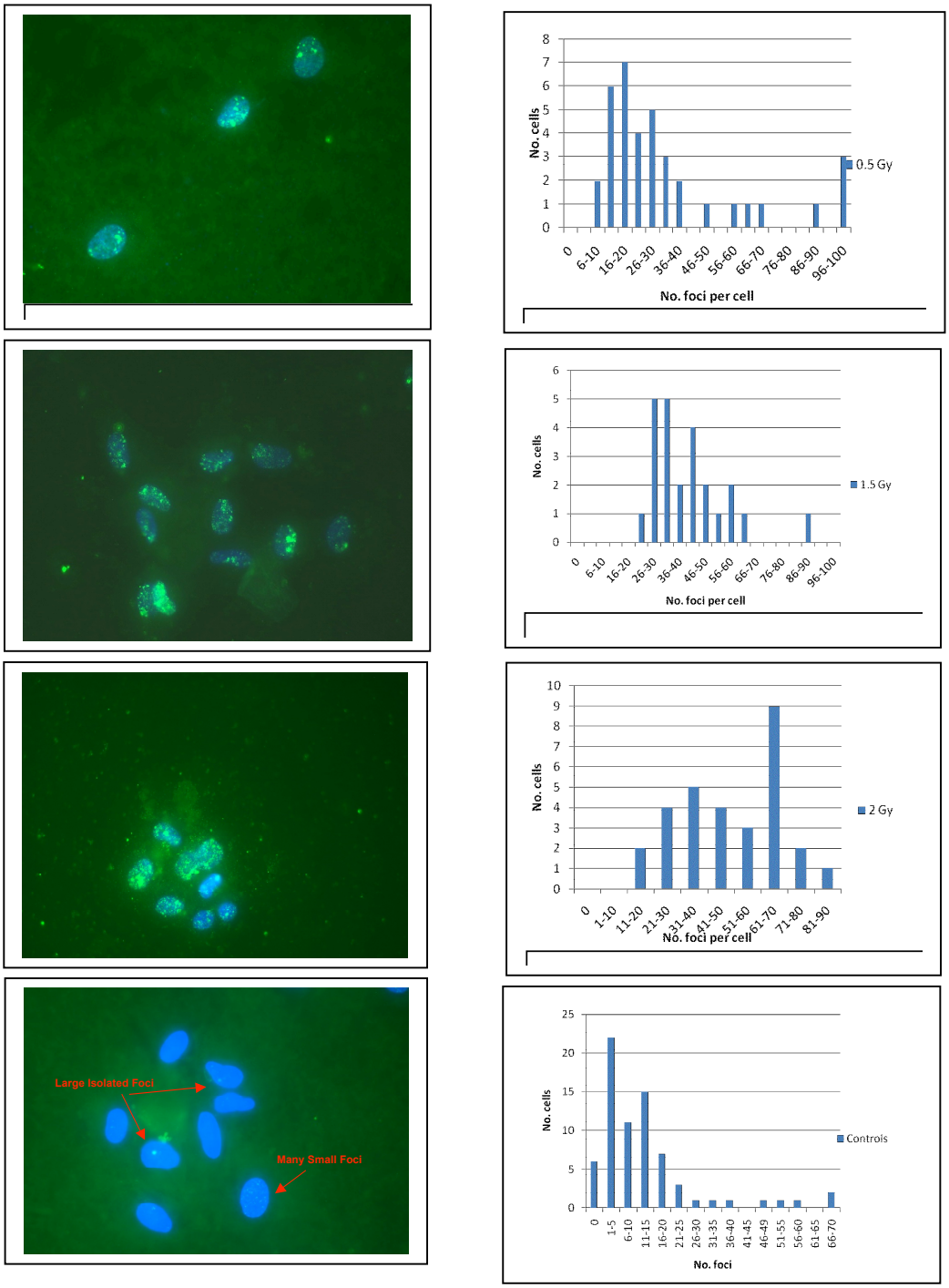

Figure 13: Left column: Fluorescent images of irradiated cells receiving (top to bottom) 0.5, 1.5, 2, and 0 Gy (control). Right column: Histogram of foci number observed. (All cells were positioned in the Bragg peak of the beam).

92% of cells in the control group show evidence of background levels of DNA damage. Damage in control cells appears in two different patterns (as also highlighted by the histogram):

Small number of isolated clear foci (<5)
Many small foci (~ 0.5 μm radius) spread throughout the nucleus

Preliminary data analysis shows foci number per cell increases linearly with dose with an average of ~33 foci/Gy. (Figure 14).

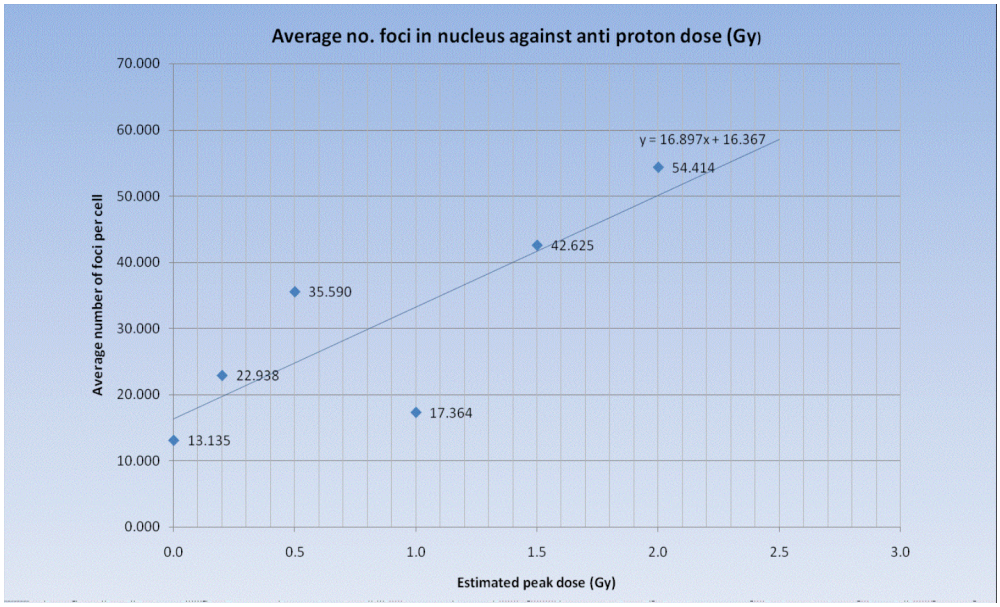

Figure 14: Linear relationship between number of foci and peak dose received by samples

Small number of isolated foci (endogenous DNA damage) are expected in control cells, based on experiments carried out in our lab with x-ray irradiation on the same cell line. Higher than expected number of foci in control cells are believed to be due to stress of transport (some samples were irradiated as much as 3 days after shipping) and infection as a result of a lack of tissue culture facilities on site at CERN.

A second control experiment has been set up in the laboratory at Queen's University to demonstrate the effect of stress on the cells and the need for tissue culture facilities on site (possibly at the University of Geneva) to achieve reliable and accurate results from the next run.

Media transfer experiments and effect of secondary particles

Unirradiated cells were cultured for 1 hour in medium, which was transferred from wells that had been irradiated with 1 Gy antiproton dose. After staining clear foci typical of DNA damage following ionizing radiation could be observed.

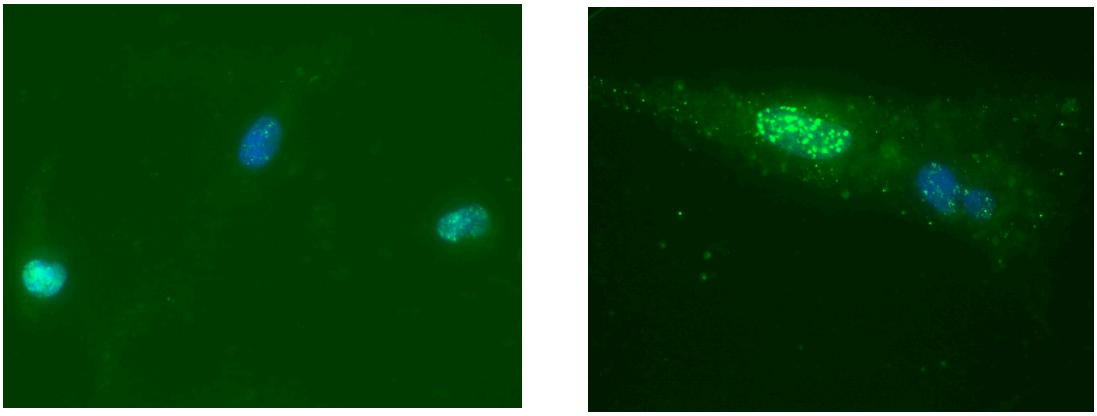

Figure 15: Unirradiated cells show foci after incubating in medium obtained from cells irradiated with one gray.

Similarly, cells outside the direct beam path, and separated by a physical barrier from cells (and medium) that were present in the water phantom at the time of the irradiation, showed clear foci. The extent of DNA damage (number of foci per cell) is less than for directly irradiated cells but still higher than for the control sample and it can only be attributed to secondary particles resulting from the antiproton annihilation. The high level of background fluorescence observed in the picture below is a result of antibody binding to contaminants in the culture media.

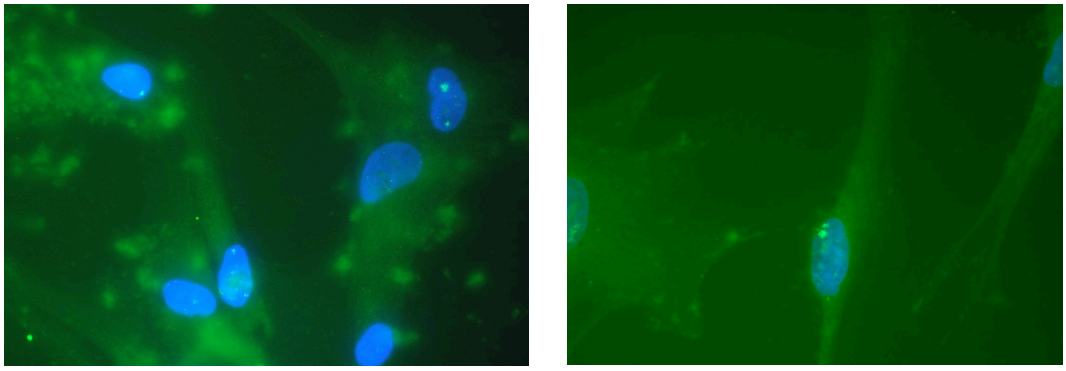

Figure 16: Foci in cells outside of the direct beam resulting from secondary particles

Conclusion and Outlook

Data from this pilot run demonstrates the potential of accurately measuring low dose DNA damage induced in cells by antiproton exposure. Despite the rudimental set-up, the preliminary data clearly show the effect of direct antiproton exposure (Bragg peak only analyzed so far) as well as medium transfer (bystander effect) and secondary particles. The sensitivity of the assay should allow us to assess each individual contribution.

V. Future Plans:

Depending on the final analysis of the data collected in 2008 we will define a scientific program for 2009. Aside from augmenting existing data on V79 cells, if necessary, and additional experiments using the FaDuD cell lines, we are discussing a number of approaches to the third question raised in the introduction, the peripheral

damage to cells outside the direct beam. Again, our approach will be based on computer calculations supported by a crucial set of experimental tests (carefully chosen to optimize beam usage) for benchmarking.

A measurement of clonogenic survival of cells in the region distal to the Bragg peak is very important as it would allow a clean assessment of the relative biological effect of secondary particles from the annihilation event. Such an experiment is also absolutely necessary for the development of a dose planning tool that includes proper restrictions on dose delivered to organs at risk in the immediate vicinity of the targeted tumour. To discern a biological effect in this region with the clonogenic assay a high dose value must be delivered to the target region, requiring a significant amount of beam time. We attempted to include an initial study of this issue at the very end of the 2008 run cycle. Unfortunately, delivery of the necessary biological samples failed as the courier service was unable to clear the cell samples through the Swiss customs at the airport on Saturday and we were unable to perform the irradiation in the remaining beam time (which was then instead used to augment our studies of the liquid ionization chamber).

As for any measurements careful initial dosimetry studies are needed and we plan to develop a program to again beneficially use 1 week (7 days) of beam time to perform several independent measurements. Aside from clonogenic cell survival experiments, which are most sensitive to exact planning, we will perform systematic study of DNA damage to cells in the beam as well as in the peripheral region and continue our development work on liquid ionization chambers. Furthermore, having added more manpower in this specific sub-category, we will pick up again on the analysis and further experimentation on the idea of real-time imaging of the annihilation vertex distribution. The exact schedule for the requested beam time will need to be decided within the collaboration to assure availability of laboratory space and personnel, but currently we favor again the time period of late October in order to stay clear of conflicts with several major international conferences in the field of radiation oncology (ESTRO, ASTRO, RSNA) which several key collaborators in AD-4/ACE must attend.

Given the necessary biological preparations and considering the limited survival time of the samples once the cells have been harvested and embedded in gelatin, a precise schedule must be established early on. The actual irradiation time can then be adjusted by a few days within the week by waiting until the beam development is completed and dosimetry has been fully established before preparing the actual samples from cell cultures started a few weeks beforehand and shipping them by personal courier to CERN. We will also study to which extent biological preparations and initial analysis can be performed at CERN or at the Geneva Hospital facilities. A grant proposal is in preparation for submission by the Queen's University Belfast team for submission to the UK's Engineering and Physical Science Research Council, to support installation of the relevant tissue culture facilities.

References:

1. Holzscheiter M H et al.: *Radiotherapy and Oncology* ***81*** *233–242(2006)*
2. A. Ferrari, P. R. Sala, A. Fasso, and J. Ranft, "FLUKA: a multi-particle transport code", CERN-2005-10 (2005), INFN/TC 05/11, SLAC-R-773.
3. Niels Bassler, Jan Alsner, Gerd Beyer, John J. DeMarco, Michael Doser, Dragan Hajdukovic, Oliver Hartley, Keisuke S. Iwamoto, Oliver Jäkel, Helge V. Knudsen, Sandra Kovacevic, Søren Pape Møller, Jens Overgaard, Jørgen

B. Petersen, Timothy D. Solberg, Brita S. Sørensen, Sanja Vranjes, Bradly G. Wouters, Michael H. Holzscheiter; *Antiproton radiotherapy*; Radiotherapy and Oncology, **86** 14–19 (2008)

4. Niels Bassler, Michael Holzscheiter; Calculated LET spectrum from antiproton beams stopping in water*; Acta Oncologica (2008) DOI: 10.1080/02841860802266730*
5. Onsager L: Intial recombination of ions. *Phys. Rev. **54**, 554-557 (1938)*
6. Kara-Michailova E and Lea D E:, The interpretation of ionization measurements in gases at high pressures, *Proc. Camb. Phil. Soc., **36**, 101-1026 (1940)*
7. Jaffé G: Zur Theorie der Ionisation in Kolonnen, *Ann d Phys, **42**, 303-344 (1913)*
8. Bassler N, Holzscheiter M H, Jäkel O, Knudsen H V, Kovacevic S and (the AD-4/ACE Collaboration), The anti-proton depth dose curve in water, *Phys. Med. Biol., **53**, 793-805 (2008)*
9. D. Blanc, J. Mathieu, P. Vermande, L.: "Torres Sur la possibilite de mesurer le facteur de qualité des rayonnements nucleaires au moyen de chambres d'ionisation remplies d'un liquide dielectrique*" Health Physics vol **11**, 63-65 (1965)*
10. S. Charalambus: "The response of a liquid ionization chamber to gamma radiation and to high-energy neutrons and protons*" Nuc. Inst. and Meth. **48** 181-192 (1967)*
11. Tölli H: Talk presented at Varenna meeting of the AD4/ACE group 2008
12. Boag J W: Ionisation Chambers, in: *Radiation Dosimetry, Vol. II, Ed. F H Attix, W C Roesch. Academic Press*, Library Number (1966) 66-26846
13. Johansson B, Wickman G and Bahar-Gogani J, General collection efficiency for liquid isooctane and tetramethylsilane in pulsed radiation, *Phys. Med. Biol., **42**, 1929-1938 (1997)*
14. K.K. Khanna, S.P. Jackson. *Nat. Genet.* **27** (2001) 247-254
15. U. Déry, J. Masson. *DNA Repair*, **6** (2007) 561-577
16. E.P. Rogakou et el., *J. Biol. Chem.* **273** (1998) 5858-5868
17. K. Rothkamm, M. Löbrich. *Proc. Natl. Acad. Sci.* **100** (2003) 5057-5062

Appendix A: Current list of Collaborators in AD-4

Aarhus University, Dept. of Phys. & Astronomy, DK-Aarhus C, Denmark
Helge KNUDSEN, Soren PAPE-MØLLER, Ulrik UGGERHØJ

Aarhus University Hospital , Nørrebrogade 44, DK-8000 Aarhus, Denmark
Jan ALSNER, Niels BASSLER, Jens OVERGAARD, Jorgen PETERSEN, Brita SINGERS-SØRENSEN

CERN, Division EP, CH-1211Geneva, Switzerland
Michael DOSER

David Geffen School of Medicine at UCLA, Los Angeles, CA 90095, USA
John J. DeMARCO, Benjamin P. FAHIMIAN, Keisuke S. IWAMOTO, William H. McBRIDE

Deutsches Krebsforschungszentrum (DKFZ), 69120 Heidelberg, Germany
Niels BASSLER, Katrin HENKNER, Rochus HERRMANN, Oliver JÄKEL, Franz-Joachim KAISER,

Geneva University Hospital, 1 rue Michel Servet, CH-1211 Geneva, Switzerland
Gerd BEYER, Oliver HARTLEY, Osman RATIB, Raymond MIRALBELL

Queen's University Belfast, Belfast BT7 1NN, UK
Frederick CURRELL, Joy KAVANAGH, Giuseppe SCHETTINO, David TIMSON

University of Athens, 157 71 Athens, Greece
Angelo ANGELOPOULOS, Ioannis KANTEMIRIS

University of Toronto, Dept. of Rad. Oncology, Toronto, ON M5G 2M9, Canada
Bradly G. WOUTERS

University of Montenegro, Nikca od Rovina 53, Podgorica, Montenegro
Dragan HAJDUKOVIC, Sandra KOVACEVIC

University of Texas Southwestern Medical Center, Dallas, TX 75390, USA
Timothy SOLBERG

University of New Mexico, Dept. of Phys. & Astr., Albuquerque, NM 87131, USA
Michael H. HOLZSCHEITER, Roy KEYES

Vinca Institute of Nuclear Sciences, 1101 Belgrade, Serbia
Sanja VRANJES

Appendix B

Radiotherapy and Oncology 86 (2008) 14—19
www.thegreenjournal.com

Antiprotons

Antiproton radiotherapy

Niels Bassler[a,b,*], Jan Alsner[a], Gerd Beyer[c], John J. DeMarco[d], Michael Doser[e], Dragan Hajdukovic[f], Oliver Hartley[c], Keisuke S. Iwamoto[d], Oliver Jäkel[b], Helge V. Knudsen[g], Sandra Kovacevic[f], Søren Pape Møller[h], Jens Overgaard[a], Jørgen B. Petersen[i], Timothy D. Solberg[j], Brita S. Sørensen[a], Sanja Vranjes[k], Bradly G. Wouters[l], Michael H. Holzscheiter[m]

[a]*Department of Experimental Clinical Oncology, Aarhus University Hospital, Aarhus, Denmark,* [b]*Deutsches Krebsforschungszentrum, Heidelberg, Germany,* [c]*Hospital Universitaire de Geneve, Geneva, Switzerland,* [d]*David Geffen School of Medicine, UCLA, Los Angeles, CA, USA,* [e]*CERN, Geneva, Switzerland,* [f]*University of Montenegro, Podgorica, Montenegro,* [g]*Department of Physics and Astronomy, and* [h]*ISA, University of Aarhus, Denmark,* [i]*Department of Medical Physics, Aarhus University Hospital, Aarhus, Denmark,* [j]*University of Nebraska Medical Center, Omaha, NE, USA,* [k]*VINCA Institute for Nuclear Sciences, Belgrade, Serbia,* [l]*University of Maastricht, Res. Institute Growth and Development, The Netherlands,* [m]*University of New Mexico, Albuquerque, NM, USA*

Abstract

Antiprotons are interesting as a possible future modality in radiation therapy for the following reasons: When fast antiprotons penetrate matter, protons and antiprotons have near identical stopping powers and exhibit equal radiobiology well before the Bragg-peak. But when the antiprotons come to rest at the Bragg-peak, they annihilate, releasing almost 2 GeV per antiproton—proton annihilation. Most of this energy is carried away by energetic pions, but the Bragg-peak of the antiprotons is still locally augmented with ~20—30 MeV per antiproton. Apart from the gain in physical dose, an increased relative biological effect also has been observed, which can be explained by the fact that some of the secondary particles from the antiproton annihilation exhibit high-LET properties. Finally, the weakly interacting energetic pions, which are leaving the target volume, may provide a real time feedback on the exact location of the annihilation peak.

We have performed dosimetry experiments and investigated the radiobiological properties using the antiproton beam available at CERN, Geneva. Dosimetry experiments were carried out with ionization chambers, alanine pellets and radiochromic film. Radiobiological experiments were done with V79 WNRE Chinese hamster cells. The radiobiological experiments were repeated with protons and carbon ions at TRIUMF and GSI, respectively, for comparison. Several Monte Carlo particle transport codes were investigated and compared with our experimental data obtained at CERN. The code that matched our data best was used to generate a set of depth dose data at several energies, including secondary particle-energy spectra. This can be used as base data for a treatment planning software such as TRiP.

Our findings from the CERN experiments indicate that the biological effect of antiprotons in the plateau region may be reduced by a factor of 4 for the same biological target dose in a spread-out Bragg-peak, when comparing with protons.

The extension of TRiP to handle antiproton beams is currently in progress. This will enable us to perform planning studies, where the potential clinical consequences can be examined, and compared to those of other beam modalities such as protons, carbon ions, or IMRT photons.
 Radiotherapy and Oncology 86 (2008) 14—19.

Keywords: Antiproton; RBE; Particle irradiation

Antiproton therapy might sound like science fiction but in fact, antiproton therapy may well be clinically beneficial for selected cases and could perhaps be economically feasible if performed in the context of a major facility producing antiproton beams for fundamental science research. Gray and Kalogeropoulus first suggested radiation therapy with antiprotons in 1984 based on Monte Carlo calculation of a significant enhancement of physical dose in the Bragg-peak [1]. Sullivan shortly afterwards measured an enhancement of the peak-to-plateau ratio of physical dose deposition by antiprotons in polyethylene by a factor of 2 compared to protons [2]. Since reducing normal tissue morbidity is one of the main goals of radiotherapy, beam modalities such as IMRT, proton beam therapy and carbon ion beams have been investigated during the last decades and have been successfully implemented in clinical use [3—7]. Other

0167-8140/$ - see front matter doi:10.1016/j.radonc.2007.11.028

particles, such as fast neutrons and pions, were applied in radiation therapy, but proved to be less successful in the clinical settings [8,9]. Antiprotons deserve closer investigation since they exhibit the precision in dose delivery of a charged particle and confine the contribution of high linear energy transfer (LET) to the Bragg-peak.

Annihilation physics

When fast antiprotons penetrate matter, they have the same stopping power as protons. The amount of primary particle loss is only slightly larger for antiprotons when compared with protons, and is less than that of carbon ions [10].

As the antiproton comes to rest, it will preferably be captured by a high-Z nucleus. For a polystyrene target ~99% of the antiprotons will therefore annihilate on a carbon nucleus, whereas the rest will annihilate with a hydrogen nucleus [11]. When captured by the target atoms, the antiproton will immediately spiral towards the nucleus and annihilate on its surface. This annihilation process releases 1.88 GeV corresponding to twice the rest-mass of the proton and the energy release is converted on average into 4 or 5 pions [12,13]. The pions created are π^+ and π^- particles, as well as π^0. The π^0 meson is highly unstable and decays instantaneously into high energy gamma-rays with roughly 70–300 MeV [12]. Due to the solid angle covered by the nucleus, 1 or 2 of the charged pions are most likely penetrating the nucleus inducing an intra-nuclear cascade, causing the nucleus to break into fragments [14–16]. Charged fragments have a very short range in the target and will deposit their kinetic energy in the immediate vicinity of the annihilation vertex. Also, we expect that some of these fragments will exhibit a high-LET and are responsible for an increase in biological effectiveness of antiproton annihilation compared to protons stopping in the target. Antiprotons annihilating on particles heavier than protons will also produce neutrons which will have a larger range and will lead to a certain level of background radiation. This needs to be studied carefully in the context of validating antiprotons for radiotherapy applications.

The total energy deposited locally by these particles has been estimated by Gray and Kalogeropoulos using Monte Carlo calculations [1] to be 30 MeV per antiproton, which has been confirmed experimentally by Sullivan [2] who used a continuous beam of antiprotons from the Low Energy Antiproton Ring (LEAR) at CERN and standard ionization chambers. This energy represents an increase of the physical dose deposition in the Bragg-peak by roughly a factor of 2, when compared to protons. In addition to this augmentation of the physical dose the secondary particles also cause the antiproton beam to have different radiobiological properties in the peak region.

Antiproton production

Currently, only few laboratories in the world produce antiparticles, and only at CERN, located near Geneva, a beam of antiprotons at clinical relevant energies is available. Antiprotons are produced from a 26 GeV proton beam, which is being dumped into a target. The peak production occurs at an antiproton energy of 3.6 GeV. Antiprotons are collected at this production energy in the antiproton decelerator (AD) ring, decelerated to lower energies, and cooled using stochastic cooling as well as electron cooling to decrease beam emittance. To date we have used both a 47 MeV and a 126 MeV antiproton beam, which have a range of approximately 2 or 11 cm in a water phantom, respectively. Every 90 s around 3×10^7 antiprotons are delivered to our experiment, which corresponds to a dose in the plateau region of 30 mGy at $\sigma = 4$ mm of the Gaussian shaped beam at 126 MeV. These antiprotons exit the accelerator vacuum through a 15 μm titanium window and pass several non-destructive beam monitors before entering the biological target. A fast current transformer gives the total charge extracted from the accelerator and a combination of a thin scintillator and a CCD camera can be used to monitor the beam position and profile. The antiproton beam focus can be changed, depending on the experimental requirements, between $\sigma = 4$ mm and $\sigma = 15$ mm. A future antiproton production facility for experimental physics is planned at the Gesellschaft für Schwerionenforschung (GSI) in Darmstadt and will offer significantly higher beam intensities.

Radiobiology

In 2006 we published an article concerning the radiobiology of a 47 MeV antiproton beam, describing the initial experiments carried out at CERN in 2003 and 2004 [17]. RBE determination was at that time not possible, since we could not assess the absolute physical dose for the pulsed antiproton beam. Instead the Biological Effective Dose Ratio (BEDR) term was conceived. Recently we have initiated a new set of measurements at higher energy at CERN and at GSI to compare the biological effects of antiprotons and carbon ions using identical experimental conditions. The energy used of 126 MeV provides a better separation of the peak from the plateau region and also enables us to produce a clinically relevant spread-out Bragg peak (SOBP). After careful dosimetry studies (see next section), we are now able to adequately assess the absolute physical dose in the peak region of the pulsed antiproton beam. This will enable us to directly determine the RBE in the peak region in future experiments, which then can be used as an input parameter for computer models used for treatment planning.

Dosimetry

Monte Carlo simulations with FLUKA 2006.3 [18,19] of a pristine beam of antiprotons are shown in Fig. 1. Here a 5×5 cm square field of 502 MeV/c (126 MeV) antiprotons on a water target was simulated. The dose was scored along the central beam axis in circular disks with a diameter of 2 cm in 0.5 mm steps. The beam momentum spread was $\Delta p/p = 5 \times 10^{-4}$ and the divergence was set to 5 mrad, mimicking the parameters of the beam at CERN. The FLUKA

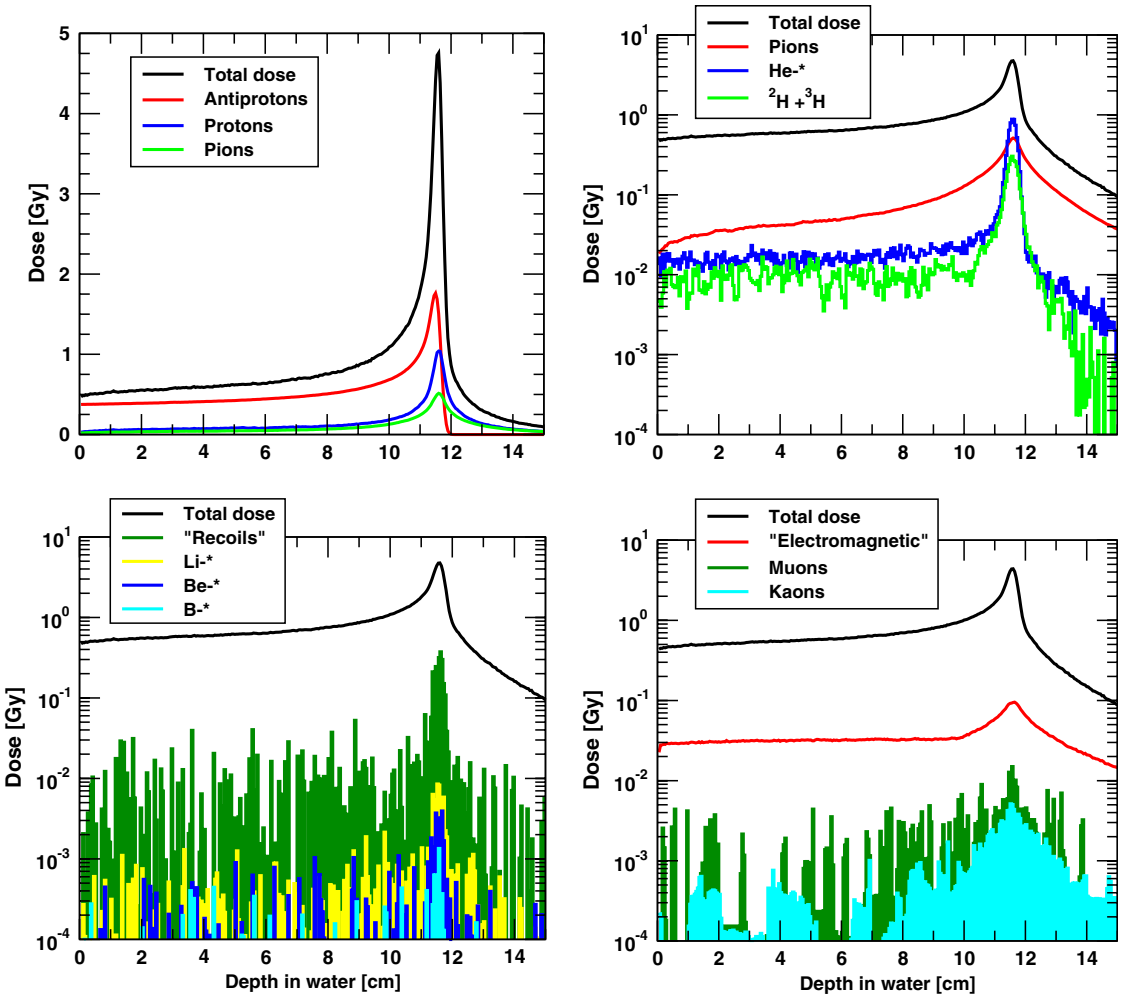

Fig. 1. FLUKA simulation of the depth dose distribution of a square 5×5 cm 126 MeV antiproton field, scaled to 10^{10} antiprotons. The dose was averaged over a central cylindrical region with a diameter of 2 cm in steps of 0.5 mm.

statistics were 500.000 simulated antiprotons, but the dose plotted here is scaled to 10^{10} antiprotons. Neutrons do not contribute directly to dose, as these particles are indirectly ionizing. They generate recoils which are further transported by FLUKA, if the energy is sufficiently high. Dose from electrons and positrons generated by photons is contained in the curve labelled ''Electromagnetic''. The curve labelled ''Recoils'' represents dose contributions from unspecified fragments with low energy (order of keV) which are not transported. They make up roughly 8% of the total dose near the annihilation peak. The asterisk in e.g. ''Li-*'' refers to all isotopes of Lithium (see Fig. 2).

Fig. 1 thus gives an overview of the contributions to the total dose. The primary antiproton beam (which, by the way, is almost identical to the depth dose curve of a primary proton beam) deposits most dose, followed by contributions from secondary protons, pions, EM-transport and helium nuclei. The remaining contributions are significantly less, and have been plotted on a logarithmic *y*-axis, else they were indistinguishable. The secondary particles are mainly created at the end of flight, and then emitted isotropically, which explains the symmetry of the curves at the annihilation vertex. Also, interesting enough, the dose contribution by transported fragments heavier than helium is in the same order as the dose contributions from muons [1] and the rather exotic kaons[2].

Dosimetry of an antiproton beam is not trivial due to the mixed particle spectrum of the secondary particles from antiproton annihilation. Most, if not all, solid state detectors respond non-linear when subjected to high-LET ionizing radiation. Often the response depends on energy and charge of the particle, and usually the behaviour of such detectors requires a detector model that describes the performance in mixed particle radiation fields. Initially, alanine detectors, thermoluminescent devices (TLDs), and radiochromic films were applied in the beam. We found that alanine detectors [20,21] could be used as an absolute dosimeter in the plateau region, and to some extent in the mixed particle environment around the annihilation peak. A model for the response of the alanine detector in various mono-energetic fields was used in conjunction with Monte Carlo simu-

[1] From pion decay.
[2] A few Σ-particles were also encountered during the simulations.

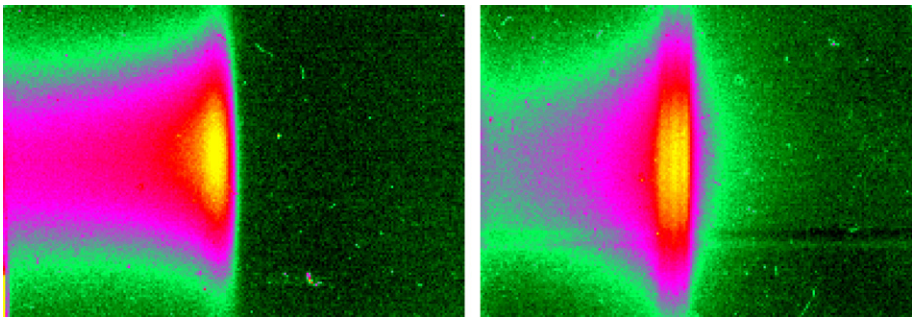

Fig. 2. Measured radiochromic film response for protons (left) and antiprotons (right) at 47 MeV. Both beams were degraded to spread-out the peak.

lations of the particle-energy spectrum in the peak. The response of alanine to the antiproton beam thus calculated was in good agreement with the measured response. This work is subject of a forthcoming publication (submitted for publication).

Apart from alanine detectors, we found that dosimetry with TLDs is not recommendable due to the lack of adequate LET models and standardised handling procedures of the detectors, which compromised the reproducibility of the response in particle fields [22]. Radiochromic films were until now primarily used for determining the width of the beam, as well as the position of the annihilation peak, but not for dosimetry, again due to the lack of models which can translate the response into dose for mixed particle spectra. Still, Fig. 2 shows effectively the key differences between a proton and antiproton beam: here two slanted radiochromic films were exposed to a Gaussian shaped beam of protons and antiprotons, respectively, entering from the left. The beam was spread-out to cover a few mm in the target region. The colour scale is normalized to match both the background and peak dose levels. Clearly, the penumbra due to secondary particles being emitted from the antiproton annihilation can be seen. Secondly, for iso-response in the peak region, the response in the entry region for the antiprotons is significantly less pronounced.

Relative dosimetry was done with a transmission ionization chamber (Advanced Roos Chamber from PTW Freiburg). Absolute dosimetry for the biology experiment using the ionization chamber alone was not possible, since the 40 mm diameter of the Advanced Roos Chamber was much larger than the ~10 mm FWHM[3] of the antiproton beam. Small beam misalignment and changes in FWHM, which seriously impact the dose delivered to the test sample, cannot be detected by the ionization chamber. Instead, the ionization chamber was used for relative dosimetry only. Due to the pulsed structure of the antiproton spills (one 300 ns spill every 90 s), it is necessary to compensate for ionic recombination effects [23,24]. The results of the ionization chamber measurements were compared with the Monte Carlo particle transport programs SHIELD-HIT v. 2.2 by Sobolevsky et al. [25] and FLUKA 2006.3. FLUKA proved to be in excellent agreement with our relative ionization chamber measurements, which is shown in Fig. 3, and therefore FLUKA was chosen to build the input data needed for the treatment planning software TRiP [26,27]. A paper concerning these findings is in preparation (submitted for publication).

[3] The FWHM is selected to be sufficiently large to give a reasonably homogeneous dose across the sample tube (which had a diameter of ~6.5 mm), while still being small enough in order to use as much as possible of the antiproton beam.

Treatment planning

The scarcity of antiprotons (we typically have access to the antiproton beam at CERN for just one week per year) dictates that we concentrate our measurements on producing the necessary database to validate our Monte Carlo codes. Then we use these codes to generate the set of input data needed for a biological treatment planning system to generate a dose plan for a virtual treatment with antiprotons that can be compared with a treatment plan calculated for protons, carbon ions, or other modalities. To date we have used TRiP to model physical dose distributions based on the depth dose base curve for antiprotons generated with FLUKA and compared this to a physical dose distribution for a carbon ion beam.

Fig. 4 is comparing a carbon ion treatment plan (left) with an antiproton plan (right). The plan is only optimized for physical dose at this time. Comparing these plans, one can see that the dose in the entry region is reduced, whereas the lateral penumbra is slightly more pronounced for antiprotons. It is still too early to derive conclusions from this, since the radiobiology optimization is still under development for antiprotons, and the RBE is expected to vary significantly along the depth dose curve for antiprotons. TRiP already uses the Local Effect Model (LEM) [28–30] for optimizing the biological dose for carbon ion beams. To optimize the treatment plan for biological dose for antiprotons, the complete particle-energy spectrum is needed for LEM to model the RBE. We have generated such spectra using FLUKA and are currently implementing these in our calculations. This will enable us to study a variety of clinical situations in order to identify those cases where antiproton therapy may offer improvements over existing particle beam modalities.

Conclusion

So far the arguments for and against antiproton radiotherapy have been mostly quantitatively. Biological experi-

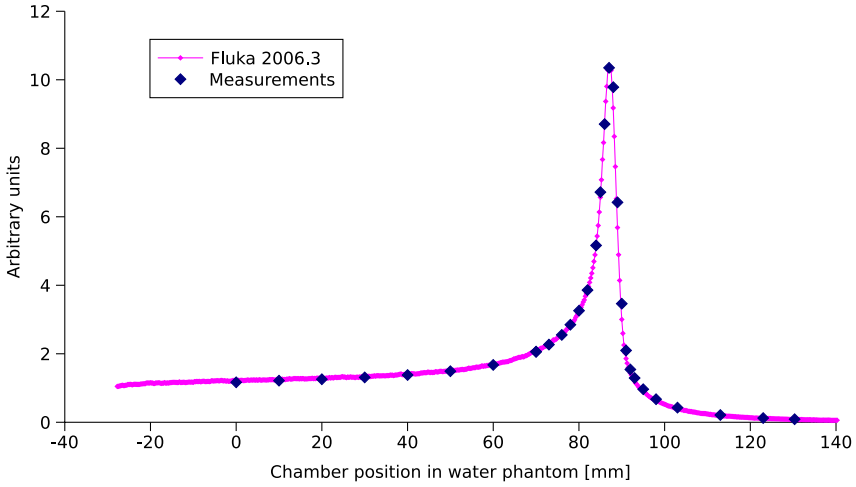

Fig. 3. FLUKA 2006.3 calculated relative dose compared with CERN ionization chamber measurements.

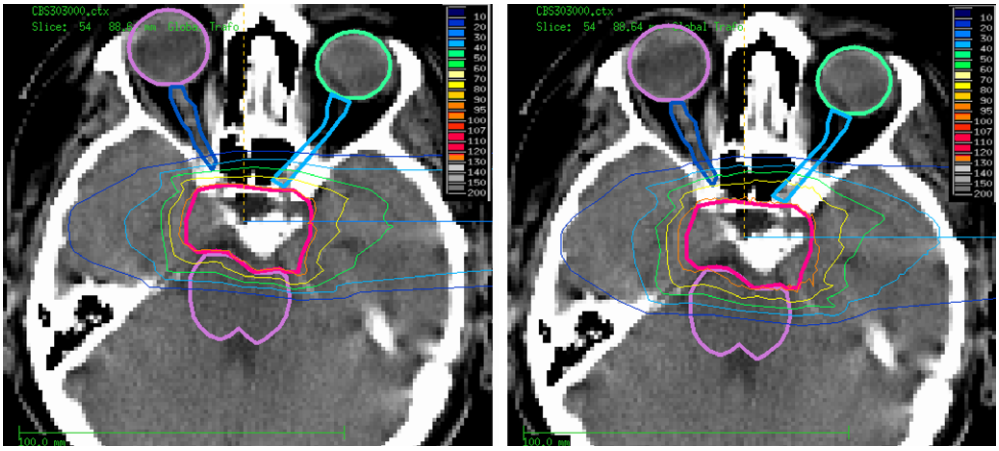

Fig. 4. Physical dose distributions for a single field of carbon ions (left) and antiprotons (right). For antiprotons the entrance dose is noticeably reduced while the lateral penumbra is slightly increased. These calculations do not include any biological effects.

ments performed by the AD-4/ACE collaboration at CERN have shown an enhanced biological effect of 4 in the peak region for antiprotons compared with protons for the same entrance dose. Careful antiproton dosimetry experiments and tests of various Monte Carlo codes have resulted in reliable computer simulations of clinical antiproton beam dose distributions. Combined with the data from the cell survival experiments the RBE can be calculated in future experiments and can then be implemented in biological treatment planning systems.

The expected possible advantage of antiproton therapy over other advanced modalities like combined IMRT/IMPT (protons)/IMPT (carbon ions) is still to be examined in treatment planning studies. One advantage of antiprotons is low-LET in the plateau (and thereby low alpha/beta ratio for late responding normal tissue) combined with high-LET, high RBE and low OER in the peak region for small targets. This suggests that antiproton therapy could be superior for small radioresistant targets surrounded by highly radiosensitive critical normal tissue. This could obviously be re-treatment of local failures in previously irradiated organs and tumours like chordomas or chondrosarcomas located between the optical pathways and close to the optic chiasm. Other anticipated uses are boost to hypoxic areas where IMRT and IMPT (protons and carbon) probably could not give the same BED conformity as fractionated antiproton therapy; this is again especially relevant in tumours surrounded by critical normal structures like hypoxic components in paranasal squamous cell carcinoma.

Acknowledgements

The Danish Cancer Society and the ICE Center under the Danish Natural Science Research Council partially supported this project with a grant. We very much appreciate the diligent efforts by the AD operations team to deliver the antiproton beam at CERN and to develop the new extraction scheme to provide the 126 MeV beam energy.

* **Corresponding author. Niels Bassler**, Deutsches Krebsforschungszentrum, E0409, Im Neuenheimer Feld 280, 69120 Heidelberg, Germany. *E-mail address:* n.bassler@dkfz.de

Received 24 September 2007; received in revised form 13 November 2007; accepted 28 November 2007; Available online 26 December 2007

References

[1] Gray L, Kalogeropoulos TE. Possible biomedical applications of antiproton beams: focused radiation transfer. Radiat Res 1984:246–52.

[2] Sullivan AH. A measurement of the local energy deposition by antiprotons coming to rest in tissue-like material. Phys Med Biol 1985;30:1297–303.

[3] Goitein Michael, Goitein Gudrun. Swedish protons. Acta Oncologica 2005;44:793–7.

[4] Olsen Dag Rune, Bruland Øjvind S, Frykholm Gunilla, Norderhaug Inger Natvig. Proton therapy – A systematic review of clinical effectiveness. Radiother Oncol 2007;83:123–32.

[5] Jäkel O, Schulz-Ertner D, Karger CP, Nikoghosyan A, Debus J. Heavy ion therapy: status and perspectives. Technol Cancer Res Treat 2003;2:377–87.

[6] Schulz-Ertner Daniela, Jäkel Oliver, Schlegel Wolfgang. Radiation therapy with charged particles. Semin Radiat Oncol 2006;16:249–59.

[7] Schulz-Ertner Daniela, Tsujii Hirohiko. Particle radiation therapy using proton and heavier ion beams. J Clin Oncol 2007;25:953–64.

[8] Budach V. The role of fast neutrons in radiooncology – A critical appraisal. Strahlenther Onkol 1991;167:677–92.

[9] Wisser L. Pion treatment of prostate carcinoma at Paul Scherrer Institute (formerly Swiss Institute for Nuclear Research (SIN)) from 1983 to 1992. Cancer Radiothérapie 2004;8:88–94.

[10] Bassler N, Holzscheiter M, Knudsen H, The AD4/ACE Collaboration. Cancer therapy with antiprotons. In: Dieter Grzonka, Rafał Czyżykiewicz, Walter Oelert, Thomasz Rożek, Peter Winter, editors. Low Energy Antiproton Physics-LEAP '05, vol. CP796 of AIP Conference Proceedings. American Institute of Physics, 2005; pp. 423–430.

[11] Ponomarev LI. Molecular structure effects on atomic and nuclera capture of mesons. Annu Rev Nucl Sci 1973:395–430.

[12] Agnew Jr Lewis E, Elioff Tom, Fowler William B, Lander Richard L, Powell Wilson M, Segrè Emilio, et al. Antiproton interactions in hydrogen and carbon below 200 MeV. Phys Rev 1960:1371–91.

[13] Inokuti M. Interactions of antiprotons with atoms and molecules. Nucl Tracks Radiat Meas 1989;16:115–23.

[14] Cugnon J, Wycech S, Jastrzębski J, Lubiński P. Geometrical effects in antiproton annihilation on nuclei. Phys Rev C 2001;63:027301.

[15] Markiel W, Daniel H, von Egidy T, Hartmann FJ, Hofmann P, Kanert W, et al. Emission of helium ions after antiproton annihiliation in nuclei. Nuclear Physics A 1988;485: 445–60.

[16] Polster D, Hilscher D, Rossner H, von Egidy T, Harmann FJ, Hoffmann J, et al. Light particle emission induced by stopped antiprotons in nuclei: energy dissipation and neutron-to-proton ratio. Phys Rev C 1995;51:1167–80.

[17] Holzscheiter Michael H, Bassler Niels, Agazaryan Nzhde, Beyer Gerd, Blackmore Ewart, DeMarco John J, et al. The biological effectiveness of antiproton irradiation. Radiother Oncol 2006;81:233–42.

[18] Fassò A, Ferrari A, Ranft J, Sala PR. FLUKA: a multi-particle transport code. CERN-2005-10, INFN/TC_05/11, SLAC-R-773.

[19] The physics models of FLUKA: status and recent developments, La Jolla, CA, USA, 2003. (paper MOMT005), eConf C0303241 (2003), arXiv:hep-ph/0306267.

[20] Hansen JW, Olsen KJ, Wille M. The alanine radiation detector for high and low LET dosimetry. Radiat Prot Dosimetry 1987;19:43–7.

[21] Palmans H. Effect of alanine energy response and phantom material on depth dose measurements in ocular protons beams. Technol Cancer Res Treat 2003;2:579–86.

[22] Niels Bassler. Experimental studies relevant for antiproton cancer therapy. Ph.D. thesis, Aarhus University, 2006.

[23] Boag JW, Currant J. Current collection and ionic recombination in small cylindrical ionization chambers exposed to pulsed radiation. Brit J Radiol 1980;53:471–8.

[24] Kanai Tatsuaki, Sudo Michio, Matsufujii Naruhiro, Futami Yasuyuki. Initial recombination in a parallel-plate ionization chamber exposed to heavy ions. Phys Med Biol 1998;43:3549–58.

[25] Gudowska Irena, Sobolevsky Nikolai, Andreo Pedro, Belkič Dževad, Brahme Anders. Ion beam transport in tissue-like media using the monte carlo code SHIELD-HIT. Phys Med Biol 2004;49:1933–58.

[26] Krämer M, Jäkel O, Haberer T, Kraft G, Schardt D, Weber U. Treatment planning for heavy-ion radiotherapy physical beam model and dose optimization. Phys Med Biol 2000;45:3299–317.

[27] Krämer M, Scholz M. Treatment planning for heavy-ion radiotherapy calculation and optimization of biologically effective dose. Phys Med Biol 2000;45:3319–30.

[28] Scholz M. Grundlagen der biologischen Bestrahlungsplanung fur die Schwerionen-Tumortherapie. Medizinische Fakultat Heidelberg, Ruprecht-Karls-Universität. Habilitationsschrift. (In German).

[29] Scholz M, Kraft G. Track structure and the calculation of biological effects of heavy charged particles. Adv Space Res 1995;18:5–14.

[30] Scholz M, Kellerer AM, Kraft-Weyrather W. Computation of cell survival in heavy ion beams for therapy. Radiat Environ Biophys 1997;36:59–66.

Appendix C

IOP PUBLISHING PHYSICS IN MEDICINE AND BIOLOGY

Phys. Med. Biol. **53** (2008) 793–805 doi:10.1088/0031-9155/53/3/017

The antiproton depth–dose curve in water

N Bassler[1,2], M H Holzscheiter[3], O Jäkel[2], H V Knudsen[4], S Kovacevic[5] and (the AD-4/ACE Collaboration)[6]

[1] Department of Experimental Clinical Oncology, Aarhus University Hospital, Aarhus, Denmark
[2] Deutsches Krebsforschungszentrum, Heidelberg, Germany
[3] University of New Mexico, Albuquerque, NM, USA
[4] Department of Physics and Astronomy, University of Aarhus, Aarhus, Denmark
[5] University of Montenegro, Podgorica, Montenegro

E-mail: n.bassler@dkfz.de

Received 19 September 2007, in final form 2 December 2007
Published 14 January 2008
Online at stacks.iop.org/PMB/53/793

Abstract

We have measured the depth–dose curve of 126 MeV antiprotons in a water phantom using ionization chambers. Since the antiproton beam provided by CERN has a pulsed structure and possibly carries a high-LET component from the antiproton annihilation, it is necessary to correct the acquired charge for ion recombination effects. The results are compared with Monte Carlo calculations and were found to be in good agreement. Based on this agreement we calculate the antiproton depth–dose curve for antiprotons and compare it with that for protons and find a doubling of the physical dose in the peak region for antiprotons.

(Some figures in this article are in colour only in the electronic version)

1. Introduction

The basic idea of antiproton radiotherapy (Gray and Kalogeropoulos 1984) is to utilize the energy from the antiproton–nucleus annihilation reactions, which occur when the antiprotons come to rest. Antiprotons behave similar to protons at high velocities, but when they slow

[6] M H Holzscheiter 1, N Bassler 2, 3, J Alsner 2, G Beyer 4, J J DeMarco 5, M Doser 6, D Hajdukovic 7, O Hartley 4, K S Iwamoto 5, O Jäkel 3, H V Knudsen 8, S Kovacevic 7, S Pape Møller 9, J Overgaard 2, J B Petersen 2, T D Solberg 10, S Vranjes 11, B G Wouters 12.
1. University of New Mexico, Albuquerque, NM, USA; 2. Department of Medical Physics and Experimental Clinical Oncology, Aarhus University Hospital, Aarhus, Denmark; 3. Deutsches Krebsforschungszentrum, Heidelberg, Germany; 4. Hospital Universitaire de Geneve, Geneva, Switzerland; 5. David Geffen School of Medicine, UCLA, Los Angeles, CA, USA; 6. CERN, Geneva, Switzerland; 7. University of Montenegro, Podgorica, Montenegro; 8. Department of Physics & Astronomy, University of Aarhus, Aarhus, Denmark; 9. ISA, University of Aarhus, Aarhus, Denmark; 10. University of Nebraska Medical Center, Omaha, NE, USA; 11. VINCA Institute for Nuclear Sciences, Belgrade, Serbia; 12. University of Maastricht, Res. Institute Growth and Development, The Netherlands.

down in the target material, they are captured by a nucleus and annihilate on its surface. Hereby twice the rest mass of the proton m_p is released (1.88 GeV) at the end of the particle trajectory. The probability for photo-emission similar to that known from the positron–electron annihilation is rather small. Instead, on average 4–5 π-mesons are created (Inokuti 1989). The photons observed from the antiproton annihilation arise primarily from π^0 decay, which has a lifetime in the order of 10^{-16} s. The energy of these photons is between 70 and 300 MeV (Agnew *et al* 1960). For antiproton–nuclei reactions, there is a high probability that one or more π-mesons will strike the nucleus[7]. Those entering the nucleus will start an intra-nuclear cascade, knocking out light nuclei (Markiel *et al* 1988). When antiprotons enter a chemical compound consisting of several materials, the majority of the annihilations will take place on high-Z materials (Ponomarev 1973). For example, in the case of polystyrene only 1% of the antiprotons will annihilate on hydrogen with the remaining 99% annihilating on carbon. Antiprotons annihilating on tissue-like material are expected to produce a particle spectrum featuring pions, neutrons, protons, deuterons, heavier nuclei and photons. A few kaons may also be created (Agnew *et al* 1960, Polster *et al* 1995). Most of the 1.88 GeV released is carried away from the annihilation vertex by the long-ranging particles (high-energy pions, protons, neutrons, and photons), but roughly 30 MeV is deposited locally near the annihilation vertex (Sullivan 1985). Even though this sounds at first sight disappointingly low (Sullivan 1985, Inokuti 1989), it represents a doubling of the peak dose at the end of the antiproton particle track, compared to protons, producing a significant clinical advantage. The loss of the primary beam due to in-flight nuclear reactions is expected to be slightly more than for protons, but still less than that of carbon ions (Bassler *et al* 2005). The antiproton depth–dose curve will therefore look similar to the depth–dose curve of protons, but with additional energy deposited in the Bragg peak from the antiproton annihilation.

Since 2002 the AD-4/ACE Collaboration has been working at CERN, using the antiproton decelerator (AD), on assessing the dosimetric and radiobiological properties of beams of antiprotons in order to estimate the suitability of antiprotons for radiotherapy (Holzscheiter *et al* 2004, 2006, Maggiore *et al* 2004, Bassler *et al* 2006, Bassler 2006). The AD has been designed and constructed for fundamental research on matter–antimatter symmetries and the availability of antiprotons for applied studies is sparse at best. Typically, we are able to obtain one week of beam time each year and have therefore concentrated on collecting few but critical data to benchmark computer models that can then be used to develop treatment planning tools. These in turn will allow us to gain a deeper insight in the potential advantages of antiprotons compared to other modalities and in selecting the most appropriate candidates of tumour indications for antiproton therapy.

Radiotherapy with antiprotons has a potential to deliver a high biological effective dose to the target while at the same time reducing the dose to normal tissue in the entrance region much more than possible with any other radiation modality. It is one of the paradigms of radiotherapy that a decrease of the irradiated volume of normal tissue is in many cases associated with an increased tolerance dose of these tissues (see, e.g., Hopewell and Trott (2000)). There are at least two situations in which antiprotons might be useful for radiotherapy. The first are tumours that cannot be controlled by conventional radiation, because the applied dose is limited by the surrounding normal tissues and where a substantial dose escalation may be beneficial, like e.g. tumours at the base of skull or paraspinal tumours. Another indication may be recurrent tumours. If the initial treatment included any kind of radiotherapy, the normal tissue surrounding the tumour will have already received a significant dose. In order to re-irradiate

[7] For nuclei with $60 \leqslant A \leqslant 200$ the probability is 85–90% according to Cugnon *et al* (2001).

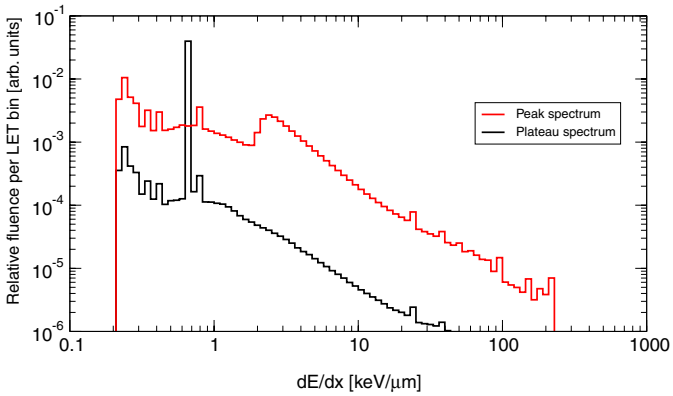

Figure 1. FLUKA calculation of charged particle LET spectrum of a 126 MeV antiproton beam. The spectrum was calculated both in the peak region and in the plateau region. Charged particles with $1 \leqslant Z \leqslant 6$ were here taken into account. The sharp line in the plateau region at 0.6 keV μm^{-1} originates from the primary antiproton beam.

this tumour one needs to assure that the dose to normal tissue does not exceed accepted tolerance level. This is facilitated by the high peak-to-plateau ratio offered by antiprotons.

Unlike protons, the relative biological effectiveness (RBE) of the antiproton beam varies sharply with depth near the end of range, as the annihilation process yields fragments with a higher linear energy transfer (LET). A calculated LET spectrum is shown in figure 1.

This enhanced LET results in an increased RBE in the peak region relative to the plateau region. The biological effect of an antiproton beam was for the first time measured by Holzscheiter *et al* (2006). However the RBE in the peak could not be measured, since the dosimetry in this region was complicated by both the mixed particle spectrum and the pulsed form of the antiproton beam. Dosimetry with alanine, thermoluminescent devices and radiochromic films were used, but these suffer from a strong, often not well understood, LET dependence of the response. Calorimetric measurements were considered as too cumbersome. Ionization chamber measurements were initially believed to be complicated due to the pulsed structure of the antiproton beam currently available at CERN.

In this paper, we report the first measurement of the dose deposited in water by a pulsed antiproton beam using ionization chambers. The high instantaneous dose rate causes a reduction in the charge collection efficiency due to general recombination effects. Using the 'Boag's two voltage method' as described by Boag and Currant (1980) we can get an estimate of the charge collection efficiency. It should be stressed that our goal is not to perform high precision dosimetry, as there are several sources of errors in the 1% range that may perturb the results which we cannot yet control. Our primary goal is instead to obtain an initial estimate of the RBE for antiprotons that will allow us to define any significant advantages of antiproton radiotherapy over other modalities. For this, uncertainties in dose of a few per cent may be tolerated.

2. Experimental methods

The antiproton decelerator (AD) at CERN is set up to provide a 502 MeV/c ($\sim$126 MeV) antiproton beam. Every 90 s a spill of roughly 2–3 $\times$ 10^7 antiprotons is ejected within 300 ns. The average number of ejected antiprotons may change depending on the actual state of the

accelerator facility. Using, e.g., arbitrarily selected 20 consecutive spills (corresponding to about 30 min of operation), the average number of antiprotons per spill was 2.5×10^7 with a standard deviation of 0.1×10^7. The number of antiprotons for each spill was recorded for each individual spill using a sensitive current transformer in the extraction beam line from the AD to our target station. While the statistical fluctuations of these measurements are low, particle loss between the transformer and our target may introduce a systematic shift ($\lesssim$10%). The momentum spread of the beam was $\Delta p/p = 5 \times 10^{-4}$, and the divergence is in the order of 5 mrad. The FWHM of the beam was slightly ellipsoid, being about 1 cm in one axis and 0.9 cm along the other axis. The beam exits the accelerator vacuum via a thin titanium window, traverses several beam monitors (scintillator viewed by CCD camera, radiochromic film) and is collimated to 1 cm diameter before entering our target. The temperature in the AD hall is maintained at 20 °C.

The target phantom is a 220 mm × 275 mm × 180 mm water tank built of PMMA material according to IAEA and ICRU standards for proton therapy (IAEA 2000, ICRU 1998). The PMMA walls are all 10 mm thick, except for the entrance window, which is 3 mm thick and had a diameter of 70 mm. We use two custom-made plane-parallel ionization chambers of the advanced Roos type from PTW Freiburg with graphite electrodes[8]. These are similar to the standard Roos chamber M34001, but with an increased diameter of 39.6 mm and a collecting volume of 2.479 cm^3. The electrode spacing is 2.013 mm. The ionization chambers are cross calibrated in absorbed dose to water using ^{60}Co γ-rays as reference radiation quality at + 400 V towards a reference ionization chamber using the in-house gammatron at the German Cancer Research Center (DKFZ) in Heidelberg (Kartal 2007). The calibration is carried out with a 10 cm × 10 cm field in a water phantom at 20 °C temperature and air pressure of 1013 hPa. The source–chamber distance was 80 cm and the measurement depth in water was 5 g cm^{-2} for the effective point. The reference chamber is a PTW Roos ionization chamber M34001-0045 and is calibrated at PTW, which is a Secondary Standard Dosimeter Laboratory (SSDL). The N_{Q_0} is found to be 1.32×10^7 Gy C^{-1} for both ionization chambers with an uncertainty of ±4%.

The measurement in the antiproton beam was performed using a pencil beam which had a diameter that was much smaller than the active area of the chamber. The dose obtained under such conditions is an integral dose over the area of the chamber at the specific depth rather than a central axis depth dose which is measured in a broad beam. Measuring such an integral dose is common for facilities using, e.g., a scanned pencil beam, like at the Paul-Scherrer institute or at GSI for carbon ions.

At the antiproton beam line at CERN, one ionization chamber is attached in front of the entrance window to the water phantom. This chamber is used for normalization of the pulse to pulse fluctuations of the antiproton beam. The second chamber is attached to a calliper which provides submillimetre precision readings of the ionization chamber position. The collected charge is read out with a UNIDOS electrometer from PTW Freiburg.

At each calliper position, data from each of several spills of antiprotons are recorded. Typically, we see around 175 pC per spill in the entry chamber and 0.2–1.4 nC in the second ionization chamber depending on the position in the water phantom. The fixed ionization chamber at the entrance window is kept at +400 V at all times. With the ionization chamber mounted in the water phantom we usually record 4–8 spills at +400 V and 4 spills at +300 V. The electrometer is read out and reset after each spill. The dark current contribution was insignificant.

[8] TM34073-1, 08-0001 and -0002.

From the measured charge q_1 and q_2 recorded at $V_1 = 400$ V and $V_2 = 300$ V, respectively, it is possible to apply Boag's theorem Boag and Currant (1980). This is done by solving

$$0 = \frac{q_1}{q_2} \cdot \frac{V_2}{V_1} - \frac{\ln(1+u_1)}{\ln(1+u_1 V_1/V_2)}. \tag{1}$$

Equation (1) is derived from equation (9) in (Boag and Currant 1980). u is related to the collection efficiency f in such a way that

$$f = \frac{1}{u}\ln(1+u). \tag{2}$$

In practice, a plug-in was written[9] for the 'Gnumeric' spreadsheet program[10], which extended the software with additional functions for calculating u and f. As an input parameter the measured charges at two voltages are needed. The functionality of the algorithms was checked by comparing the results with another independently developed program using the root-finding function provided by the Gnu Scientific Library (Galassi *et al* 2007).

Alternatively, Boag *et al* also suggest three different algorithms in Boag *et al* (1996) which enhance equation (2) with a free-electron collection effect on the recombination correction. These three algorithms are also supported in the plug-in mentioned before. In these algorithms, the free-electron fraction p is needed as an additional parameter. In this paper, f' will be the free-electron-corrected charge collection efficiency based upon equation 7 in Boag *et al* (1996):

$$f'(u) = f(u) \cdot \frac{e^{pu} - 1}{pu}. \tag{3}$$

At some calliper positions, we only measure charge at one voltage setting (400 V). Here, the charge collection efficiency is interpolated from neighbouring positions. Beyond the annihilation peak the acquired charge is small and equation (1) has no solution due to statistical fluctuations, and instead the collection efficiency is extrapolated. Similarly for the ionization chamber at the fixed entry position, the charge collection efficiency is merely estimated by extrapolation.

Linearity checks validating Boag's two voltage method are made at two calliper positions, covering the peak and the plateau region. Here the entire voltage range from the UNIDOS electrometer is applied in 50 V steps, and the q^{-1} versus V^{-1} plots are investigated for linearity.

The Boag-corrected collected charge $M_{Q,B}$ of the antiproton beam quality Q can be found by

$$M_{Q,B} = q/f. \tag{4}$$

The absolute dose D_Q is then

$$D_Q = M_{Q,B} N_{Q_0} k_{Q,Q_0} \tag{5}$$

where N_{Q_0} is the ^{60}Co calibration factor, as mentioned earlier. k_{Q,Q_0} is a beam quality correction factor, which here is set to unity. The k_{Q,Q_0} factor for the advanced Roos chamber should be nearly identical to the corresponding factor for the standard Roos chamber, the only possible difference being the chamber specific correction factors p_Q appearing in the calculation of k_{Q,Q_0} (according to equation (3.4) of IAEA (2000)). This p_Q factor is, however, taken to be unity for all chambers in a proton beam in IAEA (2000) and for photons the only effect of an increased diameter could influence the perturbation effect of the wall, p_{wall}, which is given as 1.001 for the Roos chamber. Given the large guard ring of the Roos chamber this factor should be dominated by the entrance and exit window of the chamber. Any expected

[9] The plug-in is available at http://www.phys.au.dk/~bassler/work.shtml?Boag.
[10] http://www.gnome.org/projects/gnumeric/.

difference for our chamber should not exceed the 1% level, an accuracy that is clearly beyond the level of accuracy we are aiming for in our experiment. A difference in k_{Q,Q_0} for protons and antiprotons may arise due to the different spectra of secondary particles. Even for carbon ions, where secondary particles may play a similarly important role as for antiprotons, k_{Q,Q_0} is still assumed to be of the same range as for protons, namely 1.003. Taking k_{Q,Q_0} as unity for antiprotons is thus not expected to introduce an uncertainty of more than 1–2%.

The relative measurements plotted in figures 5 and 6 are the ratio between the Boag-corrected charge measured in the ionization chamber mounted on the calliper $M_{Q,B,\mathrm{var}}(d)$ at a given depth d and the charge measured in the entry ionization chamber $M_{Q,B,\mathrm{entry}}$ corresponding to a water-equivalent (WE) depth of $d = 0$ cm:

$$\frac{M_{Q,B,\mathrm{var}}(d)}{M_{Q,B,\mathrm{entry}}} = \frac{q_{\mathrm{var}}(d)}{q_{\mathrm{entry}}} \cdot \frac{f_{\mathrm{entry}}}{f_{\mathrm{var}}(d)}. \tag{6}$$

As mentioned earlier, the average ratio was acquired from multiple spills. The absolute measurements presented in the third column in table 1 is the dose per antiproton, calculated using equation (5) and the number of antiprotons derived from the beam current monitor. The dose per antiproton presented here is averaged over multiple spills as well, and the standard deviation of the measurement is mentioned in the table as well.

3. Monte Carlo calculations

For comparison, calculations using both FLUKA v. 2006.3 (Fassò *et al* 2005, eConf C0303241:MOMT005 2003) and SHIELD-HIT v2.2 (Gudowska *et al* 2004) are applied. The geometry applied in FLUKA and SHIELD-HIT consists simply of a 502 MeV/c antiproton beam hitting a 20 × 20 × 20 cm^3 water tank. The Gaussian-shaped beam width was set to have a FWHM of 1.0 cm and 0.9 cm along the x- and y-axes. For statistical precision we used 150 000 and 100 000 primary particles, respectively, in the calculations using FLUKA and SHIELD-HIT.

The scoring region is a stack of discs placed along the beam axis. Each disc has a diameter of 39.6 mm matching the effective diameter of the ionization chamber. Since the FWHM of the beam width is only in the order of 1 cm, practically all antiprotons are contained in the active scoring region, even in the Bragg peak. This is illustrated in figure 2 which shows the lateral dose profile for the simulated beam in the plateau and the peak regions. The active scoring region also includes most low energy fragments generated in the annihilation events.

The resolution along the beam axis was in 1 mm steps for the SHIELD-HIT simulation and 0.25 mm for the FLUKA simulation. For all FLUKA calculations a beam momentum spread of $\Delta p/p = 5 \times 10^{-4}$ was used as well as a beam divergence of 5 mrad, corresponding to the characteristics of the CERN beam. In FLUKA, the default transport settings and cut-off energies from the 'HADROTHE' card are always used.

For comparison with protons (shown later in figure 7), the FLUKA calculation was repeated using a 5 cm × 5 cm square field of antiprotons, while maintaining beam energy, momentum spread and divergence. The target was a 20 × 20 × 100 cm^3 water tank placed along the beam axis. The average dose is again scored along the beam axis using flat discs, but with a radius of 0.5 cm and a thickness of 0.25 mm. Here, 400 000 particles are simulated.

Finally, the LET spectrum shown in figure 1 was obtained using 400 000 particles in a water phantom. Again, the primary beam was a 5 cm × 5 cm square field of antiprotons with unchanged beam energy, momentum spread and divergence. The track-length fluence was scored for pions and kaons (π^+, π^-, π^0, K^+, K^-, K^0), for protons and antiprotons, as well as all other nuclei with $1 \leqslant Z \leqslant 6$. The scoring region was one 2 × 2 × 1 cm^3 box placed at

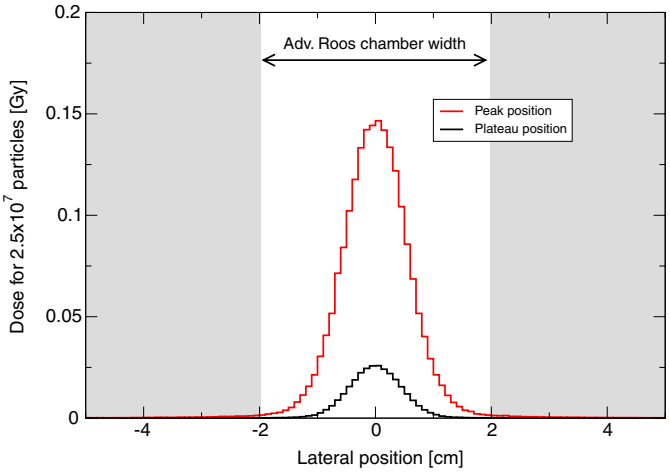

Figure 2. FLUKA calculation of the lateral dose distribution at 1.1 cm WE depth and 11.6 cm depth for the CERN beam. The entire beam is confined within the diameter of the ionization chamber.

the entrance to the water phantom in the centre of the beam with the short sides parallel to the beam axis. A similar scoring volume is also positioned around the centre of the annihilation peak at a depth of 11–12 cm.

Initial attempts to use Geant4 (Allison *et al* 2006, Agostinelli *et al* 2003) failed, as at that time the behaviour of very low energy antiprotons had not yet been fully incorporated. Meanwhile much progress in this area has been made (Kossov 2005) and future studies may include Geant4 simulations.

4. Results

The $1/q$ versus $1/V$ plot in the plateau and at the peak of the depth–dose curve is shown in figure 3. The data were normalized to $1/q$ acquired at 400 V. The choice of 400 and 300 V for the ionization chamber may not be ideal, as it is often suggested that $V_1 > 2V_2$. However, these voltage setting are within the region of linearity for the entire depth–dose curve, thereby maintaining a consistent read-out procedure.

The calculated charge collection efficiency, f, which was applied to the measured charge, is shown in figure 4 as a function of WE depth. Using the charge collection efficiency data, we can compare the measured depth–dose curve in water with SHIELD-HIT and FLUKA simulations, which is shown in figures 5 and 6, respectively. Since the measurements were recorded with an arbitrary x-scale, the measurements were shifted along the x-axis in order to match the peak of the Monte Carlo calculations. Both the Monte Carlo calculations and the measurements are normalized to unity at 88 mm WE depth in order to better show the deviations in the form of the depth–dose curve. Using this normalization, the SHIELD-HIT calculations show an overestimation of more than 20% in the peak region, whereas FLUKA matches the measured depth–dose curve very well ($\lesssim$1%). In the plateau region at 38.5 mm WE depth SHIELD-HIT underestimates the relative dose with 16%. FLUKA overestimates the dose here with less than 2%.

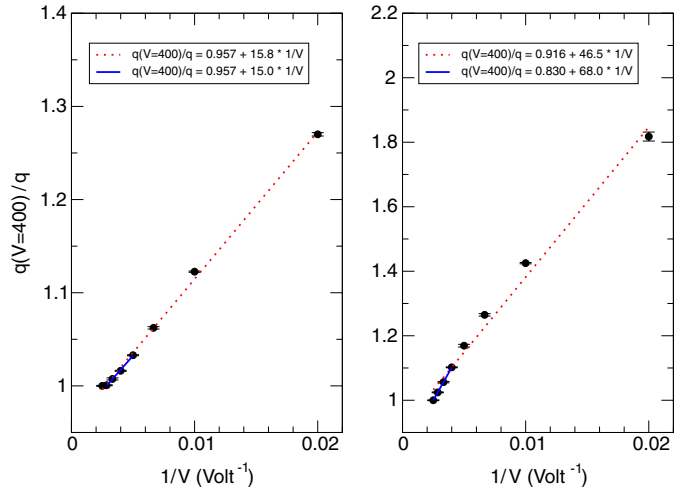

Figure 3. $1/q$ versus $1/V$ plots. Left figure shows data acquired in the plateau region, the right figure is acquired in the peak region. Results are normalized at $1/q$ $(V = 400)$.

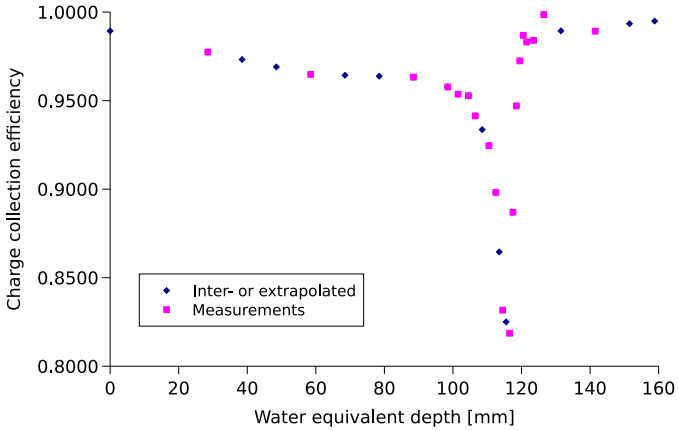

Figure 4. Calculated charge collection efficiency.

In terms of absolute values, our measurements indicate higher doses than calculated with SHIELD-HIT or FLUKA. With the entry ionization chamber we measure on average 101 $\pm$ 4 pico Gy (pGy) deposited dose per antiproton. As an estimate, we extrapolate the charge collection efficiency from the first data points of the second ionization chamber. At the second ionization chamber we see 116 $\pm$ 2 pGy of deposited dose per antiproton in a WE depth of 28 mm and 166 $\pm$ 3 pGy at a WE depth of 88 mm. In table 1, we compare these values to those calculated by SHIELD-HIT and FLUKA. The errors stated here are 1σ standard deviations.

The free-electron effect was calculated at a point in the plateau (at 28 mm WE depth) and the peak region (at 116 mm WE depth) assuming $p = 0.1$. The results are presented in table 2.

All data and data analysis are made available on the world wide web (Bassler *et al* 2007).

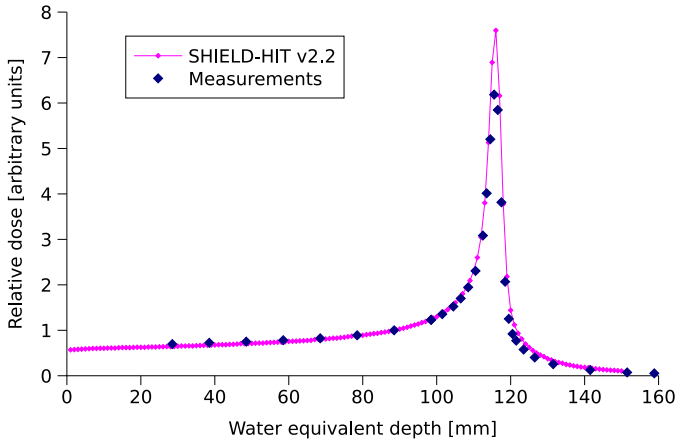

Figure 5. 126 MeV antiprotons hitting a water target. SHIELD-HIT v.2.2 Monte Carlo calculations compared with ionization chamber measurements.

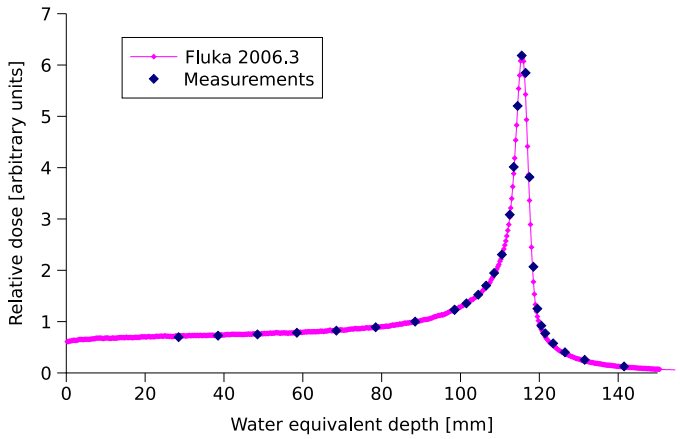

Figure 6. 126 MeV antiprotons hitting a water target. FLUKA 2006.3 Monte Carlo calculations compared with ionization chamber measurements.

Table 1. Absolute comparison of deposited dose per antiproton.

	SHIELD-HIT (pGy)	FLUKA (pGy)	Measurements (pGy)
Entry chamber at 0 mm	86.7	96.7	101 ± 4
Chamber at 27.5 mm	94.5	109	116 ± 2
Chamber at 87.5 mm	147	152	166 ± 3

5. Discussion

We found excellent agreement between ionization chamber measurements and FLUKA simulations for relative dose and reasonable agreement in the plateau regions for absolute dose (error $<$ 4–9%). The origin of the systematic deviation between experiment and models is not clear, but may possibly be attributed to several sources: first, the advanced Roos chamber

Table 2. Collection efficiency without (f) and with (f') free-electron correction; $p = 0.1$.

	u	f	f'
Chamber at plateau (27.5 mm)	0.0466	0.9774	0.9797
Chamber at peak (115.5 mm)	0.4736	0.8186	0.8383

was cross calibrated towards another ionization chamber which has an uncertainty of ±4% (Kartal 2007). Second, the calibration of the antiproton beam current monitor (which provides the amount of antiprotons) is accurate to only ±1% and may additionally have a systematic deviation of up to 10%. The difference in results from SHIELD-HIT and FLUKA is most likely related to different in-flight annihilation cross sections used by the two code packages. The in-flight annihilation cross sections of antiprotons and in-flight losses of other ions are discussed in more detail in Bassler *et al* (2005).

From the presented data it is difficult to decide which of the two code packages gives a more accurate value for the absolute antiproton dose. But based on the better agreement of the relative dose versus depth and on the fact that FLUKA simulations of protons were benchmarked by Biaggi *et al* (1999) and found in very good agreement with measurements, we tend to favour the FLUKA code package.

Finally, there is an uncertainty coming from the application of Boag's theory to the antiproton beam. The correction used is strictly valid only if the linearity of the $1/q$ versus $1/V$ plot is maintained. In figure 3, the plateau position plot reveals a deviation from linearity at a chamber voltage of 400 V. But when using points from 350 V and below, this only changed the charge collection efficiency by roughly 1.5%. The data in figures 5 and 6 are exclusively based on charge collected at 400 V and 300 V.

For pulsed beams both initial and general recombination show a linear $1/q$ versus $1/V$ dependence (Palmans *et al* 2006). In principle, it is possible to distinguish the contributions from both recombination effects. By varying the pulse length, only the general recombination is affected, as initial recombination is independent of the incident dose rate (Park *et al* 2006). Since it is not possible to significantly change the pulse length at the CERN beam line, one could instead change the angle of the ionization chamber relative to the beam axis. This was done by Kanai *et al* (1998) for a heavy ion beam, which also investigated the LET dependence of initial recombination. It could be interesting to apply similar methods to the antiproton beam in a future experiment and perhaps derive an estimate of the mean LET of the particle spectrum.

The result from Boag's free-electron-correction term in table 2 indicates only small changes to the result. The change of the charge collection efficiency when applying f' instead of f is less than 1% in the plateau region and 2% in the peak region. The other two models in Boag *et al* (1996) gave similar results within $\sim 1\%$. The estimate of $p = 0.1$ was derived from figure 3 in that reference. Here, p is plotted as a function of V for a plane-parallel ionization chamber with an electrode distance of 6.1 mm. Assuming equal field strength in the ionization chamber we read out p for a corresponding electrode distance of 2 mm. As a test, we tried to minimize the sum-of-squares deviation between measurement and FLUKA calculation and use p as a free parameter. A best fit was then achieved at $p = 0.062$, but this is regarded as being highly speculative.

At last, one may discuss whether the Bragg–Gray conditions are fulfilled for an antiproton beam. Antiprotons annihilating on the air in the ionization chamber may lead to the generation of new particles, leading to a violation of the charged particle equilibrium requirement.

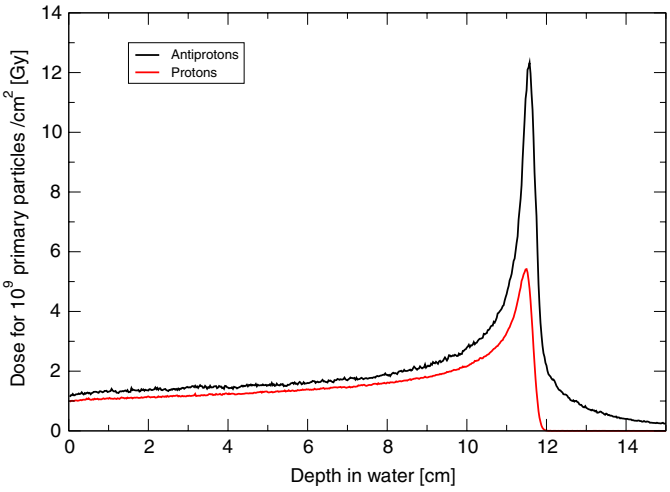

Figure 7. Comparison of the central axis depth–dose curves in water from a pristine antiproton beam with a similar proton beam. The depth–dose curves were calculated with FLUKA. The energy of the antiprotons was 126 MeV, and the field size was 5 cm × 5 cm. The momentum spread was assumed to be $\Delta p/p = 5 \times 10^{-4}$ and the beam divergence was set at 5 mrad. The dose was scored along a cylindrical region with a diameter of 1 cm in 0.25 mm steps.

Those particles may have different energy spectrum and composition. But as air mostly consists of light elements such as oxygen and nitrogen which are comparable to carbon[11] and the water environment, we do not expect significant deviations here. Despite the various uncertainties mentioned above, the overall agreement between FLUKA and our experimental data provides us with a reasonable level of confidence that we can determine dose–depth curves for antiprotons with sufficient accuracy to obtain RBE values versus depth for an antiproton beam using the measured survival values obtained in previous (Holzscheiter *et al* 2006) and future experiments conducted at CERN.

If the dosimetric evaluation is confirmed further, this will emphasize the potential of antiprotons in radiotherapy compared to protons, as presented in figure 7. Here, we used a broad beam (5 cm × 5 cm) in order to more closely match a clinical situation. In principle, this beam could be produced passively or actively to cover the target area. Scoring the central dose region, several features can be observed. In the entry region, a slight elevation of the dose level is seen as compared to protons, arising from antiprotons annihilating in-flight. The peak region itself is augmented by a factor of more than two as compared with the proton Bragg peak, at iso-fluence. When peak normalizing the depth–dose curves shown here, the dose from antiprotons at a depth of 6 cm will only be half that of the dose from protons, illustrating the significant reduction in normal tissue dose for an identical physical dose to the tumour. Combining the results obtained here and the RBE estimate in (Holzscheiter *et al* 2006) of around 2 (for a slightly spread-out annihilation peak), this imposes an even further decrease of the biologically effective dose in the entrance region as compared to a proton beam with identical biological effect in the target region.

[11] Ionization chamber electrodes consist of carbon, and the plastic housing is expected to consist of a carbon-rich compound too.

The comparison of proton and antiproton depth–doses at the same range shows the immense potential of antiprotons to reduce the dose to normal tissue in the entrance region of the particles, even without taking any increase in biological efficiency into account.

It should of course be mentioned that the dose beyond the Bragg peak is non-negligible in the case of antiprotons, which is due to the annihilation products. This dose contribution, however, is not a major concern for most clinical applications and both smaller in value and of shorter range than the dose in the fragment tail of, e.g., carbon ions. Thus, the improvement of the depth–dose characteristic of antiprotons as compared to protons seems to be undoubted. The remaining open question to be answered is the lateral dose distribution from antiprotons, especially close to the annihilation region. If the dose due to secondary particles is spread out significantly more in the lateral direction as compared to protons, this may be a serious drawback for the clinical use of antiprotons. Since the annihilation event happens at rest and is therefore isotropic in its effect we can already deduce some information from the distal edge of the Bragg peak. From our earlier measurements (Holzscheiter *et al* 2006) we expect the penumbra of antiproton beams to be only slightly larger than for protons. In addition, the effect of the diffuse and apparently weak dose from pions, gammas and neutrons on tissue far from the target area needs to be considered.

We are currently investigating this topic with model calculations along with experiments attempting to assess the peripheral dose, and this work will be the subject of a future publication which is in preparation.

6. Conclusion

Simulations with FLUKA 2006.3 are in excellent agreement with our relative measurements. In terms of absolute dose, our measurements are 6–9% higher than the FLUKA calculations, but this may be attributed to uncertainties in the saturation correction, the Monte Carlo simulation, the calibration of the ion chambers or a systematic shift in the number of antiprotons entering the target.

SHIELD-HIT v.2.2 overestimated the peak–plateau ratio, which is most likely related to the annihilation cross sections used by this code. Using ion chamber dosimetry, for the first time an absolute value of the absorbed dose in a beam of antiprotons could be determined. This enables a quantitative evaluation of the relative biological effectiveness of antiprotons and proves the superiority of the depth–dose distribution of antiprotons as compared to protons.

Acknowledgments

NB thanks the Danish Cancer Society for supporting this project with a grant. We thank Frank Fabian for assisting with the experiments and DKFZ for providing the ionization chambers and electrometers. HK thanks the ICE Center under the Danish Natural Science Research Council for support of this project. We gratefully acknowledge the AD operations team for their ongoing support and interest and for modifying the standard operating cycle of the AD machine to provide us with a higher energy antiproton beam as normally available.

References

Agnew L E Jr, Elioff T, Fowler W B, Lander R L, Powell W M, Segrè E, Steiner H M, White H S, Wiegand C and Ypsilantis T 1960 Antiproton interactions in hydrogen and carbon below 200 MeV *Phys. Rev.* 1371–91

Agostinelli S *et al* 2003 Geant4—a simulation toolkit *Nucl. Instrum. Methods* A **506** 250–303

Allison J *et al* 2006 Geant4 developments and applications *IEEE Trans. Nucl. Sci.* **53** 270–8

Bassler N 2006 Experimental studies relevant for antiproton cancer therapy *PhD Thesis* Aarhus University

Bassler N, Holzscheiter M and Knudsen H and the AD4/ACE Collaboration 2005 Cancer therapy with antiprotons *Low Energy Antiproton Physics-LEAP'05 (AIP Conference Proceedings* vol CP796*)* ed D Grzonka, R Czyżykiewicz, W Oelert, T Rożek and P Winter (New York: AIP) pp 423–30

Bassler N, Knudsen H, Møller S P, Petersen J B, Rahbek D and Uggerhøj U I and the AD4/ACE Collaboration 2006 Bubble detector measurements of a mixed radiation field from antiproton annihilation *Nucl. Instrum. Methods* B **251** 269–73

Bassler N *et al* 2007 *PBar Data* http://www.phys.au.dk/~bassler/pbar/

Biaggi M, Ballarini F, Burkard W, Egger E, Ferrari A and Ottolenghi A 1999 Physical and biophysical characteristics of a fully modulated 72 {MeV} therapeutic proton beam: model predictions and experimental data *Nucl. Instrum. Methods* B 89–100

Boag J W and Currant J 1980 Current collection and ionic recombination in small cylindrical ionization chambers exposed to pulsed radiation *Br. J. Radiol.* **53** 471–8

Boag J W, Hochhäuser E and Balk O A 1996 The effect of free-electron collection on the recombination correction to ionization measurements of pulsed radiation *Phys. Med. Biol.* **41** 885–97

Cugnon J, Wycech S, Jastrzębski J and Lubiński P 2001 Geometrical effects in antiproton annihilation on nuclei *Phys. Rev.* C **63** 027301

Fassò A *et al* eConf C0303241:MOMT005 2003 The physics models of FLUKA: status and recent developments *eConf C0303241: Paper MOMT005 (La Jolla, CA, USA, 24–28 March 2003)* (*Preprint* hep-ph/0306267)

Fassò A, Ferrari A, Ranft J and Sala P R 2005 FLUKA: a multi-particle transport code *CERN-2005-10, INFN/TC_05/11, SLAC-R-773*

Galassi M *et al* 2006 GNU Scientific Library Reference Manual—Revised Second Edition (vl.8) (Bristol: Network Theory Ltd) GSL—Gnu Scientific Library http://www.gnu.org/software/gsl/

Gray L and Kalogeropoulos T E 1984 Possible biomedical applications of antiproton beams: focused radiation transfer *Radiat. Res.* 246–52

Gudowska I, Sobolevsky N, Andreo P, Belki D and Brahme A 2004 Ion beam transport in tissue-like media using the Monte Carlo code SHIELD-HIT *Phys. Med. Biol.* **49** 1933–58

Holzscheiter M H *et al* 2004 Biological effectiveness of antiproton annihilation *Nucl. Instrum. Methods* B **221** 210–4

Holzscheiter M H *et al* 2006 The biological effectiveness of antiproton irradiation *Radiother. Oncol.* **81** 233–42

Hopewell J W and Trott K-R 2000 Volume effects in radiobiology as applied to radiotherapy *Radiother. Oncol.* **56** 283–8

IAEA (International Atomic Energy Agency) 2000 Absorbed dose determination in external beam radiotherapy: an international code of practice for dosimetry based on standards of absorbed dose to water *Technical Report 398* (Vienna: IAEA)

ICRU (International Commission on Radiation Units and Measurements) 1998 Clinical proton dosimetry: Part I. Beam production, beam delivery and measurement of absorbed dose *Technical Report 59* (Bethesda, MD: ICRU)

Inokuti M 1989 Interactions of antiprotons with atoms and molecules *Nucl. Tracks Radiat. Meas.* **16** 115–23

Kanai T, Sudo M, Matsufujii N and Futami Y 1998 Initial recombination in a parallel-plate ionization chamber exposed to heavy ions *Phys. Med. Biol.* **43** 3549–58

Kartal Ö M 2007 Cross-calibration of ionization chambers for heavy ion beams *Bachelor's Thesis* Institut für Medizinische Physik und Strahlenschutz, FH Giessen, Germany

Kossov M 2005 Simulation of antiproton–nuclear annihilation at rest *IEEE Trans. Nucl. Sci.* **52** 2832–5

Maggiore C *et al* 2004 Biological effectiveness of antiproton annihilation *Nucl. Instrum. Methods* B **214** 181–5

Markiel W *et al* 1988 Emission of helium ions after antiproton annihilation in nuclei *Nucl. Phys.* A **485** 445–60

Palmans H, Thomas R and Kacperek A 2006 Ion recombination correction in the Clatterbridge Centre of Oncology clinical proton beam *Phys. Med. Biol.* **51** 903–17

Park S H, Kim Y K, Kim H S, Kang S M and Ha J H 2006 Characteristics of the saturation curve of the ionization chambers in overlapping pulsed beams *Nucl. Instrum. Methods* A **566** 706–12

Polster D *et al* 1995 Light particle emission induced by stopped antiprotons in nuclei: energy dissipation and neutron-to-proton ratio *Phys. Rev.* C **51** 1167–80

Ponomarev L I 1973 Molecular structure effects on atomic and nuclear capture of mesons *Annu. Rev. Nucl. Sci.* 395–430

Sullivan A H 1985 A measurement of the local energy deposition by antiprotons coming to rest in tissue-like material *Phys. Med. Biol.* **30** 1297–303

Appendix D

Available online at www.sciencedirect.com
ScienceDirect
Nuclear Instruments and Methods in Physics Research B 266 (2008) 929–936
NIM B
Beam Interactions with Materials & Atoms
www.elsevier.com/locate/nimb

The antiproton depth–dose curve measured with alanine detectors

Niels Bassler [a,b,*], Johnny W. Hansen [c], Hugo Palmans [d], Michael H. Holzscheiter [e], Sandra Kovacevic [f], the AD-4/ACE Collaboration [1]

[a] Department of Experimental Clinical Oncology, Aarhus University Hospital, Aarhus, Denmark
[b] Deutsches Krebsforschungszentrum, Heidelberg, Germany
[c] Vejle Hospital, Vejle, Denmark
[d] National Physical Laboratory, Teddington, Middlesex, UK
[e] University of New Mexico, Albuquerque, NM, USA
[f] University of Montenegro, Podgorica, Montenegro

Received 24 July 2007; received in revised form 21 December 2007
Available online 12 February 2008

Abstract

In this paper we report on the measurement of the antiproton depth–dose curve, with alanine detectors. The results are compared with simulations using the particle energy spectrum calculated by FLUKA, and using the track structure model of Hansen and Olsen for conversion of calculated dose into response. A good agreement is observed between the measured and calculated relative effectiveness although an underestimation of the measured values beyond the Bragg-peak remains unexplained. The model prediction of response of alanine towards heavy charged particles encourages future use of the alanine detectors for dosimetry of mixed radiation fields.

PACS: 25.43.+t; 87.53.−j; 87.53.Qc; 87.53.Pb; 87.53.Wz; 87.66.Pm

Keywords: Alanine; Antiproton annihilation; Mixed radiation field dosimetry

1. Introduction

In radiotherapy of deep seated tumours it is advantageous to be able to deliver the dose from ionizing radiation to the tumour while at the same time sparing the surrounding normal tissue to maximum possible extend. The depth–dose profile of a proton beam is far superior to the depth–dose beam of photons in such cases, as the deposited energy peaks at the end of the range of the primary charged particle track.

In 1984, Gray and Kalogeropoulos suggested radiotherapy with antiprotons [1]. One of the anticipated advantages of antiprotons compared to protons, is the additional energy deposited at the Bragg-peak from the antiproton annihilation. Sullivan suggested in [2] that the additional local energy deposited by the annihilation products may roughly be about 30 MeV over the last 0.5 g cm^{-2} of its trajectory. Even though this value sounds low compared with

* Corresponding author. Address: Department of Experimental Clinical Oncology, Aarhus University Hospital, Aarhus, Denmark.
E-mail address: n.bassler@dkfz.de (N. Bassler).

[1] Michael H. Holzscheiter1, Niels Bassler2,3, Jan Alsner2, Gerd Beyer4, John J. DeMarco5, Michael Doser6, Dragan Hajdukovic7, Oliver Hartley4, Keisuke S. Iwamoto5, Oliver Jäkel3, Helge V. Knudsen8, Sandra Kovacevic7, Søren Pape Møller9, Jens Overgaard2, Jørgen B. Petersen2, Osman Ratib4, Timothy D. Solberg10, Sanja Vranjes11, Bradly G. Wouters12. 1 University of New Mexico, Albuquerque, NM, USA; 2 Dept. of Medical Physics and Experimental Clinical Oncology, Aarhus University Hospital, Aarhus, Denmark; 3 Deutsches Krebsforschungszentrum, Heidelberg, Germany; 4 Hospital Universitaire de Geneve, Geneva, Switzerland; 5 David Geffen School of Medicine, UCLA, Los Angeles, CA, USA; 6 CERN, Geneva, Switzerland; 7 University of Montenegro, Podgorica, Montenegro; 8 Dept. of Physics & Astronomy, University of Aarhus, Aarhus, Denmark; 9 ISA, University of Aarhus, Aarhus, Denmark; 10 University of Nebraska Medical Center, Omaha, NE, USA; 11 VINCA Institute for Nuclear Sciences, Belgrade, Serbia; 12 University of Maastricht, Res. Institute Growth and Development, The Netherlands.

0168-583X/$ - see front matter © 2008 Elsevier B.V. All rights reserved.
doi:10.1016/j.nimb.2008.01.067

the total of 1.88 GeV released by the annihilation, this still results in a substantial augmentation of the peak dose at the end of the particle track. Roughly, a proton has about 20 MeV left of kinetic energy before the onset of the Bragg-peak (corresponding to a residual range of 0.5 g cm^{-2}) and the additional 30 MeV would therefore more than double the energy deposited in the peak region. In this paper we try to characterize the antiproton annihilation peak, using alanine detectors.

To interpret a measured response of a biological system exposed to a beam of charged particles in terms of dose deposition, a prediction of the relative biological effectiveness (RBE) for the particular beam of particles is necessary. Similarly, for a radiation detector the relative effectiveness (RE) is relating the observed detector response with dose deposition. The observed response of a detector is here expressed in terms of the dose R, which is the dose as read from the ^{60}Co γ-ray response curve. This term will exclusively be used here to express response. For the dose D_{ion} deposited by ions and the secondary particles produced along the primary beam path, we have

$$R_{ion} = RE \cdot D_{ion} \quad (1)$$

Thus, R_{ion} is the response of a detector exposed to ion beams, expressed in terms of the dose by γ-rays necessary to produce an equal response. Here, "ion" means any primary particle with $Z \geqslant 1$. Note, that often the term heavy charged particles (HCPs) is used, referring to particles with $Z > 1$.

For a given biological system and chosen endpoint, RBE is a function of the target parameters, atomic number and velocity of the bombarding particle. This is why the RBE in the plateau region is different from that in the Bragg-peak. For protons one generally assumes an RBE close to unity for the entire penetration, even though an increase of RBE beyond this value has been observed for the distal edge of the Bragg-peak [3,4].

For HCPs the increase of RBE with depth becomes more pronounced and also shifts towards the entrance to the target with increasing atomic number. For antiprotons compared to protons of the same energy, the RBE is anticipated to be further enhanced in the peak region, due to the annihilation process which yields fragments with $Z > 1$. In the plateau region, antiprotons are expected to exhibit an RBE similar to that of protons.

The RE of a detector is expected to behave similar: in the peak region of the depth–dose curve we expect a lower RE due to secondary particles which may have a higher LET [5].

Attempts to measure the RBE of antiprotons directly in the peak region have failed so far [6–8], since any RBE determination requires knowledge of the dose. Dosimetry of the antiproton depth–dose curve is problematic since all applicable dosimeters known to us show non-linear effects in response when being exposed to ion beams. This is true for e.g. silicon diodes [9,10], diamond detectors [10,11], radiochromic films [12] and alanine [13].

At CERN the antiproton beam has a pulsed structure which leads to ionic recombination effects in ionization chambers [14–17]. Measurements using Boag's theorem [18,19] correcting for recombination effects have been performed and are described in [20]. Calorimetry is the most direct way to measure absorbed dose according to its definition. However, calorimeters are cumbersome to use and are not easily applicable in a low-frequency pulsed beam such as CERN's antiproton beam. Other detectors we have applied in the antiproton beam are lithium fluoride based thermoluminescent devices (TLDs) and radiochromic films [21]. This paper, however, will concentrate on the results achieved with alanine detectors.

L-α-alanine is an amino acid which occurs naturally in the human body. When alanine is irradiated with ionizing radiation, it forms the stable radical CH_3–$\dot{C}$H–COOH. Using an electron spin resonance (ESR) reader, the free electron pair at the chiral carbon atom can be detected. The magnitude of the ESR response depends on the amount of absorbed dose, and Bradshaw et al. [22] first suggested to use this detector as a dosimeter. The behaviour of alanine in photonic fields is well characterized [23]. The dynamic range of these pellets is large, ranging from 0.5 Gy to 100 kGy, being linear in the region up to 10 kGy. Kudoh et al. [24] showed that there was no dose rate effect when exposing 2.34 kGy X-rays within 70 ns. The response of alanine detectors to HCPs was investigated by Hansen and Olsen in the 80s [25,26]. A model explaining the behaviour based upon the Butts and Katz track structure idea [27,28] was developed [29]. This model has had some success in predicting the RE of alanine detectors, including fading effects – a phenomenon being of importance in the evaluation of dose–response for alanine detectors exposed to beams of HCPs: the temporal instability of the ESR signal in alanine after exposure to ionizing radiation, has been reported to be rather insignificant at low doses, but becoming more significant when approaching saturation doses of $\sim 5 \times 10^5$ Gy [25]. It was measured to be less than 1% per year for low-LET radiation, but as much as 16% after 4000 h when exposing alanine to high doses (5×10^5 Gy) of 16 MeV protons, and 22% for 10^6 Gy from stopping 21 MeV ^{7}Li-ions [23]. At lower doses (but at the same dose rate), the decay of the ESR signal from 10^4 Gy of 16 MeV protons stabilizes to 3% after 4000 h. The decay in alanine is dominant within the first 100–200 h after exposure to HCPs, and the rate of decay is different for pellets positioned in the plateau compared to those in the Bragg-peak [30].

The difference in fading rate between high and low-LET radiation and high and low dose is attributed to radical recombination effects in the microscopic high dose regions of the particle tracks [30]. Fading predictions based on the model of track structure have shown to conform to experimental data [26].

Concluding, due to the higher atomic number of annihilation fragments in the Bragg-peak of antiprotons the fading processes will be more pronounced and should from a

theoretical point of view be taken into account when comparing the radiation effect in the Bragg-peak with that of protons.

Here we shall apply the track structure model on a mixed particle-energy spectrum simulated by FLUKA, in order to calculate the RE and then the expected response of alanine pellets based on the measured ^{60}Co γ-ray dose–response curve. The predicted response as a function of penetration depth is compared to that measured from a stack of alanine pellets exposed to a beam of antiprotons.

2. Experimental methods

Two stacks of alanine pellets are irradiated with antiprotons. The pellets in stack #1 consist of finely grained crystalline alanine powder (Merck) 95% by weight mixed with 5% by weight polyvinyl-pyrrolidone (Polyvidone, Merck) as the binding agent and are manufactured by Hansen. The pellets have an outer diameter of 4.5 mm, an average thickness of 2 mm, and a density of 1.210 g cm^{-3}. Details about the dosimeter pellets are published in [29]. In this stack seven pellets are placed in the plateau, and 18 pellets are placed around the annihilation peak and are surrounded by a polystyrene phantom.

Stack #2 consists of alanine pellets which are produced by NPL and consists of 90% by weight L-α-alanine and 10% high melting point paraffin wax. The diameter of the pellets is 5 mm and the thickness is either 2.2 mm or 0.44 mm (average values for the entire batch). The average density is 1.235 g cm^{-3}. The stack is assembled from eleven 2.2 mm pellets, six 0.44 mm pellets and five 2.2 mm pellets, arranged in a 5.2 mm cylindrical hole in a PMMA phantom. We used a build-up plate of 81.8 mm polystyrene in order to position the Bragg-peak around the position of the thin pellets.

The Antiproton Decelerator (AD) at CERN provides a 502 MeV/c (∼126 MeV) antiproton beam. Every 90 s a spill consisting of roughly 3×10^7 antiprotons is ejected within 300 ns. The momentum spread of the beam is $\Delta p/p = 5 \times 10^{-4}$, and the divergence is in the order of 5 mrad. The beam exits the accelerator vacuum via a thin titanium window and is collimated to 1 cm diameter.

The absolute number of particles extracted from the AD is determined by a fast current transformer mounted downstream of the extraction septum in the beam line feeding our experimental set-up. Earlier studies show that this number possibly has a tendency to overestimate the amount of antiprotons hitting the target by 10–20%. This may be due to calibration errors and/or to losses in the final stretches of the beam line leading up to our set-up. In addition, for stack #1 we could only randomly manual check the number of antiprotons per spill, due to a temporary problem in the AD logging system. Those numbers were used to derive the best estimate of the amount of antiprotons hitting the alanine stack. The precision of this estimate is in the order of ±5%. For stack #2 the problems were solved, and every spill was logged.

We verify the alignment of the two stacks with two radiochromic films (GAFChromic HS and EBT) which are inserted along the beam. The FWHM of the beam when irradiating stack #2 is almost circular with a FWHM of 0.9 and 1.0 cm along the x and y axis. The beam which is used for stack #1 has a more ellipsoid form of about 0.6–1.0 cm FWHM along the x and y axis, respectively. The ESR signal of the pellets in stack #1 is read-out by the Radiation Research Department at the Risø, National Laboratory in Denmark, using a Bruker EMS 104 EPR alanine read-out device. Stack #1 is read-out several times at increasing time intervals, in order to detect any fading effects, as reported in [30]. At each read-out, the pellet is measured at 0° and 90° rotation and a mean signal strength is obtained. Stack #2 is read-out at the National Physics Laboratory (NPL) in the UK using the standard procedures for NPL's radiotherapy level alanine dosimetry service [31]. The spectrometer is a Bruker ESX and a standard Bruker ST4102 rectangular cavity. The acquisition time is 120 s consisting of six 20 s scans with 90° rotation of the pellet between the third and fourth scan. The pellets are introduced in the spectrometer using an automated loading system with a specially constructed sample holder to provide highly accurate positioning [32].

3. Model calculations

FLUKA [33,34] version 2006.3 is used for calculating the antiproton particle transport through the medium and the distribution of secondaries in each alanine pellet. The geometry of both stacks is carefully implemented, including correct densities and chemical compositions of target and phantom materials. The beam profiles measured with the radiochromic films is used as an input parameter for FLUKA for stack #1 and stack #2. We find for stack #1 a little misalignment of 2 mm and a rotation of the phantom of a half degree, which we include in the FLUKA calculations. 500.000 particles are used for the statistics, using the FLUKA hadron therapy "HADROTHE" default settings. The dose D for all particles (including contribution from γ-rays) is scored in every pellet position using the "USRBIN" card in FLUKA. A custom user routine is written to determine the dose D_γ from electromagnetic transport (γ-rays, electrons, positions) and D_R. D_R is a dose derived from what FLUKA defines as "kerma energy", which is energy being transferred to particles which are not transported further and again deposit their energy at the production point. These particles are not further identified in FLUKA, but it is expected to be related to low-energy neutron reactions and possibly also low-energy heavy recoils from the annihilation process.

In addition, we record the track length fluence-energy spectrum $\phi[E_j, Z_i]$ for pions, kaons and all nuclei with $1 \leqslant Z \leqslant 6$ for each pellet using the "USRTRACK" card in FLUKA. Another user routine is written in order to group all particles of equal charge. For example $Z = 1$ covers all pions (π^+, π^-, π^0), kaons ($K^+, K^-, K^0_S, K^0_L, K^0, \bar{K}^0$),

antiprotons, protons, deuterons and tritons. Higher charges $Z \geqslant 2$ includes all isotopes of the respective charge. The energy binning is done in energy per nucleon, which eases further data processing by using the fact that particles with equal charge and equal energy per nucleon have equal stopping power. For instance, pions are therefore treated as protons with mass $A = 0.15$ amu. The energy range scored ranges from 10 keV/nucleon to 1 GeV/nucleon in 100 logarithmic steps. We neglect effects of changing the charge sign, since the Barkas effect [35] is insignificant for our calculations. Thus, in all calculations antiprotons have equal stopping power as protons.

From FLUKA we can build a fluence matrix $\phi[E_j, Z_i]$ which is divided in particle types Z_i and energy bins with the mean energy per nucleon E_j.

For the relative efficiency calculations, the same approach of grouping the particles in terms of charge and energy per nucleon is taken, since the default model is not capable of treating pions, antiprotons or kaons.

The track length dose D_{TL} from these particle-energy spectra can be derived from $\phi[E_j, Z_i]$ as

$$D_{\mathrm{TL}} = \sum_{i=1}^{Z_{\mathrm{proj}}} \sum_{j=1}^{E_{\mathrm{bin}}} \phi[E_j, Z_i] \frac{1}{\rho} \frac{\mathrm{d}E}{\mathrm{d}x}(E_j, Z_i), \tag{2}$$

where $\frac{1}{\rho}\frac{\mathrm{d}E}{\mathrm{d}x}(E_j, Z_i)$ is the mass stopping power for particle Z_i at energy E_j. The stopping power is evaluated at the center of the energy bin using the PSTAR and ASTAR routines by Berger et al. [36] for $Z = 1$ and $Z = 2$, respectively, and MSTAR (by Paul and Shinner [37,38]) is used for $Z > 2$. Since we use track length dose, the energy dissipation of primary and secondary particles, when passing through the pellet of interest, is accounted for, when calculating D_{TL}.

The dose D_{TL} calculated by the track length fluence, is lower than the FLUKA dose D, since photons and low energy recoils are not included in the D_{TL} calculation. Instead these contributions are scored directly in D_γ and D_{R} as mentioned before. The contribution from D_γ and D_{R} to the total dose is about 1–2% in the plateau region and about 7–9% in the pellet(s) covering the peak region. The total summed dose D_{TOTAL} is therefore

$$D_{\mathrm{TOTAL}} = D_{\mathrm{TL}} + D_\gamma + D_{\mathrm{R}}. \tag{3}$$

D_{TOTAL} still differs from the direct way of calculating the dose D due to rounding errors from the binning, and perhaps even due to the use of external stopping power tables, which may differ from what FLUKA internally uses. The difference is 4% in the peak and 1% in the plateau.

From the track length fluence matrix $\phi[E_j, Z_i]$ the relative effectiveness of each particle-energy entry is looked up in a table. This RE table is generated using the model by Hansen and Olsen for infinitesimal thin detectors and the results are shown in Fig. 1.

By summing all individual detector responses $R_{\mathrm{ion}}(E_j, Z_i) = \mathrm{RE}(E_j, Z_i) D(E_j, Z_i)$ for each energy bin E_j and particle type Z_i, we find a total dose weighted average relative effectiveness $\overline{\mathrm{RE}}$ of the particle spectrum for the pellet of interest:

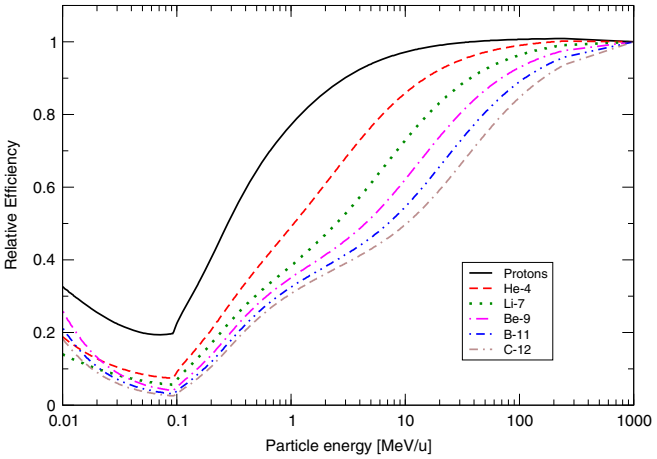

Fig. 1. Calculated relative efficiencies for infinitesimal thin detectors, without fading effects.

$$R_{\mathrm{TL}} = \sum_{i=1}^{Z_{\mathrm{proj}}} \sum_{j=1}^{E_{\mathrm{bin}}} \mathrm{RE}(E_j, Z_i) \phi[E_j, Z_i] \frac{1}{\rho} \frac{\mathrm{d}E}{\mathrm{d}x}(E_j, Z_i), \tag{4}$$

$$\overline{\mathrm{RE}} = \frac{R_{\mathrm{TL}} + \mathrm{RE}_\gamma D_\gamma + \mathrm{RE}_{\mathrm{R}} D_{\mathrm{R}}}{D_{\mathrm{TOTAL}}}, \tag{5}$$

where RE_γ and RE_{R} is the relative efficiency for the electromagnetic transport and the low-energy recoiling nuclei. Here we set $\mathrm{RE}_\gamma = 1$ per definition. Since FLUKA does not return the exact composition of the low-energy recoils, we cannot calculate RE_{R}. Fig. 1 indicates that this part the RE may lie between 0.0 and 0.2 for HCPs. since these particles are expected to have energies below 100 keV, which is the default cut-off energy for hadron transport. The Hansen and Olsen model suggest fading effects ranging from 9% to 87% for a ^{12}C nuclei with 10 keV/nucleon and 100 keV/nucleon, respectively, after 1900 h of fading. As an estimate we set RE_{R} to be $= 0.1$ with fading, and without fading we set $\mathrm{RE}_{\mathrm{R}} = 0.2$.

At last, we multiply the calculated $\overline{\mathrm{RE}}$ with the total dose D (representing the exact dose) scored by FLUKA for each pellet. This gives the response R_{ion} expressed in equivalent γ-ray dose:

$$R_{\mathrm{ion}}(D) = \overline{\mathrm{RE}} \cdot D. \tag{6}$$

4. Results

In Figs. 2 and 3, the total measured response of the alanine pellets as a function of penetration depth is plotted together with the response calculations and the predicted dose for stack #1 and #2, respectively. Fading effects are included in these calculations. The response is expressed in terms of response equivalent γ-dose.

All measurements are absolute, as the total number of antiprotons in the beam is measured upstream of the target with the beam current transformer. This possibly

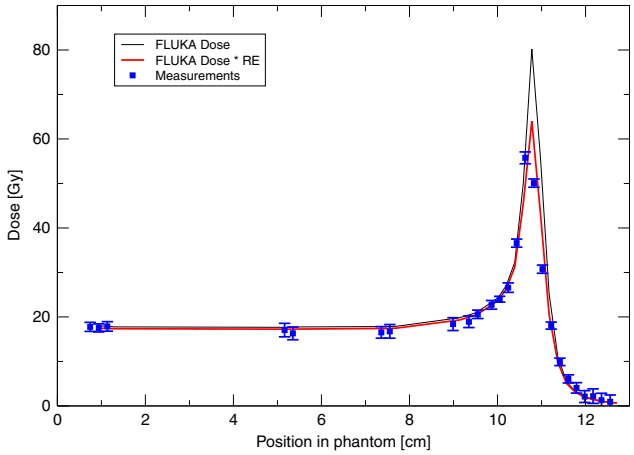

Fig. 2. Stack #1 results. The thin (black) line shows the dose for each pellet as it is calculated by FLUKA. The calculated dose multiplied with the calculated relative effectiveness is plotted as a grey (red) line, and should ideally match the measurements marked as unconnected squares. Measured response is translated to dose using the γ-ray dose–response curve. The measurements are shifted 1.5 mm upstream in order to match the results. (For interpretation of the references in colour in this figure legend, the reader is referred to the web version of this article.)

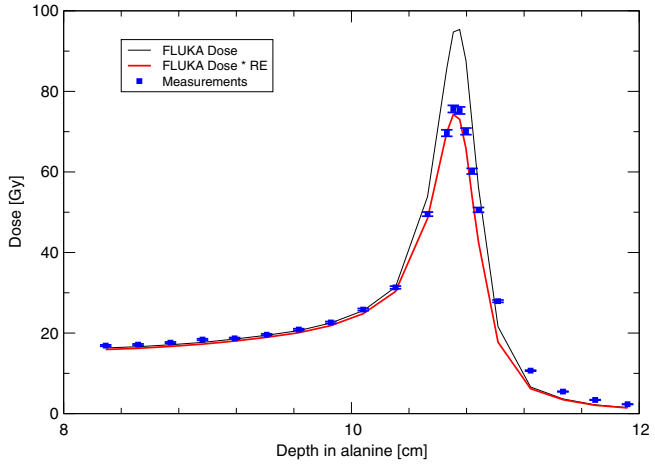

Fig. 3. Results for stack #2 plotted in the same fashion as Fig. 2. No shift along the x axis needed to be applied here.

introduces a systematic error in dose, since fractions of the beam may be lost on the way from the transformer to the experimental set-up, as mentioned earlier.

For stack #1 in Fig. 2 the measured peak was found 1.5 mm further downstream compared to the calculations. Therefore the measurements have been shifted 1.5 mm upstream the beam axis, in order to match the peaks. Investigation of the fading of the alanine tablets is attempted with alanine stack #1. Unfortunately the ESR-spectrometer for these readings turned out to be rather unstable resulting in unreliable measurements for which fading could not be determined with a sufficient accuracy. This error in precision is reflected by the 1σ standard deviation error bars in Fig. 2. From calculated predictions we expect to find a difference of less than 1% in fading between dosimeters positioned at the plateau and in the peak (see also Fig. 4). Therefore the expected fading is too small to be observable. Most of this fading in response is considered to take place within 200 h after irradiation. Here we apply 1900 h of fading for both stacks. As we mentioned earlier it is difficult to asses the amount of fading for RE_R, since the exact composition is not known.

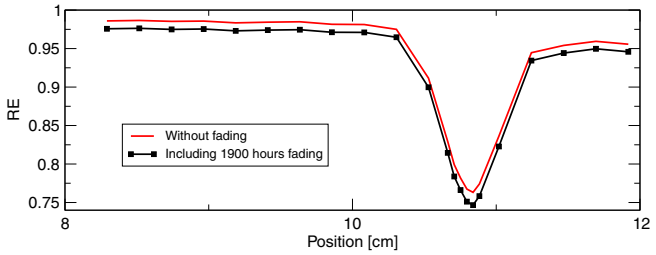

Fig. 4. Calculated relative effectiveness for stack #2 as a function of depth in phantom. The relative effectiveness drops off in the peak region due to the slowing down of antiprotons and the annihilation products with higher LET. The calculation is done twice, including and excluding fading effects.

Using Eqs. (4) and (5) the calculated relative effectiveness as a function of the particle penetration depth for stack #2 is shown in Fig. 4.

5. Discussion

One of the major differences between stack #1 and #2, is the fitting of the pellet diameter to the ∅5 mm hole drilled into the phantom. Stack #1 leaves a gap in between the pellet and the cavity wall whereas the stack #2 pellets fit the hole exactly. The presence of this gap enables some antiprotons to tunnel past the pellets. Furthermore, the pellets in stack #1 did not have a perfect cylindrical form, but had a little edge at the rim of the outer diameter. These effects are not included in the FLUKA simulations, since this is difficult to quantify. The result is that some antiprotons have a larger observed range, which in turn widens the peak, and localizes it further downstream the beam axis. This may possibly explain the shift of 1.5 mm downstream from the predicted position of the measured peak. This effect is thought to be much less pronounced for stack #2, as these pellets have perfect cylindrical form which closely matches the phantom cavity.

Another difference between both stacks is the density matching of the pellets and the surrounding phantom. For stack #1 the alanine pellets had 1.21 g cm^{-3} and are surrounded by polystyrene with 1.04 g cm^{-3}. For stack #2 the 1.235 g cm^{-3} pellets are surrounded by a PMMA phantom with a density of 1.19 g cm^{-3}. This is accounted for in the FLUKA calculations and causes the difference in the shape of the tail since antiprotons can penetrate deeper in the surrounding phantom as in the alanine stack and their annihilation can contribute to dose beyond the Bragg-peak.

The RE is fairly close to unity in the plateau region, and drops down to about 0.75 in the peak region. Compared to

the RE of e.g. low-energy carbon ions (see Fig. 1) the change in RE for antiprotons is rather small. The reason for this rather slight change in RE is due to the low atomic number of the antiproton itself but also due to the resulting mixed field of relatively light nuclei from the antiproton annihilation as described by Polster et al. [39]. Other detectors such as TLDs show a significantly higher loss of RE for light nuclei with low-energy, see e.g. [40,41].

Both stacks provide absolute dose measurements. Since the plateau region of the stack #2 fits the calculations very well, the systematic effect of a possible overestimate of the recorded particle fluence due to the upstream position of the beam current transformer seems to be minor. Absolute dose measurements for stack #1 are more problematic, since the alanine read-out device had a tendency to drift as mentioned earlier.

Due to the volume averaging effects, we focus on the stack #2. Here we see a 6% underestimation of the calculated dose in the plateau region. The agreement of the calculated dose in the annihilation peak is better than 3%, but in the tail the underestimation is almost ~40%. The nature of this underestimation is not clear, and several possible explanations exist:

- unknown accuracy of the beam current monitor;
- incorrect representation of the geometry used as input parameter for the FLUKA calculations;
- the RE model has shown to be only partially correct for HCP-energies below 2 MeV/u [26];
- limitation of the inherent model in the FLUKA code to predict the annihilation peak accurately.

On the experimental side a source of error may be the fact that the pellets consists of grains in a matrix whereas the Monte Carlo simulations assume a homogeneous mixture. Finally, the local shape of the annihilation peak is very sensitive to volume averaging effects, which may not be reproduced accurately in the Monte Carlo simulation.

Furthermore it should be noted that alanine together with model calculations of RE is a promising dosimeter in mixed radiation fields as formerly shown for neutrons [42]. In a real clinical situation, one would never use a pristine beam, but a spread out beam covering a larger treatment volume. This dilutes the RE further as the Bragg-peak is mixed with the field from primary particles and reduces the error of dosimetry in the spread out peak region further.

Models based on track structure theory by Butts and Katz [27], and derivatives of the local effect model [43–45] such as ECLaT [46] for TLDs, rely on predicting the response of a detector from the γ-response curve which is convoluted with the radial dose distribution of a track in order to achieve the relative effectiveness of the HCP radiation in question. Here we would like to speculate on the link between track interactions and saturation level of the γ-response curve. In mixed radiation fields, the track structure model and the local effect model use different approaches in calculating track interaction effects, an overview of these differences is given in [47]. In this paper though, the response calculations are further simplified since interactions between two or multiple tracks are not considered. Track interactions are most likely to happen at high fluences where the mean track distance $\sqrt{\phi^{-1}}$ becomes similar to that part of the track-radius in which "cross-overs" would lead to saturation response. For a clinical setting with a fluence of $10^9\,\mathrm{cm}^{-2}$ (per fraction) the mean track distance would be 3×10^{-5} cm. One can estimate a significant track-radius from the amorphous radial dose distribution of a track, where saturation effects occur. This radius is depending on particle-energy and particle charge, but it will decrease, the higher the onset of saturation is on the γ-response curve. If we assume 10 kGy as the onset of saturation effects for alanine, this would give a radius in the order of 10^{-6} cm for an oxygen ion with 3 MeV [30]. This radius will decrease further for decreasing charge. Neglecting of track interactions in the calculation of effectiveness should be possible due to the high saturation dose of alanine.

The region of saturation in a single particle track is smaller in a detector with a high saturation level, i.e. low radiation sensitivity, than that of a detector with a low saturation level, i.e. high radiation sensitivity. Therefore the effect of overlapping tracks is expected to be low for the alanine detector.

6. Conclusion

In this paper we have described the use of alanine detectors for the dosimetry of the mixed particle field arising from antiproton annihilation. The results could be reproduced using the relative effectiveness calculated with the track structure model by Hansen and Olsen used in conjunction with doses and particle spectra calculated with FLUKA. Forward calculation using this method shows that dose verification is possible, and in principle medical dosimetry can be reconstructed from the alanine response. We conclude that the alanine detector is an interesting detector for characterizing the mixed radiation field from antiproton annihilation. This detector could also be applied for dosimetry of medical heavy ion beams and possibly in mixed radiation fields found in space. NPL alanine dosimetry service can measure the dose from 5 Gy upwards with a precision of 1% (1σ). This is well within the dose levels used in radiotherapy. Even if ESR-spectrometers are not widespread in clinical environments and read-out may be time-consuming, this dosimeter has still some advantages: it is easy to handle, the read-out is non-destructive, and alanine has a tissue-equivalent composition.

Acknowledgments

We thank Peter Sharpe and Clare Gouldstone from NPL and Jakob Helt Hansen from Risø, for reading out

the alanine dosimeters. We also thank the AD-4 operators for providing us the antiproton beam. The Danish Cancer Society supported this project with a grant.

References

[1] L. Gray, T.E. Kalogeropoulos, Possible biomedical applications of antiproton beams: focused radiation transfer, Radiat. Res. (1984) 246.

[2] A.H. Sullivan, A measurement of the local energy deposition by antiprotons coming to rest in tissue-like material, Phys. Med. Biol. 30 (12) (1985) 1297.

[3] J.S. Loeffler, A.R. Smith, H.D. Suit, The potential role of proton beams in radiation oncology, Semin. Oncol. 24 (6) (1997) 686.

[4] B.G. Wouters, G.K.Y. Lam, U. Oelfke, K. Gardey, R.E. Durand, L.D. Skarsgard, Measurements of relative biological effectiveness of the 70 MeV proton beam at TRIUMF using chinese hamster V79 cells and the high-precision cell sorter assay, Radiat. Res. 146 (2) (1996) 159.

[5] K.J. Olsen, J.W. Hansen, Experimental and calculated effectiveness of a radiochromic dye film to stopping 21 MeV ^{7}Li and 64 MeV ^{16}O ions, Nucl. Instr. and Meth. B 5 (1984) 497.

[6] M.H. Holzscheiter, N. Agazarayan, N. Bassler, G. Beyer, J.J. DeMarco, M. Doser, T. Ichioka, K.S. Iwamoto, H.V. Knudsen, R. Landua, C. Maggiore, W.H. McBride, S.P. Møller, J. Petersen, J.B. Smathers, L.D. Skarsgard, T.D. Solberg, U.I. Uggerhøj, H. Rodney Withers, S. Vranjes, M. Wong, B.G. Wouters, Biological effectiveness of antiproton annihilation, Nucl. Instr. and Meth. B 221 (2004) 210.

[7] C. Maggiore, N. Agazarayan, N. Bassler, E. Blackmore, G. Beyer, J.J. DeMarco, M. Doser, C.R. Gruhn, M.H. Holzscheiter, T. Ichioka, K.S. Iwamoto, H.V. Knudsen, R. Landua, W.H. McBride, S.P. Møller, J. Petersen, J.B. Smathers, L.D. Skarsgard, T.D. Solberg, U.I. Uggerhøj, H. Rodney Withers, B.G. Wouters, Biological effectiveness of antiproton annihilation, Nucl. Instr. and Meth. B 214 (2004) 181.

[8] M.H. Holzscheiter, N. Bassler, N. Agazaryan, G. Beyer, E. Blackmore, J.J. DeMarco, M. Doser, R.E. Durand, O. Hartley, K.S. Iwamoto, H.V. Knudsen, R. Landua, C. Maggiore, W.H. McBride, S.P. Møller, J. Petersen, L.D. Skarsgard, J.B. Smathers, T.D. Solberg, U.I. Uggerhøj, S. Vranjes, H. Rodney Withers, M. Wong, B.G. Wouters, The biological effectiveness of antiproton irradiation, Radiother. Oncol. 81 (3) (2006) 233.

[9] E. Grusell, J. Medin, General characteristics of the use of silicon diode detectors for clinical dosimetry in proton beams, Phys. Med. Biol. 45 (9) (2000) 2573.

[10] S. Onori, C. De Angelis, P. Fattibene, M. Pacilio, E. Petetti, L. Azario, R. Miceli, A. Piermattei, L. Barone Tonghi, G. Cuttone, S. Lo Nigro, Dosimetric characterization of silicon and diamond detectors in low-energy proton beams, Phys. Med. Biol. 45 (2000) 3045.

[11] M. Sakama, T. Kanai, Y. Kase, M. Komori, A. Fukumura, T. Kohno, Responses of a diamond detector to high-LET charged particles, Phys. Med. Biol. 50 (2005) 2275.

[12] A. Piermattei, R. Miceli, L. Azario, A. Fidanzio, S. delle Canne, C. De Angelis, S. Onori, M. Pacilio, E. Petetti, L. Raffaele, M.G. Sabini, Radiochromic film dosimetry of a low energy proton beam, Med. Phys. 27 (7) (2000) 1655.

[13] H. Palmans, Effect of alanine energy response and phantom material on depth–dose measurements in ocular protons beams, Technol. Cancer Res. Treat. 2 (6) (2003) 579.

[14] F.H. Attix, Introduction to Radiological Physics and Radiation Dosimetry, John Wiley & Sons, 1986.

[15] T. Kanai, M. Sudo, N. Matsufuji, Y. Futami, Initial recombination in a parallel-plate ionization chamber exposed to heavy ions, Phys. Med. Biol. 43 (1998) 3549.

[16] H. Palmans, R. Thomas, A. Kacperek, Ion recombination correction in the clatterbridge centre of oncology clinical proton beam, Phys. Med. Biol. 51 (2006) 903.

[17] S.H. Park, Y.K. Kim, H.S. Kim, S.M. Kang, J.H. Ha, Characteristics of the saturation curve of the ionization chambers in overlapping pulsed beams, Nucl. Instr. and Meth. A 566 (2006) 706.

[18] J.W. Boag, J. Currant, Current collection and ionic recombination in small cylindrical ionization chambers exposed to pulsed radiation, Brit. J. Radiol. 53 (1980) 471.

[19] J.W. Boag, E. Hochhäuser, O.A. Balk, The effect of free-electron collection on the recombination correction to ionization measurements of pulsed radiation, Phys. Med. Biol. 41 (1996) 885.

[20] N. Bassler, M.H. Holzscheiter, O. Jäkel, H.V. Knudsen, S. Kovacevic, and the AD-4/ACE Collaboration, The antiproton depth–dose curve in water, Phys. Med. Biol. 53 (2008) 793–805.

[21] N. Bassler, Experimental studies relevant for antiproton cancer therapy, PhD Thesis, Aarhus University, May 2006.

[22] W.W. Bradshaw, D. Cadena, G.W. Crawford, H.A.W. Soetzler, The use of alanine as a solid dosimeter, Radiat. Res. 17 (1962) 11.

[23] J.W. Hansen, K.J. Olsen, M. Wille, The alanine radiation detector for high and low LET dosimetry, Radiat. Prot. Dosim. 19 (1) (1987) 43.

[24] H. Kuhdoh, M. Celina, R.J. Kaye, K.T. Gillen, R.L. Clough, Response of alanine dosimeters at very high dose rate, Appl. Radiat. Isotopes 48 (4) (1997) 497.

[25] J.W. Hansen, K.J. Olsen, Theoretical and experimental radiation effectiveness of the free radical dosimeter alanine to irradiation with heavy charged particles, Radiat. Res. 104 (1985) 15.

[26] K.J. Olsen, J.W. Hansen, The response of the alanine dosemeter to low energy protons and high energy heavy charged particles, Radiat. Prot. Dosim. 31 (1/4) (1990) 81.

[27] J.J. Butts, R. Katz, Theory of RBE for heavy ion bombardment of dry enzymes and viruses, Radiat. Res. 30 (1967) 855.

[28] R. Katz, S.C. Sharma, M. Homayoonfar, The structure of particle tracks, in: F.H. Attix (Ed.), Topics of Radiation Dosimetry, Academic Press, New York, 1972, p. 317 (Suppl. 1).

[29] J.W. Hansen, Experimental investigation of the suitability of the track structure theory in describing the relative effectiveness of high-LET irradiation of physical radiation detectors, PhD Thesis, Risø National Laboratory, DK-4000 Roskilde, Risø-R-507, 1984.

[30] J.W. Hansen, K.J. Olsen, Predicting decay in free-radical concentration in L-α-alanine following high-LET radiation exposures, Appl. Radiat. Isotopes 40 (10–12) (1989) 935.

[31] P.H. Sharpe, K. Rajendran, J.P. Sephton, Progress towards an alanine/ESR therapy level reference dosimetry service at NPL, Appl. Radiat. Isotopes 47 (11–12) (1996) 1171.

[32] P. Sharpe, J. Sephton, An automated system for the measurement of alanine/EPR dosimeters, Appl. Radiat. Isotopes 52 (5) (2000) 1185.

[33] A. Fassò, A. Ferrari, J. Ranft, P.R. Sala, FLUKA: a multi-particle transport code. CERN-2005-10, INFN/TC_05/11, SLAC-R-773.

[34] A. Fassò, A. Ferrari, S. Roesler, P.R. Sala, G. Battistoni, F. Cerutti, E. Gadioli, M.V. Garzelli, F. Ballarini, A. Ottolenghi, A. Empl, J. Ranft, The physics models of FLUKA: status and recent developments. In Computing in High Energy and Nuclear Physics 2003 Conference (CHEP2003), La Jolla, CA, USA, March 24-28 2003. (paper MOMT005), eConf C0303241 (2003), arXiv:hepph/0306267.

[35] S.P. Møller, A. Csete, T. Ichioka, H. Knudsen, U.I. Uggerhøj, H.H. Andersen, Antiprotons stopping at low energies: confirmation of velocity-proportional stopping power, Phys. Rev. Lett. 88 (19) (2002) 193201-1.

[36] M.J. Berger, J.S. Coursey, M.A. Zucker, J. Chang, Stopping-power and range tables for electrons, protons, and helium ions, <http://physics.nist.gov/PhysRefData/Star/Text/contents.html>.

[37] H. Paul, A. Schinner, MSTAR, <http://www.exphys.uni-linz.ac.at/stopping/>.

[38] H. Paul, A. Schinner, An empirical approach to the stopping power of solids and gases for ions from ^{3}Li to ^{18}Ar, Nucl. Instr. and Meth. B 179 (2001) 299.

[39] D. Polster, D. Hilscher, H. Rossner, T. von Egidy, F.J. Hartmann, J. Hoffmann, W. Schmid, I.A. Pshenichnov, A.S. Iljinov

Ye. S. Golubeva, H. Machner, H.S. Plendl, A. Grouchulska J. Jastrzebski, W. Kurcewiz, P. Lubinski, J. Eades, S. Neumaier, Light particle emission induced by stopped antiprotons in nuclei: energy dissipation and neutron-to-proton ratio, Phys. Rev. C 51 (3) (1995) 1167.

[40] J. Besserer, P. Bilski, J. de Boer, T. Kwiecien, M. Moosburger, P. Olko, P. Quicken, Dosimetry of low-energy protons and light ions, Phys. Med. Biol. 46 (2001) 473.

[41] J. Kalef-Ezra, Y.S. Horowitz, Heavy charged particle thermoluminescence dosimetry: track structure theory and experiments, Int. J. Appl. Radiat. Isotopes 33 (1982) 1085.

[42] H.M. Gerstenberg, J.W. Hansen, J.J. Coyne, J. Zoetelief, Calculations of the relative effectiveness of alanine for neutrons with energies up to 17.1 MeV, Radiat. Prot. Dosim. 31 (1/4) (1990) 85.

[43] M. Scholz, Grundlagen der biologischen Bestrahlungsplanung fur die Schwerionen-Tumortherapie, Medizinische Fakultat Heidelberg, Ruprecht-Karls-Universität, Habilitationsschrift (in German).

[44] M. Scholz, G. Kraft, Track structure and the calculation of biological effects of heavy charged particles, Adv. Space Res. 18 (1/2) (1995) 5.

[45] M. Scholz, A.M. Kellerer, W. Kraft-Weyrather, Computation of cell survival in heavy ion beams for therapy, Radiat. Environ. Biophys. 36 (1997) 59.

[46] O.B. Geiß, M. Krämer, G. Kraft, Efficiency of thermoluminescent detectors to heavy charged particles, Nucl. Instr. and Meth. B 142 (1998) 592.

[47] H. Paganetti, M. Goitein, Biophysical modelling of proton radiation effects based on amorphous track models, Int. J. Radiat. Biol. 77 (9) (2001) 911.

Appendix E

Acta Oncologica
2008, 1–4, iFirst article

informa
healthcare

ORIGINAL ARTICLE

Calculated LET spectrum from antiproton beams stopping in water

NIELS BASSLER[1,2] & MICHAEL HOLZSCHEITER[3]

[1]*Department of Experimental Clinical Oncology, Aarhus University Hospital, Aarhus, Denmark,* [2]*Deutsches Krebsforschungszentrum, Heidelberg, Germany and* [3]*University of New Mexico, Albuquerque, NM, USA*

Abstract
Introduction. Antiprotons have been proposed as a potential modality for radiotherapy because the annihilation at the end of range leads to roughly a doubling of physical dose in the Bragg peak region. So far it has been anticipated that the radiobiology of antiproton beams is similar to that of protons in the entry region of the beam, but very different in the annihilation region, due to the expected high-LET components resulting from the annihilation. On closer inspection we find that calculations of dose averaged LET in the entry region may suggest that the RBE of antiprotons in the plateau region could significantly differ from unity, which seems to warrant closer inspection of the radiobiology in this region. *Materials and Methods.* Monte Carlo simulations using FLUKA were performed for calculating the entire particle spectrum of a beam of 126 MeV antiprotons hitting a water phantom. *Results and Discussion.* In the plateau region of the simulated antiproton beam we observe a dose-averaged unrestricted LET of about 4 keV/μm, which is very different from the expected 0.6 keV/μm of an equivalent primary proton beam. Even though the fluence of secondaries is a magnitude less than the fluence of primary particles, the increased stopping power of the secondary particles causes an increase in the dose averaged LET which is expected to result in a RBE different from unity.

Antiprotons as a new beam modality in radiotherapy are being investigated by the AD-4/ACE collaboration since 2003. A beam of antiprotons hitting a water phantom exhibits a similar depth-dose curve as that known from protons, except that the Bragg peak is significantly more pronounced due the annihilation events occurring at the end of the antiproton particle tracks.

Holzscheiter et al. [1–3] investigated the radiobiology of antiprotons using an antiproton beam with kinetic energy of 50 MeV from the AD facility at CERN.

Since the dosimetry of the antiproton beam at CERN is a non-trivial matter for several reasons, the relative biological effect (RBE) in the peak region could not be measured at the time. Instead the AD-4 collaboration concentrated on measuring the ratio of the biological effect between the peak and plateau area (defined as "Biological Effective Dose Ratio", or, "BEDR"), which is measurable irrespectively of the deposited dose [3]. The BEDR value therefore expresses quantitatively, how much one can reduce the dose in the plateau for a constant effect in the peak.

In this paper we calculate the linear energy transfer (LET) spectrum and the dose averaged LET for a beam of 126 MeV antiprotons hitting a water target. This energy was chosen as it matches the beam energy in our current radiobiological experiments. All references to LET are meant to be unrestricted LET, i.e. LET_{inf}.

Since antiprotons have the same stopping power as protons in the clinical relevant energy interval, it has so far been assumed that antiprotons exhibit the same radiobiology as protons in the entrance channel. The contribution from secondary particles arising from in-flight annihilation of the primary beam was considered insignificant. Using Monte Carlo calculations for the dose of the primary beam in the peak, it is then possible to provide an estimate of the RBE in the peak region by assuming RBE = 1 in the plateau, e.g. in [3] the best estimate of the peak RBE is 2.25 for 20% clonogenic survival of V79 Chinese hamster cells.

More recently, antiproton dose calculations with FLUKA [4,5] were successfully benchmarked against experimental measurements with ionization chambers [6]. Furthermore, particle spectra

Correspondence: Niels Bassler, DKFZ E040, Im Neuenheimer Feld 280, 69120 Heidelberg, Germany. E-mail: n.bassler@dkfz-heidelberg.de

(Received 28 May 2008; accepted 10 June 2008)

ISSN 0284-186X print/ISSN 1651-226X online
DOI: 10.1080/02841860802266730

calculated with FLUKA were used in conjunction with response models in order to calculate the response of alanine detectors exposed to the mixed radiation field [7]. This allowed deducing a measurement for the dose deposit along the entire depth-dose curve. Measurements of RBE are therefore now possible and were performed in 2007. These findings are to be published in a future article.

Methods

FLUKA version 2006.3 is used for our calculations performed for this paper. A 5×5 cm^2 square field of 502 MeV/c ($\sim$126 MeV) antiprotons with a momentum spread of $\Delta p/p = 0.5\%$ and 5 mrad divergence is dumped into a water phantom. The range in water for this beam is approximately 11.5 cm. The scoring along the beam in the water target is done in rectangular boxes covering an area of 2×2 cm^2 laterally and a thickness of 1 cm along the beam line. The scoring region is thus significantly smaller than the beam width, in order to achieve lateral equilibrium of particles, which scatter into and out of the scoring volume. The other beam parameters were chosen in order to mimic the beam which we have available at CERN. Custom FLUKA user routines were written in order to extract the fluence for each particle species as a function of energy per nucleon. The stopping power used for the LET averaged calculations is provided by PSTAR, ASTAR and MSTAR routines developed by Berger et al. [8] and Paul et al. [9].

The track averaged and the dose averaged LET is calculated according to Equations 1 and 2, respectively:

$$\overline{LET}_{\phi,\mathrm{inf}} = \frac{\Sigma_{i=1}^{Z_{proj}} \Sigma_{j=1}^{E_{bin}} \phi[E_j, Z_i] \frac{dE}{dx}(E_j, Z_i)}{\Sigma_{i=1}^{Z_{proj}} \Sigma_{j=1}^{E_{bin}} \phi[E_j, Z_i]} \quad (1)$$

$$\overline{LET}_{D,\mathrm{inf}} = \frac{\Sigma_{i=1}^{Z_{proj}} \Sigma_{j=1}^{E_{bin}} D[E_j, Z_i] \frac{dE}{dx}(E_j, Z_i)}{\Sigma_{i=1}^{Z_{proj}} \Sigma_{j=1}^{E_{bin}} D[E_j, Z_i]} \quad (2)$$

where (E_j,Z_i) is the electronic stopping power in liquid water for each particle with charge Z_i at energy E_j, measured at the center of the respective energy bin, $\phi[E_j,Z_i]$ and $D[E_j,Z_i]$ are the track length fluence and dose of the corresponding particle, respectively. The sum is taken over all particle charges up to $Z_{proj} = 6$ and over the entire energy spectrum obtained from FLUKA up to 1 GeV. Being presented a highly mixed radiation field with a strong content of high LET secondary particles we choose to use the dose averaged LET for this analysis.

Results

The complete LET-spectra for those two positions are shown in Figure 1. The dose averaged LET is shown in Figure 2. A calculated depth-dose curve for antiprotons in water is added in these figures in order to guide the reader. The plateau and peak averaged values are also presented in Table I.

Antiprotons with a kinetic energy of 126 MeV have a stopping power of 0.615 keV/µm in water. In Figure 1 the primary antiproton beam is clearly visible as the stopping power bin with the highest relative fluence. Even though the track averaged LET can be shown to be comparable to the stopping power of the primary beam, the dose averaged stopping power is a magnitude higher, due to the

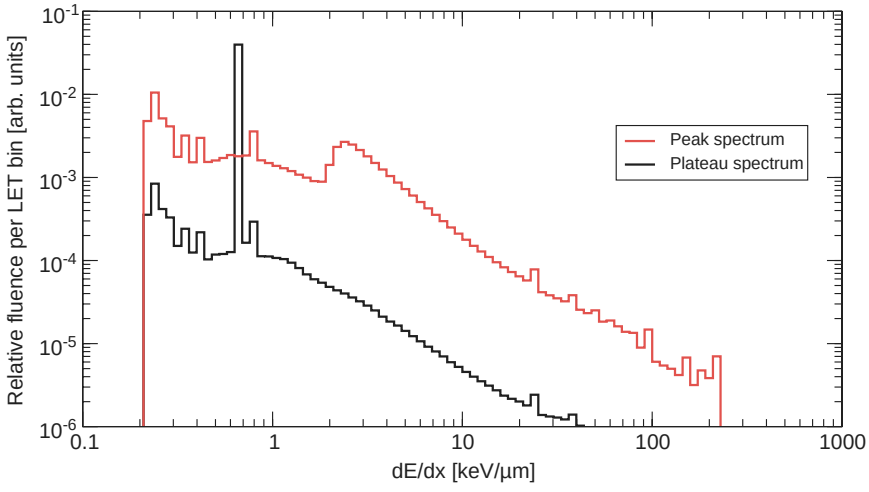

Figure 1. FLUKA calculation of charged particle LET spectrum of a 126 MeV antiproton beam as shown in [6]. The spectrum was calculated both in the peak region and in the plateau region. Charged particles with $1 \leq Z \leq 6$ were taken into account. The sharp line in the plateau region at 0.6 keV/µm originates from the primary antiproton beam.

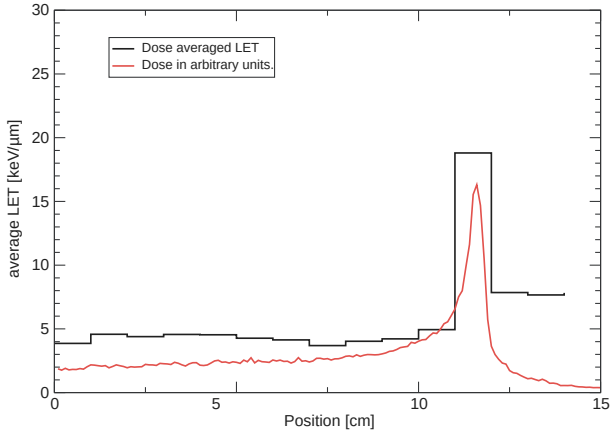

Figure 2. Dose averaged unrestricted LET plotted as a function of depth in water.

significantly higher LET of the low energy fragments present in the radiation field.

Discussion

The RBE dependence on LET has been discussed in several publications, often showing a peaking of the RBE at around 100 keV/µm. This LET corresponds to the mean distance between ionization events being comparable with the width of DNA strands, which is believed to effectively induce double strand breaks [10]. Naturally, this is rather an oversimplification of the complex biological processes, e.g. if one takes a look at Figure 11 found in the ICRU Report # 16 [11], which relates the RBE with LET, the clear dependence is less convincing. Furthermore RBE dependence cannot be single-valued, since several particles with different energies can have the same LET. However, for the discussion presented here it will be sufficient to conclude that RBE changes with LET.

Considering the work by Wouters et al. [12], where the RBE of proton beams with V79 Chinese hamster cells was investigated, one may actually get the impression that the change in dose averaged LET presented in this paper may be sufficient to significantly alter the RBE. The distribution of secondary particles from annihilation, as calculated with FLUKA, shows that mainly fragments such as pions, protons and some Helium ions contribute to the dose. Since most of these fragments have a charge $Z = 1$ we here assume that the resulting RBE may possibly be very similar to an LET equivalent field consisting of only protons with various energies. Wouters directly measured the RBE as a function of depth in a spread-out Bragg peak (SOBP) of 21 mm width and a maximum energy of 70 MeV, corresponding to a maximum depth in water of 28 mm. For three different endpoints of clonogenic survival of 3, 50, and 80% he reports a range of RBE values between 1.2 and 1.6. He also calculates the dose-averaged linear energy transfer across the width of the SOBP using the weighted sum of range-shifted pristine Bragg peaks to span the interval from 2.5 to 6.0 Kev/µm [12].

Table I. Calculated averaged LET.

	Position interval of bin [cm]	Dose averaged LET [keV/µm]
Plateau position	0–1	3.86
Peak position	11–12	18.8

Applying the dose averaged stopping power in the plateau presented here in conjunction with Figure 10 in reference [12], we find an RBE in the plateau in the region of 1.2–1.3 for 10 to 50% survival, rather than 1. This could have significant consequences for the RBE estimate in the peak area described earlier by Holzscheiter et al. [3]. For instance a RBE of 2.25 may increase to 2.7–3.0.

RBE measurements of an antiproton beam of 126 MeV energy were carried out in October 2007 and preliminary estimates sustain the findings presented here, although the Co-60 reference irradiations needed to extract a final RBE from these measurements are still to be performed.

Conclusion

Using FLUKA we have calculated the unrestricted LET spectrum of several ions. The maximum dose averaged LET in the Bragg peak region was estimated as 19 keV/µm, which suggests, that the RBE of antiprotons for V79 Chinese hamster cells may differ from unity. This would have a significant impact on earlier estimates for the RBE in the peak of an antiproton beam of 50 MeV stopping in a target of V-79 Chinese hamster cells embedded in gelatin and clearly should be considered in future analyses.

Acknowledgement

The Danish cancer society supported this project with a grant.

References

[1] Maggiore C, Agazarayan N, Bassler N, Blackmore E, Beyer G, DeMarco JJ, et al. Biological effectiveness of antiproton annihilation. NIM B 2004;214:181–5.

[2] Holzscheiter MH, Agazarayan N, Bassler N, Beyer G, DeMarco JJ, Doser M, et al. Biological effectiveness of antiproton annihilation. NIM B 2004;221:210–4.

[3] Holzscheiter MH, Bassler N, Agazaryan N, Beyer G, Blackmore E, DeMarco JJ, et al. The biological effectiveness of antiproton irradiation. Radiother Oncol 2006;81:233–42.
[4] Fassò A, Ferrari A, Ranft J, Sala PR. FLUKA: A multi-particle transport code. CERN-2005-10, INFN/TC 05/11, SLAC-R-773.
[5] Fassò A, Ferrari A, Roesler S, Sala PR, Battistoni G, Cerutti F, et al. The physics models of FLUKA: Status and recent developments. In: Computing in High Energy and Nuclear Physics 2003 Conference (CHEP2003), La Jolla, CA, USA, March 24-28 2003. (paper MOMT005), eConf C0303241 (2003), arXiv:hep-ph/0306267.
[6] Bassler N, Holzscheiter MH, Jäkel O, Kovacevic S, Knudsen HV, and the AD-4/ACE Collaboration. The antiproton depth-dose curve in water. Phys Med Biol 2008;53:793–805.
[7] Bassler N, Hansen JW, Palmans H, Holzscheiter MH, Kovacevic S, and the AD-4/ACE Collaboration. The anti-proton depth dose curve measured with alanine detectors. NIM B 2008;266:929–36.
[8] Berger MJ, Coursey JS, Zucker MA, Chang J. Stopping-power and range tables for electrons, protons, and helium ions. http://physics.nist.gov/PhysRefData/Star/Text/contents.html.
[9] Paul H, Schinner A. MSTAR. http://www.exphys.uni-linz.ac.at/stopping/.
[10] Hall EJ. Radiobiology for the Radiologist, 5th ed. Lippincott Williams & Wilkins; 2000.
[11] International Commission on Radiation Units and Measurements. Linear energy transfer. Technical Report 16, ICRU, 1970.
[12] Wouters BG, Lam GKY, Oelfke U, Gardey K, Durand RE, Skarsgard LD. Measurements of relative biological effectiveness of the 70 MeV proton beam at TRIUMF using Chinese hamster V79 cells and the high-precision cell sorter assay. Radiat Res 1996;146:159–70.

Antiproton Radiotherapy

Benjamin P. Fahimian[1], John J. DeMarco[1], Roy Keyes[2], Niels Bassler[3], Keisuke S. Iwamoto[1], Maria Zankl[4], and Michael H. Holzscheiter*[5]

1 Dept. of Radiation Oncology, University of California, Los Angeles, USA
2 Dept. of Chemical & Nuclear Engineering, UNM, Albuquerque, USA
3 Deutsches Krebsforschngszentrum Heidelberg (dkfz.), Heidelberg, Germany
4 Helmholtz Zentrum München, Neuherberg, Germany
5 Dept. of Phys. & Astronomy, University of New Mexico, Albuquerque, USA

for the AD-4 Collaboration

Keywords: Antiprotons . Particle Therapy . Peripheral Dose . Neutrons

Purpose: The AD-4 collaboration studies the biological effects of antiprotons with respect to a possible use of antiprotons in cancer therapy. *In vitro* experiments performed by the collaboration at CERN have shown an enhanced biological effectiveness for antiprotons relative to protons. One concern is the normal tissue dose resulting from medium and long range secondary particles produced in the annihilation of antiprotons on the nucleons of the target atoms. In particular, the secondary neutron dose is of interest due to the neutrons high relative biological effectiveness and long range. Here we present the first organ specific Monte Carlo calculations of normal tissue equivalent neutron dose in antiproton therapy through the use of a segmented CT-based human phantom.
Method and Materials: The MCNPX Monte Carlo code was employed to quantify the peripheral dose. Active energy and intensity modulation was used to produce a cylindrical spread out Bragg peak representing a treatment volume of 1 cm diameter and 1 cm length in the frontal lobe of a segmented whole-body phantom of a 38 year old male. The secondary neutron organ dose was tallied as a function of energy and organ. Finally, the physical neutron dose was transformed into effective dose using the energy dependent ICRP-92 radiation weighting factors. Comparisons were made to similar analogous proton treatments.
Results: For 1 Gy of physical dose delivered to the target volume in the given treatment plan,the equivalent dose from neutrons generated by annihilating antiprotons ranges from8.2E-04 Sv for the brain to 2.4 x 10^{-6} Sv for the Caecum, Colon, and Rectum . The results are dependent on the irradiation geometry and the organ equivalent neutron dose is primarily related to the proximity of the organs to the spread out Bragg peak as anticipated.
Conclusion: Using an anthropomorphic Monte Carlo model, we have presented the first calculation of neutron equivalent dose received by peripheral organs due to the annihilation process in antiproton therapy. The developed model can be utilized for similar analyses for other secondary products such as pions and high-energy photons.

Contribution presented by N. Bassler at the LEAP08, Vienna, Austria, 2008-09-21

B. P. Fahimian, J. J. DeMarco, R. Keyes, N. Bassler, K. S. Iwamoto, M. Zankl,
M. H. Holzscheiter (✉)

Dept. of Phys. & Astronomy, University of New Mexico, Albuquerque, NM 87131, USA

*e-mail: mholzscheiter@phys.unm.edu

http://www.phys.au.dk/~hk/ad4homepage.html

Introduction

Today, radiation therapy is one of the prominent treatments of cancer, both curative as well as palliative. For conventional photon irradiation, the maximum dose that can be delivered to a tumor is often limited by the tolerance of irradiated adjacent normal tissues. For many types of tumors, this has led to unacceptably low tumor control probability (TCP) and to high levels of morbidity. An alternative approach involves the use of protons and other heavier ions [1-4]. As R. R. Wilson pointed out in 1946 [5], for these charged particles, both the amount and rate of energy deposition increase dramatically as the particle nears the end of its range. This results in a large enhancement in absorbed dose at a precise depth in tissue (the Bragg peak) compared with the dose deposited at the entrance to the body. For treatment purposes, the position of the Bragg peak needs to be spread out to cover the tumor volume and the production of such a spread-out Bragg peak (SOBP) results in a build up of plateau dose and hence a reduction in the ratio of dose in the SOBP relative to the plateau. However, in contrast to photons, for a given beam direction, the dose in the SOBP that covers the tumor volume always remains larger than that in the normal tissue entrance region.

High linear energy transfer (LET) particles such as carbon ions produce a much higher ionization density in the Bragg peak region than protons and consequently provide an increase in the relative biological effectiveness (RBE) of the dose deposited in the tumor [6 – 8]. This provides a potential further therapeutic advantage, especially for tumors that have a large hypoxic fraction or for those that are resistant to conventional radiation [9]. Furthermore, since very little dose is deposited distal to the Bragg peak, charged particles are ideally suited for treatments of tumors close to radiosensitive regions.

While these favorable physical and biological characteristics have led to recent developments of proton and heavy ion cancer therapy centers worldwide, the search for possible enhancements of the therapeutic ratio (the ratio of effective dose delivered to the target region to the dose delivered to normal tissue) continues.

Antiprotons exhibit similar features as protons while in flight, are intrinsically stable particles, and deposit about twice the energy of a proton at the end of range due to annihilation at rest. This additional energy is deposited partially by high LET particles, which increases the biological effective dose even further. The enhanced biological effectiveness of antiproton annihilation in the vicinity of the Bragg peak is believed to be beneficial in the context of increasing tumor control while sparing the surrounding healthy tissue.

The AD-4/ACE collaboration is investigating the potential clinical benefit of antiproton beams using the antiproton beam available at the Antiproton Decelerator (AD) at CERN. Initial experiments with 46.7 MeV antiprotons found the biological effective dose ratio (BEDR) between peak and plateau to be 4 times higher for antiprotons than for protons [10]. Recently we have successfully performed precise measurement of the depth dose profile of antiprotons with ionization chambers [11] and alanine detectors [12], and are therefore now able to extract the relative biological effectiveness (RBE) of antiproton beams from cell survival measurements. RBE values for different cell lines and endpoints can be

extracted along the beam path and can be compared with those found from other particle beam modalities such as carbon ion and proton beams. The results of the physical dose and biological effectiveness measurements are used to benchmark particle transport and radiobiology Monte Carlo codes. Virtual treatment plans based upon the benchmarked Monte Carlo codes can then help to identify those tumor incidents where antiproton therapy may offer a decisive advantage over other modalities [13].
One important issue in the assessment of a new treatment modality is any background dose deposited outside of the primary target. In antiproton annihilation this background results from medium and long-range annihilation products, predominantly charged pions, high energy gammas, and neutrons. We have launched a major effort to address this effect using experiments and Monte Carlo calculations utilizing a variety of code packages. In this report we concentrate on the example of neutron equivalent dose to out-of-field organs using MCNPX v26F [14].

Calculation of Neutron Equivalent Dose

When an antiproton annihilates after being captured by the nucleus of a target atom, a number of neutrons, depending on the target nucleus, are emitted. The energy spectrum of these neutrons spans from thermal energies up to several hundred MeV, with a mean energy of approximately 50 MeV. The biological efficiency of these neutrons varies with energy and the International Commission on Radiological Protection (ICRP) has published weighting factors vs. energy for neutrons in human tissue. Because of the high biological effectiveness of neutrons and their abundance in the particle spectrum we decided to study the effect in detail.

Benchmarking of MCNPX

MCNPX is a Monte Carlo transport package that is widely used in clinical applications. Nevertheless, when applying it to antiproton therapy the code must be benchmarked against available experimental data to assure that correct physical models and transport parameters are utilized and the description of the annihilation process is complete. We have simulated both the bubble chamber experiments by Agnew at al. [15] and the neutron multiplicity for annihilation of antiprotons at rest in the center of slabs of ^{63}Cu reported by Polster et al. [16]. The physical models used in the simulations consisted of the Bertini model for nucleons and pions, the LAQGSM model was used for all heavy ion and light ions above 940 MeV/nucleon, and the ISABEL model was used for the remaining of the light ions [14].

Bubble Chamber Simulations 30 in^3 of Propane Liquid, 220 MeV Antiproton Beam		
	Multiplicity	
	Agnew et al.	MCNPX
$\pi^{\pm}$	3.38±0.08	3.09±0.09
π^{o}	1.6±0.5	1.83±0.05
$\kappa^{\pm}$	0.08±0.02	0.11±0.01
Heavy ions, ^{3}H , ^{3}He	1.29±0.07	1.34±0.07

Table 1: Multiplicities for pions, kaons, and heavy ion production in antiproton annihilations in a propane gas target [15].

Our calculations for Agnew's work agreed well with the experimental results after appropriate changes to the set cut-off energies were incorporated in the code [Table 1].

We also found good agreement between the general shape of the energy spectrum of neutrons produced in the annihilation of antiprotons at rest in the center of a ^{63}Cu slab obtained by MCNPX and the analytical function given by Polster et al. [16], but a slight overshoot in two distinct energy regions resulted in a higher overall neutron multiplicity than reported by Polster. The overshoot may be related to the difficulties and unknowns in modeling the Polster experiments; however, the results were found to be adequate for the purposes of establishing and upper estimate of the neutron equivalent dose.

Virtual antiproton irradiation of a voxelized phantom

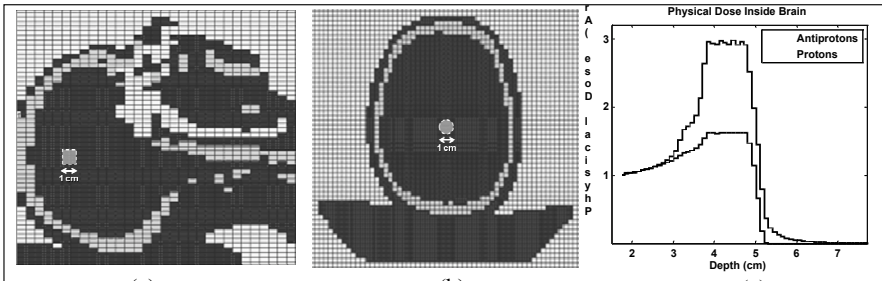

(a) (b) (c)

Fig. 1: (a),(b) Sagittal and transverse views of the voxelized phantoms' head and the PTV (c) Resulting depth dose profiles (physical dose only) in the beam direction inside the brain for the antiproton and proton simulations, normalized to the same entrance

To model the biological effect of a patient treatment with antiprotons we used a voxelized phantom of a 38 year old living man (Golem) of approximately the same dimensions as the ICRP Man [17]. Golem has a weight of 68.9 kg and a height of 176 cm. The voxel size is 34.6 mm^3. The planning target volume (PTV) consisted of a cylinder of 1 cm diameter and 1 cm length situated in the central lobe as shown in Fig. 1. Comparative simulations were performed for both antiprotons and protons using active beam modulation. Spread-out Bragg peaks were generated by modulating the intensities and beam energies between 74 and 86 MeV, resulting in the profiles shown in Fig. 1(c). The dose deposited by neutrons resulting from the annihilation in the target was tallied for the individual

organs of Golem as a function of neutron energy. The value for the normal tissue dose received by the brain was obtained by subtracting the tumor dose estimated using a mesh tally covering the target volume with a 1.5 mm margin from the total dose. Using the neutron dose as a function of energy obtained from MCNPX and the neutron radiation weighting factors given as a function of energy by ICRP, the physical dose in the different organs was then transformed to equivalent dose by integrating the product of the physical dose and radiation weighting factors over all energy bins. The resulting organ equivalent doses per gray of physical dose delivered to the target region for the antiproton and proton treatments are presented in Table 2 for a number of organs (simulation error implied by decimal point).

Comparison of Neutron Equivalent Dose Per Gy in SOBP (Sv/Gy)		
	Antiprotons (ICRP 92)	**Protons (ICRP 92)**
Brain	8.2E-04	1.2E-05
Thyroid	2.8E-05	3.1E-07
Bone	2.2E-05	3.8E-07
Lung	9.7E-06	8.4E-08
Liver	4.8E-06	3.6E-08
Caecum, Colon, Rectum	2.4E-06	1.4E-08

Table 2: Comparison of neutron equivalent dose, normalized to unit physical dose to the tumor for the given antiproton and proton treatments. For the purpose of generality, the enhanced SOBP RBE of antiprotons is not incorporated in this table.

Conclusions

Using an anthropomorphic phantom, the first Monte Carlo estimates of tissue specific neutron equivalent dose in antiproton therapy have been produced For scanning energy modulation, and a 1 cm cylindrical PTV in the brain, the calculated neutron equivalent doses for several organs range from .0001 to .8 mSv per Gy of SOBP, depending on the proximity to SOBP. In order to properly compare these results with that of proton therapy, the enhanced RBE for antiprotons in the SOBP must be considered in addition to the physical dose normalized comparisons of Table 2. Using the results from [10] this suggests that the neutron equivalent dose for antiproton therapy is roughly 60 times higher than what is obtained with protons for the given treatment plan. Here it should be noted that most proton therapy centers currently use passive scattering methods for beam delivery which increases the radiation level to the patient by 1 – 2 orders of magnitude [18]. In addition to the peripheral neutron dose described here there is also a background of pions and high-energy photons produced in the antiproton annihilation event. Preliminary calculations show that the physical dose for these components is similar to the neutron dose, but as these particles have a low linear energy transfer we expect the equivalent dose to be below the neutron dose. Monte Carlo studies of these issues are ongoing in parallel to experimental studies of biological effects in the peripheral region.

References

[1] Levin W.P., et al.: Br J Cancer **93**, 849 (2005)
[2] Suit H., et al.: Acta Oncol **42**, 800 (2003)
[3] Schulz-Ertner D., et al.: Strahlenther Onkol **179**, 598 (2003)

[4] Mazeron J.J., et al.: Radiother Oncol **73**, S50 (2004)
[5] Wilson R.R.: Radiology **47**, 487 (1946)
[6] Blakely E.A., et al.: Radiat Res **80**, 122 (1979)
[7] Weyrather W.K., Kraft G.: Radiother Oncol **73**, S161 (2004);
[8] Weyrather W.K., et al.: Int J Radiat Biol **75**, 1357 (1999)
[9] Svensson H., et al: Radiother Oncol **73**, S206 (2004)
[10] Holzscheiter M.H., et al.: Radiother Oncol **81**, 233 (2006)
[11] Bassler N., et al: Phys. Med. Biol. **53**, 793 (2008)
[12] Bassler N., et al.: Nucl. Instr. Meth. in Phys. **B 266**, 929 (2008)
[13] Bassler N., et al. Radiother Oncol **86**, 14 (2008)
[14] Waters, L.S.: MCNPX User's Manual, v2.3.0. Los Alamos Unclassified Research Report LA-UR-02-2607
[15] Agnew L.E., et al.: Phys. Rev. **118**, 1371 (1960)
[16] Polster D., et al.: Phys. Lett. **B 300**, 317 (1993)
[17] Petoussi-Henss N., et al.: Phys. Med. Biol. **47,** 89 (2002)
[18] Xu X.G., et al.: Phys. Med. Biol. **53**, R 193 (2008)